ACADEMY OF SCIENCES OF THE REPUBLIC OF UZBEKISTAN
INSTITUTE OF NUCLEAR PHYSICS

On manuscript rights

UDK 539.12.01; 539.125; 539.143

TURSUNOV ERGASH MAKHKAMOVICH

STRUCTURE OF LIGHT NUCLEI IN THE FRAME OF POTENTIAL MODELS

01.04.08 – physics of atomic nuclei and elementary particles, accelerator technics
(physics and mathematics)

DISSERTATION
on the scientific degree competition
of the doctor of sciences in physics and mathematics

Scientific consultant: doctor of sciences in physics and mathematics
Professor, Academician B.S. Yuldashev

Tashkent - 2014

CONTENTS

INTRODUCTION

Topicality and demand of the subject of dissertation. Currently, a lot of efforts are made to understand the structure of neutron rich halo nuclei like ^{6}He, ^{11}Li, ^{11}Be, ^{14}Be, ^{19}C, ^{31}Ne. These nuclei have special properties such as small binding energies and the extended one- and two-neutron low-momentum orbitals (l=0,1). Usually, these nuclei are studied in the core plus few neutrons model. Additionally, no any two-body subsystem of the three-body halo nuclei ^{6}He, ^{11}Li, and ^{14}Be is bound, a property of the Borromean system. In addition to the static properties, like energies and charge radii, the beta-decay and electromagnetic transition processes of these nuclei to two-body and three-body continuum channels are of special interest. These processes yield useful information on the internal structure and halo properties of the nuclei, since the transitions occur namely in the halo parts. In addition, there are experimental data on the beta-decay processes of the ^{6}He and ^{11}Li halo nuclei into the two-body deuteron continuum channels, which need a deep theoretical analysis. The study of the beta-decay processes of the halo nuclei ^{11}Be, ^{19}C and ^{31}Ne to the two body proton plus core continuum channels can yield new properties of these systems in addition to the static characteristics.

Among the halo nuclei a special place belongs to the ^{11}Li nucleus. Unlike other nuclei, it can decay additionally into the ^{9}Li+proton+neutron three-body continuum channel. This is the most complicated process and the theoretical model should give useful information on the process, as well as on the three-body structure of the ^{11}Li halo nucleus.

The first excited state of the ^{6}Li nucleus is the isobar analog state of the ^{6}He halo nucleus. Therefore the M1-transition process of this state to the deuteron continuum channel allows one to obtain information on its halo properties,

similar to the properties of the ^{6}He nucleus. The obtained estimations for the width of the M1-transition can be compared with the existing experimental data. The process additionally can be used when studying the parity violation effects in the strong interaction.

The nuclear-nuclear interaction models, containing forbidden states in lowest waves, have been proposed long time ago, in the seventies of the XX-th century for an adequate account of the Pauli principle as an alternative to the potential models with a repulsive core at short distances. They have a microscopic background, in other words, are based on the nucleonic degrees of freedom. However, the role of these forbidden states in the nuclear structure has not been properly studied until now. This question is of special interest for nuclei containing several alpha clusters. The exclusion is the Moscow nucleon-nucleon potential model with forbidden states in lowest waves: its properties in the three-body nuclei have been studied in details. On the other hand, a role of forbidden states in the Moscow model is different and it is connected with the quark structure of the nucleon. But in light nuclei containing several nuclear clusters, the models with forbidden states are introduced exclusively for the adequate account of the Pauli principle. They have got a special actuality in view of the discovery of the halo structure of some light nuclei.

The nuclei which consist of several alpha clusters play an important role in astrophysics. Although the two alpha particles are unbound, but the nuclei, containing three (^{12}C) and four (^{16}O) alpha clusters, have large binding energies and belong to the group of the Borromean nuclei. For these nuclei, the obtaining realistic wave functions for the bound, as well as continuum states, which can be applied to the estimation of the cross-section of the astrophysical synthesis reactions, is the most difficult problem. On the other hand, study of the structure of these nuclei become even more actual in view of predictions of the existence of the "alpha-condensation".

The topic of the dissertation is included into the list of the priority direc-

tions of the fundamental research developed by the Academy of Sciences of the Republic of Uzbekistan. Needs for the dissertation topic are connected with the necessity of development of fundamental knowledge on matter structure, nuclear forces and processes occurring in the microworld. Developed theoretical models of strong interaction allow one to describe structure of nuclei and to predict their new properties. Fundamental knowledge of nuclear structure and nuclear forces will be a reliable basis for the development of nuclear power which becomes basic and practically inexhaustible energy source in the near future.

Conformity of research to priority directions of development of science and technologies of the Republic of Uzbekistan. This work has been carried out in accordance with development priorities of science and technology of the Republic of Uzbekistan F2 "Physics, Astronomy, Power engineering and engineering industry".

Review of international scientific research on dissertation subject. Theoretical models for the structure of light nuclei are being developed in different scientific centers of the world. The most successful models for the structure of bound states of light nuclei are based on variational methods on Gaussian (theoretical groups in Niigata and Kyoto, Japan and Moscow State University, Russia) and Lagrange mesh (theoretical group at the University Libre de Bruxelles, Belgium) bases. They have been applied to the study of the structure of the three-body nuclei ^{3}H, ^{3}He, ^{6}He, ^{6}Li, ^{11}Li, ^{9}Be. The energy spectra, root-mean square radii, electric and magnetic form factors have been estimated. However, a theoretical study of the ^{12}C nucleus in the 3α model does not give satisfactory results. The bound spectrum of this nucleus obtained with the help of the local $\alpha - \alpha$-potential with a repulsive core lays much higher than the experimental data. At the same time the microscopical models underestimate the spectrum by several MeV. And the three-body calculations using potential models with $\alpha\alpha$-forbidden states, meet big problems connected with

the orthogonalization of the solution on forbidden states. In order to overcome these difficulties it is necessary to examine carefully the sensitivity of the energy spectrum of the ^{12}C nucleus to the description of the $\alpha - \alpha$-forbidden states.

The three-body continuum structure of light nuclei is being studied through the break-up reaction in the experiments (RIKEN, Japan), as well as by theoretical way on the basis of the Faddeev equation approach (theoretical group at the Aarhus University, Denmark), the complex scaling and analytical continuation methods (theoretical group at the MSU, Russia). However, these methods have limited possibilities. In particular, the Faddeev equation approach meets difficulties when dealing with the Coulomb forces. And the complex scaling method, as well as the analytical continuation method can be applied only to the resonance states.

In the past the R-matrix approach has been applied to the two-body continuum problems. However, a recent application of this method in the literature to the three-body continuum in the frame of the hyperspherical method (groups of the Kurchatov Atomic Energy Institute, Russia and of the Copenhagen University, Denmark) meets serious problems due-to the extended three-body binding potential.

As was noted above, during the last years the properties of the two-body ^{11}Be, ^{19}C, ^{31}Ne and three-body ^{6}He, ^{11}Li, ^{14}Be halo nuclei present a special interest. Currently, all the above mentioned theoretical groups are being interested to study the bound and continuum structure of these systems and the electromagnetic and beta-transition processes to the continuum channels.

Degree of study of the problem. The role of forbidden states in nuclear interactions has been studied in the 3α problem several times. But, up to now it was impossible to separate completely the three-body allowed subspace for this system. The obtained solutions of the Schrödinger equation for the bound states of the ^{12}C nucleus in the 3α model with the BFW potential with forbidden states contain some piece of forbidden states therefore the obtained

theoretical results for the energy spectrum are not realistic. The application of the orthogonalising pseudopotential method for the exclusion of forbidden states allows to find out special features of the ^{12}C nucleus that have not been studied in the literature.

Serious problems connected with the extended three-body effective potential when describing the three-body continuum of halo nuclei, can be overcome in the R-matrix approach in a combination with the propagator method. This way allows to match the wave function with its asymptotics at large distances. The method can be applied to the three-body continuum structure of the halo nuclei ^{6}He and ^{14}Be that has not been studied in the literature.

The existing experimental data on the beta-decay processes of the halo nuclei ^{6}He and ^{11}Li into the two-body continuum channels with the deuteron emission have not been explained adequately up to now in theoretical models, although there were several papers devoted to this problem. The theoretical researches on the ^{6}He beta-decay have concluded that the $\alpha - d$-potentials with forbidden states describe the experimental data better than the models with forbidden states which have a microscopical background. Additionally, a potential dependence of the beta-transition probability of the ^{11}Li nucleus into the deuteron continuum channel has not been studied, although obtained results are somehow close to the experimental data. Also, a role of the S-wave resonance in the ^{9}Li+d system has not been studied for the correct description of the experimental data.

The halo properties of the isobar-analog state ^{6}Li(0^{+}) have not been studied in details in the three-body model in the literature. Only some simplified estimations have been obtained. Here one has to develop complete three-body formalism with the extraction of analytical expressions for the matrix elements of the M1-transition with the further numerical realization.

Also, there were no studies of the beta-decay processes of the one-neutron halo nuclei ^{11}Be, ^{19}C and ^{31}Ne to the two-body continuum channels with emis-

sion of a proton.

As was noted above, the most complicated process is the beta-decay of the halo nucleus ^{11}Li into the three-body continuum channel ^{9}Li+p+n. This process was studied neither in theoretical works, nor in the experiment. Therefore the theoretical analysis of the process with application of the modified Coulomb functions allows finding out new halo properties of this nucleus.

Connection of dissertational research with the plans of scientific-research works is reflected in next projects performed in the frame of the State Scientific-Technical Programs on fundamental research:

N.F-2.1.33 "Study of the multiphonon states of the vibrational nuclei" (2003-2007);

N.FA-F2-F076+F074 "Study of the structure of the symmetrical and neutron rich nuclei in the transfer and breakup reactions" (2007-2011);

N.F2-FA-0-10117 "Study of the formation of light elements and properties of exotic nuclei formed in the low-energy reactions" (2011-2016).

Purpose of research is to establish special features of the potential model of the interaction between nuclear clusters for the bound and continuum structure of light nuclei and for the description of processes with these nuclei at low energies.

To achieve this goal the following **tasks of research** are formulated:

- to estimate the energy spectrum of the ^{12}C nucleus in the 3α cluster model and to clarify special features of the potential model with forbidden states;

- to develop the R-matrix approach in the combination with the propagator method for the study of the three-body continuum structure of light nuclei, to estimate three-body phases for the two-neutron halo nuclei ^{6}He and ^{14}Be;

- to analyze the beta-decay processes of the halo nuclei ^{6}He and ^{11}Li into the $\alpha + d$ and ^{9}Li+d two-body continuum channels in the three-body cluster potential model and to clarify potential dependence of the transition probabilities;

- to study halo properties of the the isobar-analog state ^{6}Li(0+) in the magnetic M1-transition processes to the ^{6}Li(1+) ground state and to the $\alpha + d$ continuum in the three-body model and to study potential dependence of the transition probabilities;

- to estimate the transition probabilities of the ^{11}Li nucleus beta-decay to the ^{9}Li+$p + n$ three-body continuum channel in the cluster potential model;

- to to estimate the transition probabilities of the beta-decay of the one-neutron halo nuclei ^{11}Be, ^{19}C and ^{31}Ne to the two-body continuum channels in the frame of cluster potential model.

Objects of research are the bound spectrum of the ^{12}C nucleus, transition probabilities of the beta-decay of the halo nuclei ^{6}He, ^{11}Li, ^{11}Be, ^{19}C and ^{31}N to the two-body and three-body continuum channels, the probability of the M1-transition of the isobar-analog state ^{6}Li(0^+) to the ^{6}Li(1^+) ground state and to the $\alpha + d$ continuum, three-body continuum structure of the ^{6}He and ^{14}Be halo nuclei.

Subjects of research are two-body and three-body structure of light nuclei, including halo nuclei, electromagnetic and weak transitions in nuclei, nuclear interaction potentials, mechanisms of the strong interaction.

Methods of research. Cluster potential model based on variational methods on Gaussian and hyperspherical Lagrange-mesh bases for the calculations of the two-body and three-body bound state wave functions and corresponding energy spectrum; Numerov algorithm for the calculation of the two-body scattering wave functions; R-matrix approach in the hyperspherical Lagrange-mesh basis for the calculation of the three-body continuum wave functions with the help of the propagation method on the basis of the Numerov algorithm; method of orthogonalizing pseudopotentials for the elimination of Pauli forbidden states.

Scientific novelty of the research, presented in the dissertation consists in the following:

- For the first time an extremely high sensitivity of the energies of the compact 0_1^+ and 2_1^+ states of the ^{12}C nucleus to the description of the two body Pauli forbidden states was established, which leads to the occurrence of the so called "almost forbidden states" in the three-body functional space.

- For the first time the R-matrix approach is developed in combination with the propagator method for the study of the three-body continuum structure of light nuclei ^{6}He and ^{14}Be in the frame of the hyperspherical harmonics method on a Lagrange-mesh basis. It is shown that for the convergence of the results the wave function has to be matched with its asymptotics at large distances (about 1000 fm). The diagonal- and eigen-phases of the three-body collision matrix have been calculated and a new ^{14}Be(2^+) resonance is predicted near E_x=3.4 MeV.

- Theoretical estimations for the transition probabilities per time and energy units of the beta-decay of the two-neutron halo nucleus ^{6}He to the $\alpha + d$ continuum channel have been obtained. For the first time it was shown that for the reproduction of the experimental data on the beta-decay, it is necessary to use microscopically found $\alpha - d$-potentials containing a forbidden state in the S-wave, reproducing phase shifts and the ground state energy. It was shown also that the convergence of matrix elements requires to know wave functions up to 30 fm and hypermomentum components up to K=24. It was demonstrated that the halo effects play an important role in the description of the process because of mutual suppression of the internal and external parts of the matrix elements.

- For the first time the theoretical estimations for the probabilities of the M1-transition per time and energy units of the isobar-analog state ^{6}Li(0^+) to the $\alpha + d$ continuum have been obtained. It was shown that only in the case of using the potentials with forbidden states the integral width of the transition 0.9 meV is well consistent with the previous simplified calculations. It was shown also that the convergence of the results requires to take the upper limit

of the effective integral around 25-30 fm and the hypermomentum components up to K=20.

- For the first time the theoretical estimations for the transition probabilities per time and energy units of the ^{11}Li to the two-body ^9Li+d continuum channel have been obtained, very consistent with new experimental data. It was shown that in this case, a resonance in the S-wave of the ^9Li+d system at the energy position of about 0.7 MeV plays the main role, not depending on which potential model is used: with a repulsive core or with a forbidden state. The ^9Li+d-potential which reproduces this resonance, describe well the shape and absolute values of the transition probabilities with the help of absorbing imaginary term due-to open decay channels.

- For the first time theoretical estimations for the beta-decay probabilities per time and energy units of the ^{11}Li halo nucleus to the $^9Li+p+n$ three-body continuum channel have been obtained.

- For the first time theoretical estimations for the beta-decay probabilities per time and energy units of the one-neutron halo nuclei ^{11}Be, ^{19}C and ^{31}Ne to the two-body $core+p$ continuum channels have been obtained in the potential cluster model. It was demonstrated that the transition probabilities are strongly sensitive to the separation energy of the valence neutron.

Reliability of the obtained results is provided by the followings: modern methods of quantum mechanics and the theoretical nuclear physics and highly effective numerical methods and algorithms are used; careful check of a consistence of the received theoretical results with experimental data and results of other authors is performed; conclusions are well consistent with the main provisions of the theory of structure of light nuclei.

Theoretical and practical value of research results. The theoretical and practical values of the results, presented in the dissertation, consist in the possibility to use them for the development of the theory of nuclear structure, of the cluster model of light nuclei. The methods developed in the thesis can be

applied for the solution of few-body quantum mechanical problems in molecular, atomic and nuclear physics. The obtained theoretical estimations for the transition probabilities of the two-neutron halo nucleus ^{11}Li into the ^{9}Li+p+n three-body continuum channel and one-neutron halo nuclei ^{11}Be, ^{19}C and ^{31}Ne to the two-body continuum channels can be used when planning experiments on these processes. The theoretical estimations for the M1-transition probabilities of the isobar-analog state ^{6}Li(0^+) to the $\alpha + d$-continuum can be used when planning experiments on this process and also when examining the parity violating effects in the strong interaction.

Realization of the research results. The new resonance ^{14}Be(2^+) around E_x=3.4 MeV predicted in the dissertation was confirmed recently in the experiment with E_x(exp)=3.54(16) MeV: Aksyutina Yu., Aumann T., Boretzky K., et al. "Study of the ^{14}Be continuum: Identication and structure of its second 2^+ state", Phys. Rev. Lett. - New York, 2013. - vol. 111, N. 24. - 242501. The methods developed in the dissertation work have been used by 1)P. Descouvemont in Journal of Physics G: Nuclear and Particle Physics, 2010. - vol. 37.- id.064010 when the three-body continuum structure of the 12C nucleus is studied and by 2) E. C. Pinilla, et al. in Physical Review, 2012, - vol. C 85. - id.054610 when the three-body breakup of the ^{11}Li nucleus is studied in the frame of the Interuniversity Attraction Pole Program P6/23 "Spectroscopy of light nuclei and nuclear reactions in microscopical models" (2010-2012) initiated by the Belgian-State Federal Services for Scientific, Technical and Cultural Affairs. The theoretical results presented in the thesis have been used when planning the last experiments on the beta-decay of halo nuclei ^{6}He and ^{11}Li into the deuteron channel by R. Raabe, J. Buescher, et al. in Phys. Rev. C, V. 80, N.5, 054307, 2009 and by R. Raabe, A. Andreyev et al. in Phys. Rev. Lett., V. 101, N. 21, 212501, 2008. In recent papers of M. Grieser et al., Eur. Phys. J., Special Topics, v. 207, N. 1, pp.2012 and M.J.G. Borge et al. J. Phys. G: Nucl. Part. Phys. 40, 2013, 035109 the results on the beta-decay

of one-neutron halo nuclei ^{11}Be, ^{19}C and ^{31}Ne into two-body and ^{11}Li into the three-body continuum channels, presented in the thesis have been used to help devising a storage ring for the ISOLDE facility at CERN.

Approbation of the work. Main results of the dissertation have been reported at the seminars of the Nuclear physics department of the INP of the UzAS, of the National University of Uzbekistan, of the Brussels Free University (ULB), of the Surrey University (England), of the Inha University (Korea), at 6 International Conferences "50 Years of the Nuclear Shell Model" (Heidelberg, Germany, 1999), "SOTANCP-2010" (Brussels, Belgium, 2010), "Modern Problems of Nuclear Physics" (Samarkand, 2003; Tashkent, 2009), "Nuclear and Radiation Physics" (Almaty, Kazakhstan, 2011), "Nuclear science and its application", (Samarkand, 2012).

Publication of results. The main results of the dissertation have been published in 20 scientific works, 9 of them are in international leading journals (1 of them is as Proceedings of the International Conference), 1 paper is published in Uzbek Journal of Physics (as Proceedings of the International Conference), 1 paper is in the Proceedings of the International Conference (Niigata, Japan, 2003), 1 preprint is in the Los-Alamos e-arXiv and 8 Abstracts are of International Nuclear Physics Conferences.

Structure and volume of the dissertation. The dissertation consists of an introduction, eight chapters, conclusion, a reference list and two appendices. The dissertation is printed on 181 pages,and includes 33 figures and 14 tables.

Acknowledgements

First and foremost the author deeply thanks and expresses his profound gratitude to Prof. Daniel Baye and Prof. Pierre Descouvemont for the close and fruitful collaboration during the long period. He is grateful to Prof. Academician B.S. Yuldashev and Prof. U.S. Salikhbaev for the valuable support during the dissertation work. He thanks all the staff of the Institute of Nuclear Physics of the Uzbekistan Academy of Sciences and the scientific staff of the

PNTPM, University Libre de Bruxelles, Brussels, Belgium, especially Dr. J-M. Sparenberg, Prof. Ch. Willain, Dr. P. Capel for the kind scientific atmosphere during his visits to Brussels, Prof. L.D. Blokhintsev and Dr. N. Timofeyuk for the support and very useful discussion of the results, Prof. A. Faessler, Prof. Th. Gutsche, Prof. S. Krewald, Prof. E. Oset and Prof. A.M. Rakhimov, Prof. V. Petrov, Prof. H.S. Kim, Dr. U. Yakhshiev for useful discussions of the results and valuable advices. Author is thankful to Prof. R. Yarmukhamedov, Prof. M. Karimov and Z. Fazilova for the help in fulfilling the formalities of the Dissertation. Finally, the author acknowledges his wife Nilufar, his daughter Munisa and his sons Jamshid and Jahongir for their patience and support during the long period of his work on the Dissertation.

List of published papers:

1. Tursunov, E.M. Variational calculations of the 12C nucleus structure in a 3- alpha model using a deep potential with forbidden states // Journal of Physics G: Nuclear and Particle Phys.- London, 2001. - vol. **27**, N. 7. - pp. 1381-1389.

2. Tursunov, E.M., Baye D., Descouvemont P. Comparative variational studies of 0+ states in three-alpha models// Nuclear Physics. - Amsterdam, 2003. - vol. **A723**, N. 3-4. - pp. 365-374.

3. Descouvemont P., Tursunov E.M., Baye D. Three-body continuum states on a Lagrange mesh // Nuclear Physics A. - Amsterdam, 2006.- vol. **765**, N. 3-4. - pp. 370-389.

4. Tursunov E.M., Baye D., Descouvemont P. Analysis of the 6He beta-decay into alpha + d continuum in a three-body model // Physical Review C. - New York, 2006. - vol. **73**, N. 1 - 014303 (9 p.).

5. Baye D., Tursunov E.M., Descouvemont P. 11Li beta-decay into 9Li and deuteron within a three-body model // Physical Review C. - New York, 2006.- vol. 74, N. 6 - 064302 (7 p.)

6. Tursunov E.M., Baye D., Descouvemont P. Three-body systems with the

Lagrange-mesh technique // Proc of the Int. Symp. A new era of Nucl. Struct. Phys., Niigata, Japan, Nov 19-22, 2005. Ed. Y. Suzuki et al. - World Scien. Publ. Singapore, 2006 - pp. 325-326.

7. Tursunov E.M., Descouvemont P., Baye D. Gamma-delayed deuteron emission of the 6Li (0+ ; T=1) halo state // Nuclear Physics A. - Amsterdam, 2007.- vol. **793**, N. 1. - pp. 52-66.

8. Tursunov E.M., Baye D., Descouvemont P. Electromagnetic and weak processes with light halo nuclei // Uzbek. Phys. Journal - Tashkent, 2010. - vol. **12**, N. 4-6. - pp. 280-289.

9. Tursunov E.M. On the convergence of the many-body Pauli projector // arXiv:1002.0455, Los-Alamos, 2010. - (3 p.).

10. Baye D., Descouvemont P., Tursunov E.M. Unique decay process: beta-delayed emission of a proton and a neutron by the 11Li halo nucleus // Phys. Rev.C - New York, 2010 - vol. **82**, N. 5 - 054318 (6 p.).

11. Baye D., Tursunov E.M. Beta-delayed emission of a proton by a one-neutron halo nucleus // Phys. Lett. B - Amsterdam, 2011.- vol. **696**, N. 5 - pp. 464-467.

12. Tursunov E.M., Baye D., Descouvemont P. Theoretical study of the 11Li beta-decay into the deuteron channel in a cluster model // Int. J. Mod. Phys.E. - Singapore, 2011. - vol. **20**, N. 4 - pp. 803-806.

I. EFFECTIVE POTENTIAL MODELS FOR THE STRUCTURE OF LIGHT NUCLEI

A central place in nuclear physics belongs to the NN- interaction models. In nuclear physics, one starts with a realistic NN-potential, with parameters, fitted to reproduce the NN-scattering data and deuteron observables. The NN-potential is required to be consistent with the OPE-mechanism of Yukawa at large distances (from 1.5 - 2 fm). At intermediate distances (from 0.5 fm) the potential parameters are defined mostly from the scalar σ-meson exchange mechanism which yields an attraction. At short distances (up to 0.5 fm) the behavior of the NN-interaction potential is repulsive and it is a challenge for the nuclear physics community around the world. All the gluon-, vector meson(ρ and ω)-, quark-exchange mechanisms are believed to be responsible for the short-range NN-repulsion. The realistic Reid [1], Argonne [2], Bonn OBE [3] potential models of the NN- interaction, containing a repulsive core at short distances yield an overall good description of the few-nucleon observables. However, without additional 3N-forces these models underbind the lightest ^3He and ^3H nuclei by about 1 MeV. A serious problem is an understanding of the difference between the theoretical estimations and experimental data for the polarization observables in the $p+d$ -scattering process [4], the so-called A_y-puzzle. Recent effective chiral field theory [5] calculations also did not resolve this problem.

At the same time, in nuclei due to overlap of nucleons with the size of about 0.8 fm, the average distance between the centers of nucleons is estimated to be about 1.8 fm. Consequently, at short distances, a quark structure of nucleons comes into the game. An exchange mechanism between valence quarks directly contributes to the exchange forces between the two nucleons. One can note at

this point, that strong nuclear forces are originated from the strong interaction physics between valence quarks.

A valuable information on the NN-interaction and on nuclear forces at short distances can be extracted from the study of the excited nucleon and delta spectrum (see recent experimental data [6] and review [7] and references therein). These studies are believed, in particular, to answer the question: what is the most important exchange mechanism between valence quarks in hadrons, hence between nucleons at short distances (in the quark-core region) [8, 9]. The Scientific Programs of the International Workshops on Physics of Excited Nucleons (NSTAR) which are held every two years in hadronic physics centers around the world (Florida, USA, 2005; Bonn, Germany, 2007; Beijing, China, 2011; Thomas Jefferson Laboratory, USA, 2011; University of Valencia, Spain, 2013 [10]) include all the theoretical and experimental developments in current field (see also Ref. [11]).

In Refs. [12–17] we have applied a relativistic chiral quark potential model (ChQPM) [18–20] to the excited nonstrange baryon spectroscopy and demonstrated that the model can describe the excited baryon spectrum fairly well.

There are very few models of the NN-interaction which incorporate the quark structure of the nucleon [21]. The quark motivated realistic Moscow NN-potential model [22, 23] does not have a traditional repulsive core at short distances. Instead of the core, the potential contains forbidden states at lowest partial S- and P-waves, which are required to be projected out during the solution of the dynamical many-body Schrödinger equation. The parameters of the model are fitted only to the NN-scattering data, while the deuteron appears as the first excited state in the coupled $^3S_1 -^3 D_1$ channel without any fitting parameters. It is important to note, that there is a SUSY-transformation [24] between the deep Moscow NN-potential [23] and the Reid soft core NN-potential [1]. Detailed studies of the structure of the ^3He and ^3H nuclei have demonstrated [22, 23], that the Moscow NN-potential underbinds three-nucleon

systems by about 2.5 MeV, which means that three-body forces in this case should give a larger contribution in comparison with the case of the traditional NN-potential models (Reid, Argonne, Bonn).

The existence of forbidden states in the Moscow NN-potential model is motivated by the quark structure of the interacting nucleons [25]. From the Constituent Quark Model studies it was found that the six-quark wave function component s^4p^2 has a dominant projection on the NN-channel compared to the bag-like symmetric s^6-configuration [22, 23]. The orthogonality of these two six-quark components is believed to yield a strong repulsion in the NN-channel which is modeled by the deep attractive potential with forbidden states at lowest partial S- and P-waves.

The first suggestion for the deep potentials came from Neudatchin et al. [26]. Then this idea has been realized by Buck, Friedrich and Wheatley for the description of the $\alpha - \alpha$ interaction [27]. These potentials have a strong microscopic background, and yield a node at short distances for the scattering wave functions. The $\alpha - \alpha$ potential suggested contains two Pauli forbidden states in the S-wave and a single forbidden state in the partial D-wave. The phase shifts in these waves are well described with only two fitted parameters of the potential. The role of forbidden states is expected to be very important for the compact ground (0^+) and first excited (2_1^+) states of the ^{12}C nucleus in the 3α cluster potential model. On the other hand, the ^{12}C nucleus is a three-body Borromean system, that means that no any two-body subsystems are bound and it is the lightest bound alpha-cluster system [28]. Structure of this nucleus is still one of the hot topics in the literature [29–35]. The microscopic 3α potential models of the ^{12}C nucleus structure [36–41] yield a strong overbinding by 7-10 MeV for the ground 0_1^+ ($E_{exp} = -7.27$ [42]) and first excited 2_1^+ states, while the macroscopic 3α potential model of Ali and Bodmer (AB) [43] yields a strong underbinding. The application of the alternative deep potential model of Buck, Friedrich and Wheatley (BFW) [27] with forbidden states in the lowest S- and

D- waves met serious problems related to the elimination of Pauli forbidden states in the three-body functional space [44, 45]. A method of orthogonalizing pseudopotentials for the elimination of forbidden states, which will be developed in chapter 2, is expected to clarify the question, is it possible to describe the ^{12}C nucleus structure in a macroscopic 3α model [46, 47]. This question raised a lot of activity last years [48–51].

Models of the deep potentials with forbidden states for the interaction between nuclear clusters are expected to present a special interest for the structure of light halo nuclei, including their continuum structure. The deep potential models have a microscopic background and are consistent with the realistic models of the NN-interaction. It would be very important to see a difference between the theoretical results for the deep and shallow potential models when studying the processes at low energies, such as beta-decay and electromagnetic transition of the halo nuclei to the two-body and three-body continuum channels.

Currently, there is a big effort for the understanding of the structure of neutron rich and proton rich halo nuclei, which do not exist in Nature but are produced at nuclear facilities [52–56]. The halo nuclei are the most popular objects in nuclear physics for the last two decades beginning from the discovery of the halo effect near the neutron drip line [57–59]. This discovery triggered many experimental and theoretical works on exotic nuclei, such as ^{6}He, ^{11}Li or ^{14}Be. They are weakly bound and have very extended halo structure. The large radii are interpreted as arising from an extended spatial density of a few neutrons [58, 60, 61]. Three-body halo systems present a large variety of interesting features [62–64]. Their bound-state spectroscopy is now relatively well known. On the experimental side, current intensities of radioactive beams are high enough for precise measurements of spectroscopic properties, such as energies, r.m.s. radii or quadrupole moments. On the theoretical side, several methods have been developed, and provide accurate solutions of the three-

body Schrödinger equation. The hyperspherical harmonic method (HHM) is known to be well adapted to three-body systems [65, 66]. It has been applied to many exotic nuclei. In Ref. [67], the HHM has been combined with the Lagrange-mesh technique. The information provided by continuum states is a natural complement to the bound-state spectroscopy. Experimentally, three-body continuum states are investigated through breakup experiments (see for example Ref. [68]). On the theoretical point of view, various methods have been developed [69–85]. Some of them, such as the Complex Scaling Method [86], or the Analytic Continuation in the Coupling Constant [87] deal with resonances only, they cannot be applied to non-resonant states. Other methods, such as the R-matrix theory [88] are more difficult to apply, but can be used for non-resonant, as well as for resonant states. Applications of the R-matrix method to two-body systems have been performed for many years in nuclear as well as in atomic physics. In nuclear physics, applications to three-body systems are more recent [89], however, it raises problems owing to the long range of the coupling potentials. This can be solved by using propagation techniques [90]. In chapter 3 we will extend the R-matrix method in the frame of HHM on a Lagrange mesh to the three-body continuum study [91]. We show applications to the α+n+n and ^{12}Be+n+n halo systems, for which two-body potentials are available in the literature.

Among their remarkable properties, nuclei with a neutron halo display unusual β decay channels. There is indeed the possibility that the decay occurs in the halo, releasing the halo nucleons. This process has been observed in the β delayed deuteron decay of ^{6}He and ^{11}Li [92–98]. The β decay with emission of a deuteron, also known as β delayed deuteron decay, is energetically possible for nuclei with a two-neutron separation energy S_{2n}, limited by the energy conservation condition

$$S_{2n} < B(^2\mathrm{H}) + (m_n - m_p - m_e)c^2 \approx 3.007 \text{ MeV} \tag{1.1}$$

where $B(^2\mathrm{H})$ is the binding energy of the deuteron, and m_n, m_p, and m_e are the neutron, proton, and electron masses, respectively. Only a few nuclei have low enough separation energies to allow this decay: ^{6}He, ^{8}He, ^{11}Li, ^{14}Be, ^{17}B, ^{27}F. The measured spectrum shapes of these decay processes offer a unique opportunity of probing the halo properties and the examination of potential models, models with a repulsive core and alternative models with forbidden states in the lowest partial waves. The β decay of the ^{6}He halo nucleus into α and a deuteron,

$$^6\mathrm{He} \rightarrow \ ^4\mathrm{He} + d + e^- + \tilde{\nu}_e \tag{1.2}$$

has been observed in several experiments [92–94] in spite of the fact that the branching ratio was smaller than expected from simple R-matrix [92], two-body [99], and three-body [100] models. Various values of the branching ratio have been obtained, i.e., $(2.8 \pm 0.5) \times 10^{-6}$ [92], $(7.6 \pm 0.6) \times 10^{-6}$ [93], and $(1.9 \pm 0.8) \times 10^{-6}$ [94], for a deuteron cutoff energy of about 350 keV. A semi-microscopic model study [101] of the process has been able to explain that the low value of the branching ratio is the result of a cancellation between the "internal" and "external" parts of the Gamow-Teller matrix element. The overlaps of the ^{6}He ground state and $\alpha + d$ scattering wave functions in the internal ($R < 5$ fm) and external ($R > 5$ fm) regions have very close magnitudes but opposite signs. It is clear that the external part of the Gamow-Teller matrix element reflects the properties of the halo structure of the ^{6}He nucleus. An improved microscopic wave function of ^{6}He confirmed this interpretation [102]. It was also confirmed by a fit in the R-matrix framework [103] which yields a satisfactory description of the deuteron spectrum shape and branching ratio of Ref. [93]. A fully microscopic description of the β decay of the ^{6}He nucleus to the ^{6}Li ground state and to the $\alpha + d$ continuum [104] was performed in a dynamical microscopic cluster model with consistent fully antisymmetrized wave functions for the initial bound state and the final scattering state. This

model provided a reasonable agreement with the data of Ref. [93]. Without any fitted parameter, those data were underestimated by about a factor of 2. Hence, the same microscopic results now *overestimate* the recent data of Ref. [94] by a similar factor. Since new data [94] with much better statistics are now available which provide an even lower branching ratio, it is timely to reexamine the interpretation of the β delayed deuteron decay. Since improving the microscopic model of Ref. [104] is not easy, we prefer to base our discussion on an $\alpha + N + N$ three-body model. Very accurate wave functions of ^{6}He are available in hyperspherical coordinates [67]. A previous calculation based on the same model [100] contains several limitations which led to a significant overestimation of the data of Ref. [93]: the calculations were restricted to very small values of the hypermomentum, $K = 0$ and 2 and the halo description may not have been sufficiently extended. In chapter 4 we will study the β decay of the ^{6}He halo nucleus into $\alpha + d$ continuum channel within the HHM on a Lagrange mesh and examine different $\alpha + d$ potential models, with a forbidden state in S-wave, and alternatively, with a strong repulsive core [105, 106].

Electromagnetic transition processes provide a useful tool for the study of the nuclear structure and the reaction mechanisms. The theoretical study of such processes yields estimates for the different static and dynamical observables of a nucleus. In ^{6}Li, the $(0^+; T = 1)$ state has raised interest as a good candidate for observing parity violation [107, 108]. Indeed, its decay into the $\alpha + d$ continuum is forbidden by parity conservation. Since electromagnetic M1 transitions into this continuum are allowed, they have been also studied because they may compete with the parity-violating decay and make its detection difficult. However, the $^6\mathrm{Li}(0^+; T = 1)$ state is also interesting by itself. It is most likely a halo state, as it is the isobaric analog of the ^{6}He ground state [109]. The M1 transition process to the continuum

$$^6\mathrm{Li}(0^+) \rightarrow \ ^4\mathrm{He} + d + \gamma \tag{1.3}$$

is in fact also an excellent tool to explore these halo properties [110] and compare them with those of ^{6}He [105]. As was discussed above, in the beta-decay of ^{6}He halo nucleus the deuteron spectrum is strongly sensitive to the halo structure. Similarities between this process and the γ-delayed deuteron emission of ^{6}Li(0^+) are expected, and should test charge symmetry in exotic light nuclei. The branching ratio of the total transition probability to the $\alpha + d$ continuum and the transition probability to the ^{6}Li(1^+) ground state was estimated as 8×10^{-5} under a number of simplifying assumptions [108]. However the shape and magnitude of the transition probability to the continuum as a function of the deuteron energy were not studied. In addition, the sensitivity with respect to the $\alpha + d$ potential, as well as convergence problems, were not addressed. In chapter 5 we will study the M1 transition processes from the ^{6}Li(0^+) excited state to the $\alpha + d$ continuum, as well as to the ^{6}Li(1^+) ground state in the two-body and three-body models.

The most interesting halo nucleus is probably ^{11}Li [63]. Its two-neutron separation energy is particularly small: 300 ± 19 keV according to the atomic mass evaluation [111] or 376 ± 5 keV according to recent results [112–115]. This nucleus can be considered as a ^{9}Li core surrounded by two halo nucleons distant from each other by more than 6 fm [116] in agreement with theoretical expectations [117]. It differs from ^{6}He by the fact that its core does not correspond to a closed shell. The halo structure is understood as due to a virtual state in the s wave of the $^9\mathrm{Li} + n$ interaction [118]. Another difference with ^{6}He is that the core is unstable. Therefore many more β decay channels are open. This complicates experiments but also offers many opportunities to test models [96,97,119]. Among the possible channels, the delayed deuteron β decay

$$^{11}\mathrm{Li} \rightarrow \ ^9\mathrm{Li} + d + e^- + \tilde{\nu}_e. \tag{1.4}$$

remains especially interesting because this decay essentially occurs inside the halo and can probe its properties. In experiments however, the deuteron decays

can not easily be separated from the delayed triton channel [120]. Anyway the β delayed deuteron decay has been observed [96, 97] with a branching ratio of $(1.5\pm0.2)\times10^{-4}$ [97]. This order of magnitude is consistent with predictions of a simple model [121] and of a model based on a limited hyperspherical-harmonics expansion [122]. In chapter 6 we reexamine this process at the light of the knowledge gained on the ^{6}He decay in chapter 4. Experiments have revealed the important role played by a resonance around 18 MeV in the excitation spectrum of ^{11}Be [97]. Taking also that information into account, the transition probability per time and energy units will be calculated. The total transition probability is constrained with the branching ratio. It will be analyzed by comparison with the ^{6}He decay with emphasis on the role of the node structure of the scattering wave functions, which are different for deep potentials with forbidden states and the potentials with a repulsive core. On the basis of this analysis we try to explain new data [98] which yield an energy-dependence, by modifying our potential parameters [123, 124].

A theoretical study is also possible for the beta-decay of the ^{11}Li nucleus to the $^9Li + n + p$ channel [125]:

$$^{11}\mathrm{Li} \rightarrow\ ^{9}\mathrm{Li} + n + p + e^- + \tilde{\nu}_e \tag{1.5}$$

This process is even more severely restricted, i.e. a decay of a halo neutron releasing a free neutron and a free proton. The condition is

$$S_{2n} < (m_n - m_p - m_e)c^2 \approx 0.782 \text{ MeV}. \tag{1.6}$$

Among nuclei with known two-neutron separation energy, the unique nucleus where this decay is allowed is ^{11}Li. This process should be observable if the branching ratio is large enough. However, the small energy available for the decay indicates that the phase space is much smaller than for the deuteron emission. In chapter 7 we will develop the three-body model for the study of this process and estimate the transition probability and the branching ratio with

the help of the modified Coulomb functions for the continuum, which simulate the real continuum wave function corresponding to the nuclear plus Coulomb interaction potentials.

Some neutron-rich halo nuclei can simply emit a proton in a delayed beta-decay process [126]. This process is possible if the neutron separation energy is very small. Indeed a weakly bound halo neutron may β decay by emitting a proton.

A one-neutron halo nucleus can be viewed as a normal nucleus, the core, to which a neutron is bound in an orbital with a large radius. The β decay of the bound halo neutron may occur, releasing the proton, under the condition of energy conservation

$$S_{\rm n} < (m_n - m_p - m_e)c^2 \approx 0.782 \text{ MeV}, \tag{1.7}$$

where $S_{\rm n}$ is the neutron separation energy of the decaying nucleus. Among one-neutron halo nuclei for which S_n is known with sufficient precision, this decay is allowed at least for ^{11}Be and ^{19}C, and probably for ^{31}Ne. It should be observable if the branching ratio is large enough. In chapter 8 we will study this rare decay mode within a two-body potential model. The initial halo nucleus is treated as a core+neutron bound state. The final states lie in the core+proton continuum. How rare is this decay is the main question raised in the present exploratory study.

In view of above discussion, the aim and tasks of the Dissertation have been formulated, which were given in the Introduction on pages 10 and 11.

II. VARIATIONAL STUDY OF THE ^{12}C NUCLEUS STRUCTURE IN A 3α MODEL

[1] As was indicated in chapter 1, in this chapter we study the 3α-problem by using the l-independent (ABd$_0$) and l-dependent (ABd) versions of the Ali-Bodmer $\alpha - \alpha$ potential [43], and also BFW potential [27] in the framework of the cluster potential model [129] for light nuclei based on a high accuracy variational method on Gaussian basis (VGM) in comparison with the results of the Lagrange-mesh (LMM) and Hyperspherical harmonics (HHM) methods. The Gaussian basis variational method (VGM) has been used successfully in many structure calculations of various atomic and nuclear systems [23, 130–133]. The two alternative potential models differ from each other in describing the Pauli repulsion part of the alpha-alpha interaction. As a result, the local on-shell equivalent potential models give still different wave functions for the ^8Be ground state: while the BFW potential yields a nodal behavior, the AB potential does not describe this microscopically substantiated property. For the elimination of forbidden states we use the method of orthogonalizing pseudopotentials (OPP) which allows to work in the complete functional space. The main feature of this chapter is the description of the convergence of the orthogonalizing procedure for the ground and lowest excited states of the ^{12}C nucleus. When using the OPP method one can examine the convergence of the three-body energy as a function of the projecting constant λ [23, 134]. We check also the convergence in respect to the description of the two-body forbidden states fixed by chosen $\alpha\alpha$ potential. We show that the convergence of the orthogonalizing procedure has different character for the compact shell-model like bound states and for

[1] This chapter is based on the results of Refs. [46, 47, 127, 128]

the resonance states with a well developed cluster like structure.

2.1. Model

The Hamiltonian of the 3α system consists of the kinetic energy operator and interaction terms between the α-particles:

$$\hat{H} = \hat{H}_0 + V_{12}(\vec{r}_{12}) + V_{23}(\vec{r}_{23}) + V_{31}(\vec{r}_{31}). \tag{2.1}$$

In common case of three particles with mass numbers A_1, A_2 and A_3 (expressed in units of nucleon mass m_N) and space coordinates $\vec{r}_1$, $\vec{r}_2$ and $\vec{r}_3$, the Jacobi coordinates $(\vec{x}_k, \vec{y}_k)$ in the k-set are defined as:

$$\begin{aligned} \vec{x}_k &= \sqrt{\mu_{ij}}(\vec{r}_j - \vec{r}_i) \\ \vec{y}_k &= \sqrt{\mu_{(ij)k}}\left(\vec{r}_k - \frac{A_i\vec{r}_i + A_j\vec{r}_j}{A_i + A_j}\right), \end{aligned} \tag{2.2}$$

where (i,j,k) is even permutation of (1,2,3) and the dimensionless reduced masses are defined as

$$\begin{aligned} \mu_{ij} &= A_iA_j/(A_i + A_j) \\ \mu_{(ij)k} &= (A_i + A_j)A_k/(A_i + A_j + A_k). \end{aligned} \tag{2.3}$$

In these coordinates the kinetic energy operator of the relative motion of three particles is expressed simply [22, 130]:

$$\hat{H}_0 = -\frac{\hbar^2}{2m_N}\left[\left(\frac{\partial}{\partial\vec{x}_k}\right)^2 + \left(\frac{\partial}{\partial\vec{y}_k}\right)^2\right]. \tag{2.4}$$

A probe wave function of the 3α- system is expanded over symmetrized Gaussian basis [130]:

$$\Psi_s^{JM} = \sum_{\gamma j} c_j^{(\lambda,l)} \varphi_{\gamma j}^s, \tag{2.5}$$

with

$$\varphi_{\gamma j}^s = \varphi_{\gamma j}(1;2,3) + \varphi_{\gamma j}(2;3,1) + \varphi_{\gamma j}(3;1,2),$$

$$\varphi_{\gamma j}(k;l,m) = N_j x_k^\lambda y_k^l exp(-\alpha_{\lambda j} x_k^2 - \beta_{lj} y_k^2) \mathcal{F}_{\lambda l}^{JM}(\widehat{\vec{x}}_k, \widehat{\vec{y}}_k), \tag{2.6}$$

where the orbital momenta λ and l are conjugate to the Jacobi coordinates $\vec{x}_k$ and $\vec{y}_k$, respectively, and

$\gamma = (\lambda, l, J, M) = (\gamma_0, J, M)$,

while N_j is a normalization factor.

The nonlinear variational parameters $\alpha_{\lambda j}, \beta_{lj}$ are chosen as nodes of the Chebyshev grid:

$$\alpha_{\lambda j} = \alpha_0 tan(\frac{2j-1}{2N_\lambda}\frac{\pi}{2}), j = 1, 2, ...N_\lambda,$$

$$\beta_{lj} = \beta_0 tan(\frac{2j-1}{2N_l}\frac{\pi}{2}), j = 1, 2, ...N_l, \tag{2.7}$$

where α_0 and β_0 are scale parameters for each (λl) partial component of the three-body wave function. When we use the Chebyshev grid, the basis frequencies $\alpha_{\lambda j}, \beta_{lj}$ cover larger and larger intervals around the scale parameters as the numbers N_λ and N_l increase. This allows us to take into account both short-range and long-range correlations of particles. The extraordinary flexibility of the many-particle Gaussian basis makes it possible to describe three-body configurations that are formed in the ground and excited states of multicluster systems, and which exhibit an extremely high degree of clustering [130].

The angular part of the Gaussian basis is factorized into the angular component and the internal wave functions $\phi(i)$ of the α-particles [130]:

$$\mathcal{F}_{\lambda l}^{JM}(\widehat{\vec{x}}_k, \widehat{\vec{y}}_k) = \{Y_\lambda(\widehat{\vec{x}}_k) \bigotimes Y_l(\widehat{\vec{y}}_k)\}_{JM} \phi(1)\phi(2)\phi(3). \tag{2.8}$$

By using the above expansion the energy functional is minimized according to the variational principle. The method was firstly suggested in the Ref. [135] and successfully employed for the study of the structure of light nuclei with $A = 6$ and $A = 3$ [23, 130, 131, 134]. A high accuracy of the method has been demonstrated in a number of works [23, 130–133]. A general formalism of the method and analytical expressions of the matrix elements of the overlapping integral, the kinetic energy operator, central, spin-orbital and tensor interaction potentials for the system of three identical fermions with a spin value 1/2 have been given in Ref. [130]. A corresponding part of these matrix elements can be used for the 3α-system.

In the case when we use a deep $\alpha\alpha$- potential, the method of OPP is employed for the elimination of forbidden states from the solution of the three-body Schrödinger equation. In this method one has to replace the interaction potential $V_{jk}(r) = V_i(r)$ by the pseudopotential of the form [46]

$$\widetilde{V}_i(r) = V_i(r) + \sum_f \lambda_f \hat{\Gamma}_i^{(f)}, \tag{2.9}$$

where λ_f is the projecting constant,

$\hat{\Gamma}_i^{(f)}$ is the projecting operator to the f-wave forbidden state in the two-body subsystem $(j + k)$, $(i, j, k) = (1, 2, 3)$, and their cyclic permutations.

We note that the OPP method includes only the first term in the expansion of the complete three-body projector [37]

$$\hat{P} = \sum_{i=1}^{3} \hat{P}_i - \sum_{i,j=1}^{3} \hat{P}_i \hat{P}_j + \sum_{i,j,k=1}^{3} \hat{P}_i \hat{P}_j \hat{P}_k - \cdots, \tag{2.10}$$

where

$$\hat{P}_i = \sum_f \hat{\Gamma}_i^{(f)}. \tag{2.11}$$

While using the OPP approach, we neglect three-cluster (triple) Pauli forces.

Nevertheless, it allows us to obtain the solution of the Schrödinger equation at large values of λ_f which is orthogonal to the two-body forbidden states.

2.2. Numerical results

The first model of the $\alpha - \alpha$ interaction used in our work is the potential of Ali and Bodmer [43] with a Gaussian form-factor:

$$V_{AB}(r) = V_1 exp(-\eta_1 r^2) + V_2 exp(-\eta_2 r^2) + V_{coul}(r), \tag{2.12}$$

where the last term presents a Coulomb potential between two α particles. The parameters of the repulsive and attractive parts of the l-independent version of the Ali-Bodmer potential (ABd$_0$)are $V_1 = 500$ MeV, $\eta_1 = 0.49\ fm^{-2}$ and $V_2 = -130$ MeV, $\eta_2 = 0.225625\ fm^{-2}$ respectively. The Coulomb interaction potential in our calculations is taken in the form

$$V_{Coul}(r) = 4e^2 erf(br)/r, \tag{2.13}$$

where b=0.75 fm^{-1}, which corresponds to the α particle charge distribution being the Gaussian form with a width of $1/b$.

In the l-dependent version of the Ali-Bodmer potential (ABd), the parameters are as in the S-wave, except $V_1 = 320$ MeV for $l = 2$, $V_1 = 0$ for $l > 2$ and $b = \sqrt{3}/2.88$ fm^{-1} in the Coulomb potential for all l. We use $\hbar^2/m_\alpha = 10.4465$ MeV fm^2 and e^2=1.44 MeV fm in our calculations.

The second alternative deep potential model of Buck, Friedrich and Wheatley [27]

$$V_{BFW}(r) = V_0 exp(-\eta r^2) + V_{Coul}(r), \tag{2.14}$$

with V_0=-122.6225 MeV, $\eta = 0.22$ fm^{-2} . This potential describes well the experimental phase shifts of the $\alpha\alpha$-scattering $\delta_L(E)$ with $L = 0, 2, 4$ up to 40 MeV. The potential has three nonphysical bound states forbidden by the Pauli

principle in each $\alpha\alpha$-subsystem, with the energy values $E(0_1^+) = -72.625691755$ MeV , $E(0_2^+) = -25.618638588$ MeV, $E(2^+) = -22.000501732$ MeV. The 0_1^+ state corresponds to the shell configuration s^8, while the 0_2^+ and 2^+ states correspond to the s^6p^2. These forbidden states in our three-body calculations are eliminated by using the method of orthogonalising pseudo-potentials (OPP) briefly described above. This method allows us to obtain the solution of the Schrödinger equation at large values of λ_f which is orthogonal to the two-body forbidden states.

Table 2.1.

The energy spectrum of the ^{12}C nucleus calculated with the Ali-Bodmer $\alpha - \alpha$ potential in different variational approaches in MeV

(J^π, T)	LMM	ABd$_0$ (l-indep.) HHM	VGM	
$(0_1^+, 0)$	-0.58427008	-0.58407	-0.584266	with Coulomb
$(0_1^+, 0)$	-5.122093595	-5.122	-5.1220936	no Coulomb
$(0_2^+, 0)$	-1.3606	-1.2	-1.36062	
$(0_3^+, 0)$	-1.338	-0.8	-1.33873	
$(2_1^+, 0)$		-1.15	-1.3398	
		ABd (l-dep.)		
$(0_1^+, 0)$		-1.523	-1.523	with Coulomb
$(0_1^+, 0)$		-6.423	-6.423	no Coulomb
$(0_2^+, 0)$		-1.92	-1.934	

First we note that a very large symmetrized Gaussian basis is used in our calculations. For the estimation of the energy levels with $(J^\pi, T) = (0^+, 0)$ we include the three-body channels $(\lambda, l) = \{(0,0); (2,2); (4,4)\}$ and for the levels with $(J^\pi, T) = (2^+, 0)$ we take the three-body channels (λ, l) ={(0,2); (2,0); (2,2); (2,4); (4,2); (4,4)}. The results indicate that a further extension of the basis does not have a remarkable influence on the accuracy of the expansion.

The numerical results obtained with the Ali-Bodmer $\alpha - \alpha$ potential are presented in Table 2.1 in comparison with the LMM and HHM, developed by D. Baye and P. Descouvemont. The calculations with the additional Coulomb term were performed only for the ground state. We note that all three methods yield close numbers for the ground state. However, for the excited states the convergence of the HHM is poor, while other two methods give very close and accurate numbers. In addition, the estimations for the ground state are far from the experimental energy value $E = -7.275$ MeV [42] due to strong off-shell effect of the repulsive core presented in the Ali-Bodmer potential.

In the calculations within the VGM the number of Gaussians is 680 and 1264 for the 0^+ and 2^+ levels, respectively. We note, however, that a good saturation was already obtained with 372 Gaussians for the 0^+ levels (-5.12205, -1.35234 and -0.87654 MeV) and with 875 Gaussians for the 2+ levels (-1.2369 MeV). Even 280 Gaussians yield a good accuracy for the ground state energy value, although the 0_3^+ excited state is estimated roughly (-5.1215, -1.341 and -0.5564 MeV).

In the case of the BFW deep $\alpha\alpha$- potential we use the OPP method [22, 135] for the elimination of forbidden states from the solution of the three-body Schr$\ddot{o}$dinger equation.

The explicit form of the projector on the **f**-wave forbidden state in each two-body subsystem is written as:

$$\hat{\Gamma}_i^{(f)} = \frac{1}{2f+1} \sum_{m_f} \mid \varphi_{fm_f}(\vec{x}_i) >< \varphi_{fm_f}(\vec{x'}_i) \mid \delta(\vec{y}_i - \vec{y'}_i), \tag{2.15}$$

where the forbidden state wave function is expanded over Gaussian basis:

$$\varphi_{fm_f}(\vec{x}_i) = x_i^f \sum_m N_m^{(f)} b_m^{(f)} exp(-\frac{r_i^2}{2r_{0m}^{(f)2}}) Y_{fm_f}(\hat{\vec{x}}_i). \tag{2.16}$$

Here r_0 is the "projector radius", and $N_m^{(f)}$ is the normalizing multiplier:

$$N_m^{(f)} = 2^{f+7/4} \frac{\alpha_m^{(2f+3)/4}}{\pi^{1/4}[(2\lambda+1)!!]^{1/2}}, \qquad \alpha_m = \tau^2/(2r_{0m}^2). \tag{2.17}$$

In order to check the behavior of the 3α-energy when improving the accuracy

Table 2.2.

Sets of Gaussian approximations for the forbidden states wave functions of the $\alpha\alpha$ system and corresponding energy values in MeV

N (Gaussian numbers)	$E(0_1^+)$	$E(0_2^+)$	$E(2^+)$
≤ 2	-72.5445	-25.106	-21.676
3	-72.6126	-25.5558	-21.8837
4	-72.6233	-25.6111	-21.9576
7	-72.624905	-25.6173	-21.999098
15	-72.625691755	-25.618638588	-22.000501732

of the expansion of the two-body $\alpha\alpha$ forbidden states wave functions, we choose several sets of the Gaussian approximations. The corresponding approximate values of the $\alpha\alpha$ forbidden states energies are shown in the Table 2.2. In Set 1 the $\alpha\alpha$- forbidden state wave function of the 0_1^+-level is approximated via N=1 Gaussian, and wave functions of the forbidden 0_2^+- and 2^+-states are approximated via N=2 Gaussian, etc. The values of the two-body forbidden states energies are given in corresponding squares. By comparison of these numbers with the corresponding exact values of the two-body $0_1^+, 0_2^+, 2^+$-forbidden states energies, one can conclude about the quality of the approximation for the given number N. We note that the wave function of the 0_2^+- $\alpha\alpha$ forbidden state contains a node due to orthogonality to the first 0_1^+-level, hence it can not be expressed by a single Gaussian.

The spectrum of the energy levels of the ^{12}C nucleus with $(J^\pi, T) = (0^+, 0)$

Table 2.3.

The energy spectrum of the ^{12}C nucleus with $(J^{\pi}, T) = (0^{+}, 0)$ in MeV for the several sets of Gaussian approximations of the $\alpha\alpha$ forbidden states at several values of the projecting constant

N	λ (MeV)	10	10^2	10^3	10^4	10^5	10^6	10^7	10^8
≤ 2	E_1	-210.80	-45.194	-20.665	-18.999	-14.882	-12.85	-12.56	-12.44
	E_2	-150.72	-20.037	-0.677	+0.274	1.210	1.284	1.39	1.42
	E_3	-109.37	-15.878	+1.239	1.306	+2.98	3.446	3.99	4.01
	$< P >$	29.83	30.36	0.847	1.133	1.73	0.300	6.E-2	5.E-2
3	E_1	-210.71	-43.298	-19.776	-16.492	-6.387	-3.666	-3.35	-3.311
	E_2	-150.05	-17.183	-0.411	-0.021	1.238	1.331	1.42	1.463
	E_3	-109.53	-15.652	+1.344	1.380	+2.553	3.361	4.07	4.046
	$< P >$	29.93	28.78	1.017	2.837	3.100	0.322	1.E-2	1.E-2
4	E_1	-210.72	-44.149	-20.15	-16.227	-.463	0.051	0.406	0.468
	E_2	-150.28	-17.423	-0.512	-0.417	1.357	1.424	1.522	1.571
	E_3	-109.37	-15.430	+1.336	1.355	+2.979	3.319	4.059	4.087
	$< P >$	29.92	28.76	1.120	3.647	0.397	0.242	6.4E-2	8.7E-3
7	E_1	-210.69	-44.207	-20.15	-16.106	-.830	-0.435	-0.307	-0.283
	E_2	-150.32	-17.585	-0.531	-0.422	1.353	1.407	1.513	1.551
	E_3	-109.32	-15.310	+1.334	1.353	+3.019	3.316	4.038	4.055
	$< P >$	29.95	28.92	1.130	3.777	0.721	8.76E-2	2.3E-2	4.7E-3

and $(2^{+}, 0)$ for the several variants of the Gaussian expansion of the forbidden state wave functions are shown in Tables 2.3 and 2.4. For the sake of convenience we use an identical value of the projecting constant λ_f for all forbidden states. In all three tables the symbol "$< P >$" denotes the total admixture of the forbidden states to the energy of the 3α-system:

$$< P >=< \Psi_s \mid \lambda(\hat{P}_1 + \hat{P}_2 + \hat{P}_3) \mid \Psi_s > . \tag{2.18}$$

From Tables 2.3 and 2.4 one can see a reasonable saturation of the energy levels of the ^{12}C nucleus when increasing the projecting constant λ to the infinity

for a given set of approximation of the two-body forbidden states. However, beginning from the value of the projecting constant $\lambda \geq 10^3$ MeV the ground and first excited 2_1^+ states energies of the ^{12}C nucleus begin to display a high sensitivity to the description of the two-body forbidden states. Moreover the energy decreases sharply when increasing the value of the projecting constant from 10^4 to 10^5. The unexpected results when increasing the parameter λ is that the second 0_2^+ state with the energy -0.422 MeV at $\lambda = 10^4$ MeV becomes the lowest state. In other words, the ground state is lost. The same situation can be observed in the 2^+-sector. This unusual behavior of the energies was found in our work more than ten years ago [46]. To examine this unusual behavior

Table 2.4.

The energy spectrum of the $(J^\pi, T) = (2^+, 0)$ levels of the ^{12}C nucleus in MeV for the several sets of Gaussian approximations of the $\alpha\alpha$ forbidden states at several values of the projecting constant

N	λ (MeV)	10^3	10^4	10^5	10^6	10^7	10^8
≤ 2	E_1	-17.19	-16.15	-14.55	-12.103	-11.176	-11.04
	E_2	0.944	0.95	0.952	0.965	1.022	1.079
	$< P >$	0.923	0.95	1.024	0.807	0.136	2.E-2
3	E_1	-17.213	-15.665	-11.142	-5.953	-3.950	-3.80
	E_2	1.029	1.032	1.034	1.047	1.141	1.19
	$< P >$	1.024	0.918	2.842	1.495	5.E-2	8.5E-3
4	E_1	-17.433	-15.725	-8.578	1.042	1.082	1.157
	E_2	1.029	1.032	1.034	1.694	2.656	3.038
	$< P >$	1.075	1.095	5.85	9.1E-3	2.9E-2	2.8E-2
7	E_1	-17.361	-15.649	-8.243	1.042	1.086	1.162
	E_2	1.030	1.032	1.034	1.475	2.524	2.643
	$< P >$	1.062	1.127	5.974	1.2E-2	3.1E-2	2.7E-2

of the three α energy, we look on the values of the admixture of the forbidden states in the last row of Table 2.3. We can see that this variable decreases

from 30 MeV for the $\lambda = 10$ MeV up to 1.130 MeV for $\lambda = 1000$ MeV, that is normal. However, after this value the variable $< P >$ begins to increase, which means that admixture of forbidden states is going up. We found minimum of $< P >$=1.032 MeV at λ =1450 MeV. This point is the beginning of the high sensitivity of the 3 α energy to the description of the Pauli forbidden states. For this value $E(0_1^+) = -19.763$ MeV and $E(2_1^+) = -16.931$ MeV.

As was found by Fujiwara and soauthors [136], the high sensitivity of the 3α energy on the two-body Pauli forbidden states results in the so-called three-body "almost forbidden state".

It can be shown explicitly [128], that the complete three-body projector Eq. (2.10) and the sum of the two-body projectors $\hat{\Gamma} = \hat{P}_1 + \hat{P}_2 + \hat{P}_3$ have identical kerns (eigenstates with the zero eigenvalue), which define the 3-body allowed subspace of the full Hilbert space. This means that one can expand a probe wave function for the 3α Schrödinger equation over the eigenfunctions of the operator $\hat{\Gamma}$ with the zero eigenvalue. In this way one can develop an alternative direct method for the orthogonalization in the three-body problem. Fujiwara et al have used a different way to come to the same method: as the two body projectors $\hat{P}_i$, i=1, 2, 3 are positive operators, then the system of equations $\hat{P}_i = 0$, i=1, 2, 3, is equivalent to the relation $\hat{\Gamma} = \hat{P}_1 + \hat{P}_2 + \hat{P}_3 = 0$.

When applying the direct orthogonalization method, Fujiwara et al. for the first time found a three-body "almost forbidden state". We have applied this method and found such a state with an energy $E_0 = 1.1847E - 4$ MeV. If we describe it and other eigenstates of the operator Γ with eigenvalues $E > E_0$ as forbidden states (if we remove these states from the allowed subspace), then we come to the weak binding E=-0.645 MeV for the 3α -ground state. But if we describe this "almost forbidden state" as belonging to the allowed functional space, then we have the 3α-energy value at about E=-20 MeV which was obtained above in our method at the extremum point of $\lambda = 1450$ MeV and which is close to the results of the microscopic calculations.

In Table 2.5 we give the final results for the energy spectrum of the Borromean ^{12}C nucleus in the macroscopic 3α model. The results with the BFW potential correspond to the allowed "almost forbidden state" and are close to the results of the semi-microscopic and microscopic studies [137]. The results for the ground and first excited 2_1^+ states are far from the experimental data, which means that the local potential models are not able to describe well these compact states. But, the astrophysical significant 0_2^+ state is reproduced quite well.

As noted above, the existence of the "almost forbidden state" is the result of the high sensitivity of the compact ground 0_1^+ and first excited 2_1^+ states energies of the 3α system on the two-body forbidden states. The authors of Ref. [136] suggested to use microscopically defined two-body $\alpha - \alpha$ forbidden states instead of forbidden states fixed from the deep $\alpha - \alpha$-potential. This way, as stated by the authors of this reference, strongly separates the three-body functional space into two orthogonal subspaces, an allowed and forbidden states. And this way does not result any "almost forbidden state".

We suggest another possible solution of the 3α problem, to fit parameters of the deep potential to the $\alpha\alpha$-forbidden states fixed from the microscopic calculations. Then one can check a description of the phase shifts in S- and D-waves.

Table 2.5.

The energy spectrum of the ^{12}C nucleus calculated in the VGM with the Ali-Bodmer and BFW $\alpha - \alpha$ potentials in MeV

(J^π, T)	ABd_0	ABd	BFW	Exp [42]
$(0_1^+, 0)$	-0.584266	-1.523	-19.763	-7.275
$(0_2^+, 0)$			-0.50189	0.3796
$(2_1^+, 0)$			-16.931	-2.836

2.3. Conclusion

The energy spectrum of the ^{12}C nucleus with $(J^\pi, T) = (0^+, 0)$ and $(J^\pi, T) = (2^+, 0)$ was studied in the framework of the cluster potential model using different $\alpha\alpha$-potentials: the Ali-Bodmer potential with a strong repulsive core and a deep potential of Buck, Friedrich and Wheatley with forbidden states in the S and D waves. For the elimination of forbidden states the method of orthogonalising pseudo-potentials (OPP) has been used.

The numerical results indicate that a local Ali-Bodmer $\alpha\alpha$ -potential with a repulsive core yields a very weak binding for the 3α-system.

It was shown that the energies of the $(0_1^+, 0)$ and $(2_1^+, 0)$ states of the ^{12}C nucleus with a compact shell-model like structure display a very high sensitivity to the description of the two-body forbidden states. This strong sensitivity of the energy values directly results in an "almost forbidden state" in the 3α functional space. Whether this "almost forbidden state" allowed or forbidden, the 3α-system has a strong or weak binding. This very interesting phenomena shows an importance of the microscopical description of the Pauli principle when studying a structure of the 3α-system.

The results with allowed "almost forbidden states" are close to the results of the semi-microscopic and microscopic studies.

III. THREE-BODY CONTINUUM STATES ON A LAGRANGE-MESH

As was noted in chapter I , the hyperspherical harmonic method (HHM) is well adapted to three-body systems [65, 66]. [1] The six Jacobi coordinates are replaced by five angles, and a single dimensional coordinate, the hyperradius. The HHM transforms the three-body Schrödinger equation into a set of coupled differential equations depending on the hyperradius. In previous chapter we have compared the three methods (HHM, VGM and Lagrange mesh) in the 3 α bound state problem. The HHM has been also applied to many exotic nuclei. In the Ref. [91] we extended the formalism of Ref. [67] to three-body continuum states. The R-matrix theory allows the use of a variational basis to describe unbound states. It is based on an internal region, where the wave function is expanded over the basis, and on an external region, where the asymptotic behavior can be used.

In two-body systems, the Lagrange-mesh technique associated with the R-matrix formalism has been applied in single- [138] and multi-channel [139, 140] calculations. Our goal is to extend the method to three-body systems within the HHM by using the propagation techniques [90]. Another development concerns the application to charged systems. Many exotic nuclei are unbound, even in their ground states, due to the Coulomb force. We show applications to the α+n+n and ^{12}Be+n+n systems, for which two-body potentials are available in the literature. The mirror systems are also investigated.

We first summarize the three-body formalism, and present the R-matrix method. Then the method is applied to ^{6}He and ^{14}Be, with the mirror systems.

[1] This chapter is based on the results of Ref. [91]

3.1. Three-body continuum states

3.1.1. Hamiltonian and wave functions

Let us consider three particles with mass numbers A_i (in units of the nucleon mass m_N), and space coordinates $\boldsymbol{r}_i$. A three-body Hamiltonian is given by

$$H = \sum_{i=1}^{3} T_i \; + \; \sum_{i>j=1}^{3} V_{ij}(\boldsymbol{r}_j - \boldsymbol{r}_i), \tag{3.1}$$

where T_i is the kinetic energy of nucleon i, and

V_{ij} is a nucleus-nucleus potential. We neglect three-body forces in this presentation.

The HHM is known to be an efficient tool to deal with three-body systems. This formalism is well known, and we refer to Refs. [63, 66] for detail. Starting from coordinates $\boldsymbol{r}_i$, we define the Jacobi coordinates $\boldsymbol{x}_k$ and $\boldsymbol{y}_k$ ($k = 1, 2, 3$) as was done in chapter 2 (see Eq. (2.2) and Ref. [67]). The hyperradius ρ and hyperangle α_k are then defined as

$$\begin{aligned} \rho^2 &= x_k^2 + y_k^2, \\ \alpha_k &= \arctan \frac{y_k}{x_k}. \end{aligned} \tag{3.2}$$

The hyperangle α_k and the orientations Ω_{x_k} and Ω_{y_k} provide a set of angles Ω_{5k}. In this notation the kinetic energy reads [67, 91]

$$T_\rho = \sum_{i=1}^{3} T_i - T_{cm} = -\frac{\hbar^2}{2m_N}\left(\frac{\partial^2}{\partial\rho^2} + \frac{5}{\rho}\frac{\partial}{\partial\rho} - \frac{K^2(\Omega_{5k})}{\rho^2}\right), \tag{3.3}$$

where T_{cm} is the c.m. kinetic energy, and

K^2 is a five-dimensional angular momentum whose eigenfunctions (with eigenvalues $K(K+4)$) are given by [91, 141]

$$\begin{aligned}\mathcal{Y}^{\ell_x\ell_y}_{KLM_L}(\Omega_5) &= \phi^{\ell_x\ell_y}_K(\alpha)\left[Y_{\ell_x}(\Omega_x)\otimes Y_{\ell_y}(\Omega_y)\right]^{LM_L},\\ \phi^{\ell_x\ell_y}_K(\alpha) &= \mathcal{N}^{\ell_x\ell_y}_K(\cos\alpha)^{\ell_x}(\sin\alpha)^{\ell_y}P_n^{(\ell_y+\frac{1}{2},\ell_x+\frac{1}{2})}(\cos 2\alpha),\end{aligned} \tag{3.4}$$

where

$\mathcal{N}^{\ell_x\ell_y}_K$ a normalization factor [66],

K is the hypermomentum,

(ℓ_x,ℓ_y) are the orbital momenta associated with $(\boldsymbol{x},\boldsymbol{y})$,

n is a positive integer defined by

$$n=(K-\ell_x-\ell_y)/2, \tag{3.5}$$

$P_n^{(\alpha,\beta)}(x)$ is a Jacobi polynomial. Introducing the spin component χ^{SM_S} yields the hyperspherical function with total spin J

$$\mathcal{Y}^{JM}_{\gamma K}(\Omega_5)=\left[\mathcal{Y}^{\ell_x\ell_y}_{KL}(\Omega_5)\otimes\chi^S\right]^{JM}, \tag{3.6}$$

where index γ stands for (ℓ_x,ℓ_y,L,S).

A wave function $\Psi^{JM\pi}$, solution of the Schrödinger equation associated with Hamiltonian Eq. (3.1), is expanded over basis functions Eq. (3.6) as [91]

$$\Psi^{JM\pi}(\rho,\Omega_5)=\rho^{-5/2}\sum_{\gamma K}\chi^{J\pi}_{\gamma K}(\rho)\ \mathcal{Y}^{JM}_{\gamma K}(\Omega_5), \tag{3.7}$$

where $\pi=(-1)^K$ is the parity of the three-body relative motion,

$\chi^{J\pi}_{\gamma K}(\rho)$ are hyperradial wave functions which should be determined. Rigorously,

the summation over (γK) should contain an infinite number of terms. In practice, this expansion is limited by a maximum K value, denoted as K_{max}. For weakly bound states, it is well known that the convergence is rather slow, and that large K_{max} values must be used. Typically $100 - 200$ terms are necessary for realistic K_{max} values.

The radial functions $\chi^{J\pi}_{\gamma K}(\rho)$ are derived from a set of coupled differential equations [91]

$$\left[-\frac{\hbar^2}{2m_N}\left(\frac{d^2}{d\rho^2} - \frac{\mathcal{L}_K(\mathcal{L}_K+1)}{\rho^2}\right) - E\right]\chi^{J\pi}_{\gamma K}(\rho) + \sum_{K'\gamma'} V^{J\pi}_{K\gamma,K'\gamma'}(\rho)\,\chi^{J\pi}_{\gamma' K'}(\rho) = 0, \tag{3.8}$$

with $\mathcal{L}_K = K + 3/2$. The potential terms are given by the contribution of the three nucleus-nucleus interactions

$$V^{J\pi}_{K\gamma,K'\gamma'}(\rho) = \sum_{i=1}^{3}(V^{J\pi(Ni)}_{K\gamma,K'\gamma'}(\rho) + V^{J\pi(Ci)}_{K\gamma,K'\gamma'}(\rho)), \tag{3.9}$$

where we have explicitly written the nuclear (N) and Coulomb (C) terms.

Assuming the use of $(\boldsymbol{x}_1, \boldsymbol{y}_1)$ for the coordinate set, the contribution $i = 1$ is directly determined from

$$V^{J\pi(1)}_{K\gamma,K'\gamma'}(\rho) = \int \mathcal{Y}^{JM*}_{\gamma K}(\Omega_5)\, V_{23}\left(\frac{\rho\cos\alpha}{\sqrt{\mu_{23}}}\right)\mathcal{Y}^{JM}_{\gamma' K'}(\Omega_5)d\Omega_5, \tag{3.10}$$

where $\mu_{ij} = A_iA_j/(A_i + A_j)$. The terms $i = 2, 3$ are computed in the same way, with an additional transformation using the Raynal-Revai coefficients [141]. Definition Eq. (3.10) is common to the nuclear and Coulomb contributions. Integrations over Ω_x and Ω_y are performed analytically, whereas integration over the hyperangle α is treated numerically. For the Coulomb potential, the ρ dependence is trivial; we have

$$\sum_{i=1}^{3} V^{J\pi(Ci)}_{K\gamma,K'\gamma'}(\rho) = z^{J\pi}_{K\gamma,K'\gamma'}\frac{e^2}{\rho} \tag{3.11}$$

where $z^{J\pi}_{\gamma K,\gamma',K'}$ is an effective charge, independent of ρ, and calculated numerically from Eq. (3.10) and from Raynal-Revai coefficients [142, 143]. Examples of matrices $z^{J\pi}$ are given in Ref. [142] for the α+p+p system. Knowing the analytical ρ-dependence of the potential is crucial for continuum states (see below). Notice that, to derive Eq. (3.11), one assumes the $1/|\boldsymbol{r}_j - \boldsymbol{r}_i|$ dependence of the Coulomb potential. Using a point-sphere definition is straightforward, as the difference can be included in the nuclear part.

3.1.2. Asymptotic behaviour of the potential

For small ρ values the potential must be determined by numerical integration of Eq. (3.10). However, analytical approximations can be derived for large ρ values. For the Coulomb interaction, definition Eq. (3.11) is always valid. Let us now consider the nuclear contribution. After integration over Ω_x and Ω_y, a matrix element between basis states Eq. (3.4) is written as [91]

$$\begin{aligned}
V^{\ell_x\ell_y,\ell'_x\ell'_y}_{KL,K'L'}(\rho) &= \delta_{LL'}\delta_{\ell_y\ell'_y}\int_0^{\pi/2}\phi^{\ell_x\ell_y}_K(\alpha)V_N\left(\frac{\rho\cos\alpha}{\sqrt{\mu_{23}}}\right)\phi^{\ell'_x\ell_y}_{K'}(\alpha)\sin^2\alpha\cos^2\alpha d\alpha \\
&= \mathcal{N}^{\ell_x\ell_y}_K\mathcal{N}^{\ell'_x\ell_y}_{K'}\delta_{LL'}\delta_{\ell_y\ell'_y}\frac{1}{\rho^3}\int_0^{\rho}P_n^{(\ell_y+\frac{1}{2},\ell_x+\frac{1}{2})}\left(2\frac{u^2}{\rho^2}-1\right)V_N\left(\frac{u}{\sqrt{\mu_{23}}}\right) \\
&\times\ P_{n'}^{(\ell_y+\frac{1}{2},\ell'_x+\frac{1}{2})}\left(2\frac{u^2}{\rho^2}-1\right)\left(1-\frac{u^2}{\rho^2}\right)^{\ell_y+\frac{1}{2}}\left(\frac{u}{\rho}\right)^{\ell_x+\ell'_x}u^2du. \qquad (3.12)
\end{aligned}$$

To deal with the spin, the coupling order in Eq. (3.6) is modified in order

to introduce the total spin of the interacting particles $\boldsymbol{j_x} = \boldsymbol{\ell_x} + \boldsymbol{S}$. This is achieved with standard angular-momentum algebra, involving $6j$ coefficients. If the tensor force is not included, we also have $\ell_x = \ell'_x$. For large ρ values, and if the potential goes to zero faster than $1/u^2$, we can use the following expansions [91, 144]

$$
\begin{aligned}
P_n^{(\alpha,\beta)}(2x-1) &= \sum_{m=0}^{n} c_m^{(\alpha,\beta)} x^m, \\
c_m^{(\alpha,\beta)} &= \frac{(-1)^{n+m}}{m!(n-m)!} \frac{\Gamma(\beta+n+1)\Gamma(\alpha+\beta+n+m+1)}{\Gamma(\beta+m+1)\Gamma(\alpha+\beta+n+1)}, \\
(1-x)^\alpha &= \sum_{m=0}^{\infty} \begin{pmatrix} \alpha \\ m \end{pmatrix} (-x)^m,
\end{aligned} \tag{3.13}
$$

and we end up with the asymptotic expansion of the potential

$$
V_{KL,K'L'}^{\ell_x\ell_y,\ell'_x\ell'_y}(\rho) \approx \delta_{LL'}\delta_{\ell_y\ell'_y} \frac{1}{\rho^{\ell_x+\ell'_x+3}} \sum_{k=0}^{\infty} \frac{v_k}{\rho^{2k}}, \tag{3.14}
$$

where

$$
\begin{aligned}
v_k &= \mathcal{N}_K^{\ell_x\ell_y} \mathcal{N}_{K'}^{\ell'_x\ell_y} \int_0^\infty u^{\ell_x+\ell'_x+2k+2} V\left(\frac{u}{\sqrt{\mu_{23}}}\right) du \\
&\times \sum_{m_1,m_2} (-1)^{k-m_1-m_2} \begin{pmatrix} \ell_y + \frac{1}{2} \\ k - m_1 - m_2 \end{pmatrix} c_{m_1}^{(\ell_y+\frac{1}{2},\ell_x+\frac{1}{2})} c_{m_2}^{(\ell_y+\frac{1}{2},\ell'_x+\frac{1}{2})}.
\end{aligned} \tag{3.15}
$$

Owing to the finite range of the potential, the upper limit in the integrals Eq. (3.12) has been replaced by infinity. Up to a normalization factor, the contribution of each k value is a moment of the potential. As it is well known [89], the leading term is v_0/ρ^3 for $\ell_x = \ell'_x = 0$. Expansion Eq. (3.14) is carried out for the three nucleus-nucleus potentials with additional Raynal-Revai transformations for the second and third terms. Analytic expansions of potentials

Eq. (3.10) are finally obtained with [91]

$$\sum_{i=1}^{3} V^{J\pi(Ni)}_{K\gamma,K'\gamma'}(\rho) \approx \frac{1}{\rho^{l_x+l'_x+3}} \sum_{k=0}^{\infty} \frac{\tilde{v}_k}{\rho^{2k}}, \tag{3.16}$$

where coefficients $\tilde{v_k}$ are obtained from v_k after Raynal-Revai and spin coupling transformations.

Let us evaluate coefficients $\tilde{v_k}$ for ^{6}He=α+n+n, with the $\alpha - n$ potential taken from Kanada *et al.* [145]. Coefficients $\tilde{v_0}$ to $\tilde{v_4}$ are given in Table 3.1 for $J = 0^+$. We also provide the amplitude of the centrifugal term

$$v_{cent} = \frac{\hbar^2}{2m_N}(K + 3/2)(K + 5/2), \tag{3.17}$$

which depends on ρ as $1/\rho^2$. It is clear from Table 3.1 that coefficients $\tilde{v_k}$ are large and increasing with k. Integrals in Eq. (3.15) must be computed with a high accuracy. Special attention must be paid to partial waves involving two-body forbidden states. In this case, we use a supersymmetry transform of the potential [24], in order to remove forbidden states in the three-body problem. This transformation is carried out numerically, and the resulting potential presents a singularity at short distances.

From Table 3.1, we evaluate the ρ value where the nuclear part is negligible with respect to the centrifugal term. In other words, ρ_{max} is defined as

$$\frac{|\tilde{v_0}|}{\rho^3_{max}} = \epsilon \times \frac{v_{cent}}{\rho^2_{max}}. \tag{3.18}$$

Values of ρ_{max} are given in Table 3.1 by assuming $\epsilon = 0.01$. In general they are larger for low K values for two reasons: (i) the centrifugal term is of course lower, and (ii) low partial waves generally involve forbidden states which lead to singularities in the potential, and hence to larger values of $\tilde{v_0}$.

From the ρ_{max} values displayed in Table 3.1, it is clear that the channel radius a of the R matrix must be very large. Using basis functions valid up to

Table 3.1.

Coefficients $\tilde{v_0}$ to $\tilde{v_4}$ in ^{6}He for $J = 0^+, L = S = 0$, and for typical partial waves (energies are expressed in MeV and lengths in fm). The bracketed values represent the power of 10, and $\gamma = \ell_x, \ell_y$.

K, γ	K', γ'	$\tilde{v_0}$	$\tilde{v_1}$	$\tilde{v_2}$	$\tilde{v_3}$	$\tilde{v_4}$	v_{cent}	ρ_{max}
0,0,0	0,0,0	3.40(3)	-7.46(3)	-2.02(4)	-1.53(5)	-1.78(6)	78	4370
4,0,0	4,0,0	1.18(3)	-1.20(5)	7.31(6)	-2.13(8)	2.87(9)	741	160
8,0,0	8,0,0	-2.59(3)	-1.19(5)	5.46(7)	-6.66(9)	4.98(11)	2068	125
4,2,2	4,2,2	2.61(4)	-1.27(6)	5.40(7)	-1.39(9)	1.81(10)	741	3520
8,2,2	8,2,2	5.49(4)	-7.82(6)	1.06(9)	-1.02(11)	6.78(12)	2068	2660
0,0,0	4,0,0	-3.41(3)	8.04(4)	-1.09(6)	4.27(6)	1.43(7)		
0,0,0	8,0,0	1.19(3)	-1.08(5)	6.21(6)	-1.75(8)	2.33(9)		
0,0,0	4,2,2	9.62(3)	-2.41(5)	3.47(6)	-1.37(7)	-4.61(7)		
0,0,0	8,2,2	1.40(4)	-9.90(5)	4.80(7)	-1.30(9)	1.71(10)		

these distances would require tremendous basis sizes. This is solved by using a propagation technique which is presented in next section.

In the analytical expansion of the potential, the maximum value k_{max} is determined from the requirement

$$\frac{\tilde{v}_{k_{max}+1}}{a^{2k_{max}+2}} \ll \frac{\tilde{v}_{k_{max}}}{a^{2k_{max}}}. \tag{3.19}$$

This yields typical values $k_{max} \approx 3-4$, depending on the system and on the partial wave.

3.1.3. Three-body R-matrix

Principle of the R matrix

The R-matrix theory is well known for many years [88]. It allows matching a variational function over a finite interval with the correct asymptotic solutions of the Schrödinger equation. We summarize here the main ingredients of the R-matrix theory and emphasize its three-body aspects. The R-matrix method is based on the assumption that the configuration space can be divided into two regions: an internal region, with radius a, where the solution of (3.8) is given by some variational expansion, and an external region where the exact solutions of Eq. (3.8) are known. This is formulated as

$$\chi^{J\pi}_{\gamma K,int}(\rho) = \sum_{i=1}^{N} c^{J\pi}_{\gamma Ki}\, u_i(\rho), \tag{3.20}$$

where the N functions $u_i(\rho)$ represent the variational basis, and

$c^{J\pi}_{\gamma Ki}$ are the corresponding coefficients. In the external region, it is assumed that only the Coulomb and centrifugal potentials do not vanish; we have, for an entrance channel $\gamma' K'$,

$$\chi^{J\pi}_{\gamma K,ext}(\rho) = A^{J\pi}_{\gamma K}\left[H^{-}_{\gamma K}(k\rho)\delta_{\gamma\gamma'}\delta_{KK'} - U^{J\pi}_{\gamma K,\gamma' K'} H^{+}_{\gamma K}(k\rho)\right], \tag{3.21}$$

where the amplitude is chosen as

$$A^{J\pi}_{\gamma K} = i^{K+1}(2\pi/k)^{5/2}, \tag{3.22}$$

and $\boldsymbol{U}^{J\pi}$ is the collision matrix, and

$k = \sqrt{2m_N E/\hbar^2}$ is the wave number [89]. If the three particles do not interact, Eq. (3.21) is a partial wave of a 6-dimension plane wave [141]

$$\exp\left[i(\boldsymbol{k_x}.\boldsymbol{x}+\boldsymbol{k_y}.\boldsymbol{y})\right] = \frac{(2\pi)^3}{(k\rho)^2}\sum_{\ell_x\ell_y LM_L K} i^K J_{K+2}(k\rho) \times\mathcal{Y}^{\ell_x\ell_y}_{KLM_L}(\Omega_{5\rho})\,\mathcal{Y}^{\ell_x\ell_y *}_{KLM_L}(\Omega_{5k}). \tag{3.23}$$

For charged systems, we have

$$H^{\pm}_{\gamma K}(x) = G_{K+\frac{3}{2}}(\eta_{\gamma K},x) \pm iF_{K+\frac{3}{2}}(\eta_{\gamma K},x), \tag{3.24}$$

where $G_{K+3/2}$ and $F_{K+3/2}$ are the irregular and regular Coulomb functions, respectively [146]. The Sommerfeld parameters $\eta_{\gamma K}$ are given by

$$\eta_{\gamma K} = z^{J\pi}_{\gamma K,\gamma K}\frac{m_N e^2}{\hbar^2 k}, \tag{3.25}$$

where $\boldsymbol{z}^{J\pi}$ is the effective-charge matrix Eq. (3.11); η therefore depends on the channel. Notice that we neglect non-diagonal terms of the Coulomb potential. This is in general a good approximation as these terms are significantly smaller than diagonal terms [142, 143]. For neutral systems, the ingoing and outgoing functions $H^{\pm}_{\gamma K}(x)$ do not depend on γ and are defined as

$$H^{\pm}_{\gamma K}(x) = \pm i\left(\frac{\pi x}{2}\right)^{1/2}\left[J_{K+2}(x) \pm iY_{K+2}(x)\right], \tag{3.26}$$

where $J_n(x)$ and $Y_n(x)$ are Bessel functions of first, and second kind, respectively. The phase is chosen to recover the plane wave in absence of interaction ($\boldsymbol{U}$=$\boldsymbol{I}$).

For bound states ($E<0$), the external wave function is written as

$$\chi^{J\pi}_{\gamma K,ext}(\rho) = B^{J\pi}_{\gamma K}\,W_{-\eta_{\gamma K},K+2}(2\kappa\rho), \tag{3.27}$$

where $B^{J\pi}_{\gamma K}$ is the amplitude ($\kappa^2 = -2m_N E/\hbar^2$),

$W_{ab}(x)$ is a Whittaker function. For neutral systems, we have

$$\chi^{J\pi}_{\gamma K,ext}(\rho) = C^{J\pi}_{\gamma K}\,(\kappa\rho)^{1/2} K_{K+2}(\kappa\rho), \tag{3.28}$$

where $K_n(x)$ is a modified Bessel function.

The Bloch-Schrödinger equation

The basic idea of the R-matrix theory is to solve Eq. (3.8) over the internal region. To restore the hermiticity of the kinetic energy, one solves the Bloch-Schrödinger equation [91]

$$(H + \mathcal{L}(\boldsymbol{L}) - E)\,\Psi^{JM\pi} = \mathcal{L}(\boldsymbol{L})\Psi^{JM\pi}, \tag{3.29}$$

with the Bloch operator $\mathcal{L}(\boldsymbol{L})$ defined as

$$\mathcal{L}(\boldsymbol{L}) = \frac{\hbar^2}{2m_N}\sum_{\gamma K} |\mathcal{Y}^{JM}_{\gamma K} > \delta(\rho - a_0)\frac{1}{\rho^{5/2}}\left(\frac{\partial}{\partial\rho} - \frac{L_{\gamma K}}{\rho}\right)\rho^{5/2} < \mathcal{Y}^{JM}_{\gamma K}|, \tag{3.30}$$

where $\boldsymbol{L}$ is a set of arbitrary constants $L_{\gamma K}$. In the following, we assume $L_{\gamma K} = 0$ for positive energies. Formulas presented in this subsection are given for any channel radius a_0, which can be different from a, defined in 2.3.1.

Let us define matrix $\boldsymbol{C}^{J\pi}$ as [91]

$$C^{J\pi}_{\gamma K i,\gamma' K' i'} =< u_i \mathcal{Y}^{JM}_{\gamma K}|H + \mathcal{L}(\boldsymbol{L}) - E|u_{i'}\mathcal{Y}^{JM}_{\gamma' K'} >_I, \tag{3.31}$$

where subscript I means that the matrix element is evaluated in the internal region only, i.e. for $\rho \leq a_0$. Using the partial-wave expansion Eq. (3.7) and the continuity of the wave function at $\rho = a_0$, we obtain the R-matrix at a_0 from [91]

$$R^{J\pi}_{\gamma K,\gamma' K'}(a_0) = \frac{\hbar^2}{2m_N a_0}\sum_{i,i'} u_i(a_0)\left(\boldsymbol{C}^{J\pi}\right)^{-1}_{\gamma K i,\gamma' K' i'} u_{i'}(a_0). \tag{3.32}$$

R-matrix propagation and collision matrix

As shown in previous section, the nuclear potential extends to very large distances, even for short-range nucleus-nucleus interactions. In other words, the asymptotic behaviour Eq. (3.21) is not accurate below distances which may be as large as 1000 fm or more. This is a drawback of the hyperspherical method, where even for large ρ values, two particles can still be close to each other and contribute to the three-body matrix elements.

It is clear that using basis functions valid up to distances of 1000 fm is not realistic, as the size of the basis would be huge. On the other hand, using a low channel radius (typically $30 \sim 40$ fm) would keep the basis size in reasonable limits, but would not satisfy the key point of the R-matrix theory, namely that the wave function has reached its asymptotic behaviour at the channel radius a_0. This problem can be solved with propagation techniques, well known in atomic physics [90]. The idea is to use a_0 as a starting point for the R matrix; its value is small enough to allow reasonable basis sizes. The R matrix is then propagated from a_0 to a, where the Coulomb asymptotic behaviour Eq. (3.21) is valid. Between a_0 and a, the wave functions $\chi^{J\pi}(\rho)$ are still given by Eq. (3.8), but with the potential replaced by its (analytical) asymptotic expansion.

More precisely, the internal wave functions in the different intervals are given by

$$\begin{aligned} \chi^{J\pi}_{\gamma K,int}(\rho) &= \sum_{i=1}^{N} c^{J\pi}_{\gamma Ki}\, u_i(\rho) \text{ for } \rho \leq a_0, \\ &= \tilde{\chi}^{J\pi}_{\gamma K}(\rho) \text{ for } a_0 \leq \rho \leq a, \end{aligned} \tag{3.33}$$

where $\tilde{\chi}_{\gamma K}(\rho)$ are solutions of Eq. (3.8) with the analytical expansion Eq. (3.16) of the potential term.

The R matrix is first computed at a_0 with Eq. (3.32) (typical values are $a_0 \approx 20 - 40$ fm). Then we consider N_0 sets of initial conditions for $\tilde{\chi}(\rho)$, where

N_0 is the number of γK values (from now on we drop the $J\pi$ index for clarity). We combine these sets as matrix $\tilde{\boldsymbol{\chi}}_{\mathbf{0}}(\rho)$, and choose

$$\tilde{\boldsymbol{\chi}}_{\mathbf{0}}(a_0) = \boldsymbol{I}, \tag{3.34}$$

where $\boldsymbol{I}$ is the unit matrix.

According to the definition of the R matrix [88], we immediately find the derivative at a_0

$$\tilde{\boldsymbol{\chi}}_{\mathbf{0}}{}'(a_0) = \frac{1}{a_0}\boldsymbol{R}^{-1}(a_0)\tilde{\boldsymbol{\chi}}_{\mathbf{0}}(a_0) = \frac{1}{a_0}\boldsymbol{R}^{-1}(a_0). \tag{3.35}$$

Knowing functions $\tilde{\chi}_{0\gamma K}$ and their derivatives at a_0, they are then propagated until a by using the Numerov algorithm [147], well adapted to the Schrödinger equation. The analytical form Eq. (3.16) of the potential is used, with a summation limited to a few k values. The R matrix at a is then determined by using Eq. (3.35) with $\tilde{\boldsymbol{\chi}}_0(a)$ and $\tilde{\boldsymbol{\chi}}_0'(a)$. We have

$$\boldsymbol{R}(a) = \frac{1}{a}\tilde{\boldsymbol{\chi}}_{\mathbf{0}}(a)\left(\tilde{\boldsymbol{\chi}}_{\mathbf{0}}{}'(a)\right)^{-1}. \tag{3.36}$$

Notice that the propagated R matrix Eq. (3.36) does not depend on the choice of $\tilde{\chi}_0(a_0)$. In Ref. [90], the propagation is performed through the Green function defined in the intermediate region, and expanded over a basis. The method presented here uses the Numerov algorithm, and does not rely on the choice of a basis. The analytical form of the potential in this region makes calculations fast and accurate.

Finally the collision matrix is obtained from the R matrix at the channel radius a with [91]

$$\boldsymbol{U}^{J\pi} = \left(\boldsymbol{Z}^{J\pi\star}\right)^{-1}\boldsymbol{Z}^{J\pi}, \tag{3.37}$$

and

$$Z^{J\pi}_{\gamma K,\gamma' K'} = H^-_{\gamma K}(ka)\delta_{\gamma\gamma'}\delta_{KK'} - ka(H^-_{\gamma K}(ka))' R^{J\pi}_{\gamma K,\gamma' K'}(a), \tag{3.38}$$

where the derivation is performed with respect to ka.

Lower values of the channel radius a can be used by employing the Gailitis method [148]. In this method the asymptotic forms Eq. (3.24) are generalized with the aim of using them at shorter distances. This means that the propagation should be performed in a more limited range (typical values for a are $a \sim 200 - 400$ fm). However this does not avoid propagation which, in any case, is very fast. In addition, the Gailitis method cannot be applied to charged systems, as it assumes from the very beginning that the coupling potentials decrease faster than $1/\rho$.

The extension of the R-matrix formalism to bound states is well known for two-body systems [149]. Basically, the $L_{\gamma K}$ constants are defined so as to cancel the r.h.s. of Eq. (3.29). Then, the problem is reduced to a matrix diagonalization with iteration on the energy [149, 150].

Wave functions

Once the collision matrix is known, the internal wave function Eq. (3.33) can be determined in both intervals. Although the choice of $\tilde{\boldsymbol{\chi}}_{\mathbf{0}}(a_0)$ is arbitrary, functions $\tilde{\boldsymbol{\chi}}(\rho)$ entering Eq. (3.33) do not depend on that choice. In the intermediate region $a_0 \leq \rho \leq a$, functions $\tilde{\boldsymbol{\chi}}(\rho)$ and $\tilde{\boldsymbol{\chi}}_0(\rho)$ are related to each other by a linear transformation

$$\tilde{\boldsymbol{\chi}}(\rho) = \tilde{\boldsymbol{\chi}}_{\mathbf{0}}(\rho)\boldsymbol{M}. \tag{3.39}$$

Matrix $\boldsymbol{M}$ is deduced by using the asymptotic behaviour Eq. (3.21) at $\rho = a$,

$$\tilde{\boldsymbol{\chi}}(a) = \tilde{\boldsymbol{\chi}}_0(a)\boldsymbol{M} = \boldsymbol{\chi}_{ext}(a), \tag{3.40}$$

where $\boldsymbol{\chi}_{ext}(a)$ is the matrix involving all entrance channels [see Eq. (3.21)]. It depends on the collision matrix.

Coefficients $c^{J\pi}_{\gamma Ki}$ defining the internal wave function in the interval $\rho \leq a_0$ are finally obtained by

$$c^{J\pi}_{\gamma Ki} = \frac{\hbar^2}{2m_N} \sum_{\gamma' K' i'} \left(\boldsymbol{C^{-1}}\right)^{J\pi}_{\gamma Ki,\gamma' K' i'} \left(\frac{d\tilde{\chi}^{J\pi}_{\gamma' K'}}{d\rho}\right)_{\rho=a_0} u_{i'}(a_0). \tag{3.41}$$

The Lagrange-mesh method

Up to now, the basis functions $u_i(\rho)$ are not specified. We use here the Lagrange-mesh method which has been proved to be quite efficient in two-body [151] and three-body [67] systems. Notice however that its application to three-body continuum states is new.

When dealing with a finite interval, the N basis functions $u_i(\rho)$ are defined as [138]

$$u_i(\rho) = (-1)^{N-i} \left(\frac{1-x_i}{a_0 x_i}\right)^{1/2} \frac{\rho P_N(2\rho/a_0 - 1)}{\rho - a_0 x_i}, \tag{3.42}$$

where the x_i are the zeros of a shifted Legendre polynomial given by

$$P_N(2x_i - 1) = 0. \tag{3.43}$$

The basis functions satisfy the Lagrange condition

$$u_i(a_0 x_j) = (a_0 \lambda_i)^{-1/2} \delta_{ij}, \tag{3.44}$$

where the λ_i are the weights of the Gauss-Legendre quadrature corresponding to the [0,1] interval, i.e. half of the weights corresponding to the traditional interval [-1,1].

The main advantage of the Lagrange-mesh technique is to strongly simplify the calculation of matrix elements Eq. (3.31) if the Gauss approximation is used. Matrix elements of the kinetic energy $(T + \mathcal{L})$ are obtained analytically [138]. Integration over ρ provides matrix elements of the potential by a single evaluation of the potential at $\rho = a_0 x_i$. The potential matrix is diagonal with respect to i and i'.

In Ref. [67], the Lagrange-mesh technique has been applied to bound states of three-body systems. As the natural interval ranges from zero to infinity, the Laguerre mesh was used. It was shown that the Gauss quadrature is quite accurate for the matrix elements, and that computer times can be strongly reduced.

3.2. Applications

3.2.1. Conditions of the calculations

Here we apply the method to the ^{6}He and ^{14}Be nuclei. The α-n and ^{12}Be-n interactions are chosen as local potentials. They contain Pauli forbidden states (one in $\ell = 0$ for α-n, and one in $\ell = 0, 1$ for ^{12}Be-n) which should be removed for a correct description of three-body states [67, 89]. For bound states, two methods are available: the use of a OPP method [135], and a supersymmetric transformation of the nucleus-nucleus potential [24]. Although both approaches provide different wave functions, spectroscopic properties are similar [67]. For unbound systems, it turns out that the projector technique is quite difficult to apply with a good accuracy. Expansions similar to Eq. (3.16) for the projection operator provide non-local potentials. Consequently, all applications presented here are obtained with supersymmetric partners of the nucleus-nucleus potentials.

As collision matrices can be quite large, it is impossible to analyze all elements. To show the essential information derived from the collision matrix, we rather present some eigenphases. Those presenting the largest variation in the considered energy range are shown.

Analyzing the collision matrix in terms of eigenphases raises two problems. First, it is in general not obvious to link the eigenphases at different energies.

As eigenphases cannot be associated with given quantum numbers, there is no direct way to draw continuous eigenphases. The procedure can be strongly improved by analyzing the eigenvectors. Starting from a given energy, eigenphases for the next energy are chosen by minimizing the differences between the corresponding eigenvectors.

A second problem associated with eigenphases arises from the Coulomb interaction. As matrix elements of the Coulomb force are not diagonal, the corresponding phase shifts do not appear in a simple way, as in two-body collisions. A new method was suggested by D. Baye in Ref. [91]. According to this method, in order to extract the nuclear contribution $\boldsymbol{U_N}$ from the total collision matrix $\boldsymbol{U}$, we perform two calculations: a full calculation providing $\boldsymbol{U}$, and a calculation without the nuclear contribution, providing the Coulomb collision matrix $\boldsymbol{U_C}$. Then we define the nuclear collision matrix $\boldsymbol{U_N}$ by

$$\boldsymbol{U} = \boldsymbol{U_C}^{1/2}\boldsymbol{U_N}\boldsymbol{U_C}^{1/2}. \tag{3.45}$$

As $\boldsymbol{U}$ and $\boldsymbol{U_C}$ are symmetric and unitary, the same properties hold for $\boldsymbol{U_N}$. Examples of Coulomb phase shifts will be given in the next sections.

3.2.2. Application to ^{6}He and ^{6}Be

The conditions of the calculation are those of Ref. [67]. The α-n potential $V_{\alpha-n}$ has been derived by Kanada *et al.* [145]. It contains spin-orbit and parity terms. The n-n potential is the Minnesota interaction [152]. As bare nucleus-nucleus potentials cannot be expected to reproduce the ^{6}He ground-state energy with a high accuracy, the potential $V_{\alpha-n}$ was renormalized by a factor $\lambda = 1.051$ (note that this value was misprinted in Ref. [67]). This value reproduces the ^{6}He experimental energy -0.97 MeV and provides 2.44 fm for the r.m.s. radius [91]. The convergence with respect to K_{max} and to the Lagrange-mesh parameters has already been discussed in Ref. [67].

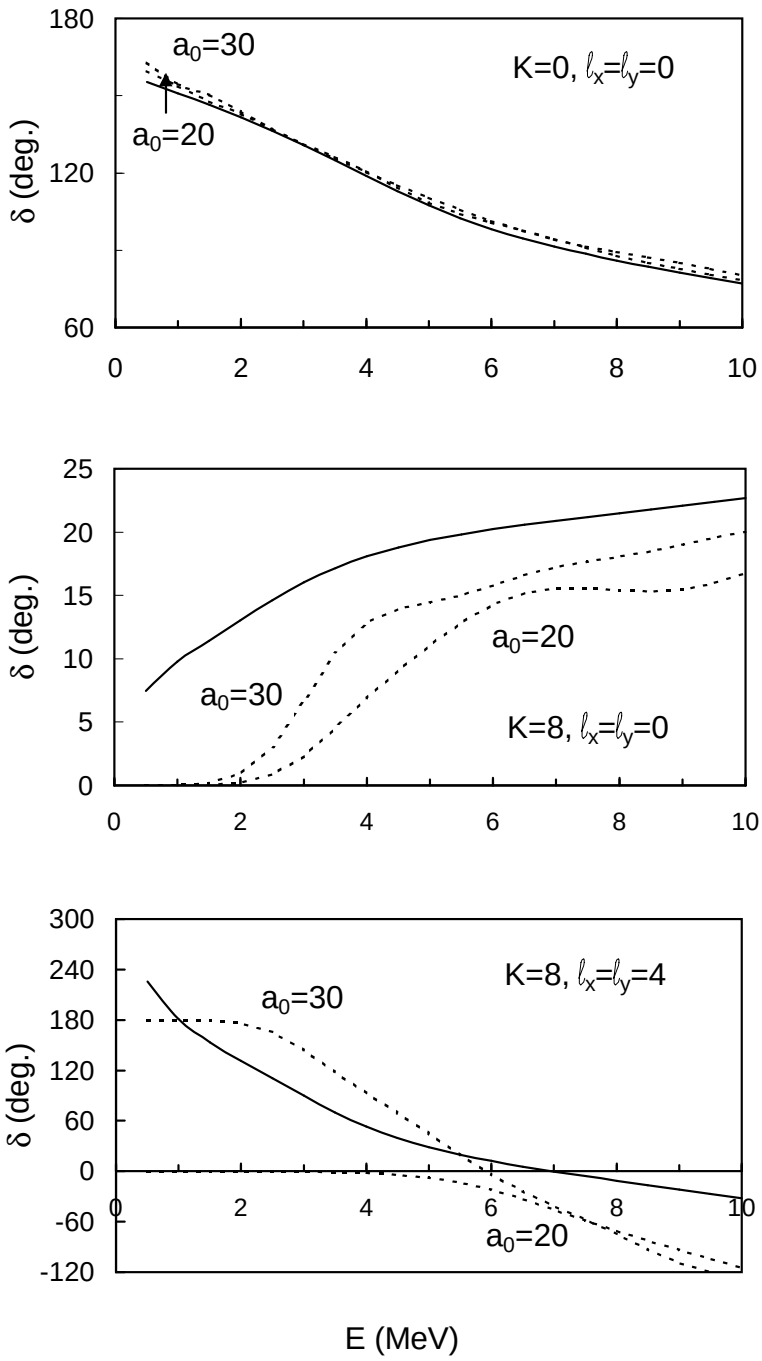

Fig. 3.1. **α+n+n phase shifts ($J = 0^+$) for channel radii $a_0 = 20$ fm ($N = 20$) and $a_0 = 30$ fm ($N = 30$), and for different partial waves. Solid lines are obtained with propagation up to $a = 250$ fm of the R matrix (curves corresponding to different a_0 are undistinguishable), and dashed lines without propagation.**

Let us first illustrate the importance of the propagation technique. In Fig. 3.1, we plot some elements of the $J = 0^+$ collision matrix under different conditions. In each case, we compare the phase shifts for two channel radii: $a_0 = 20$ fm and $a_0 = 30$ fm. The calculation is performed with and without propagation. For $K = 0$, reasonable values can be obtained without propagation. However, for larger K values ($K = 8$ is displayed with $\ell_x = \ell_y = 0$ and $\ell_x = \ell_y = 4$), the channel radius should be quite large to reach convergence. To keep the same accuracy, the number of basis functions should be increased. However, one basis function per fm is a good estimate, and this leads to unrealistically large basis sizes. This convergence problem is due to the long range of the potential. The propagation technique (performed here up to $a = 250$ fm) allows us to get a very high stability (better than $0.1°$ at all energies) even for rather small channel radii. Consequently calculations with high K values are still feasible.

To illustrate the diagonalization of the collision matrix, we compare in Fig. 3.2 the diagonal phase shifts with the corresponding eigenphases. The diagonal phase shifts correspond to the collision matrix before diagonalization, while the eigenphases correspond to the diagonalized collision matrix. We have selected a particular case, with $J = 2^+$, and $K_{max} = 2$. With these conditions the collision matrix is 4×4, and presents a narrow resonance near 2 MeV. In the upper part of Fig. 3.2, we plot the diagonal phase shifts. One of them presents a $180°$ jump, characteristical of narrow resonances. This resonant behaviour is also observable in two other partial waves. After diagonalization of the collision matrix (Fig. 3.2, lower part) the resonant behaviour shows up in one eigenphase only. The three other eigenphases smoothly depend on energy.

The convergence with respect to K_{max} is illustrated in Fig. 3.3 with the $J = 0^+$ eigenphases. It turns out that, at low energies, high hypermomenta are necessary to achieve a precise convergence. However, above 4 MeV, $K_{max} = 20$ is sufficient to obtain an accuracy of $2°$.

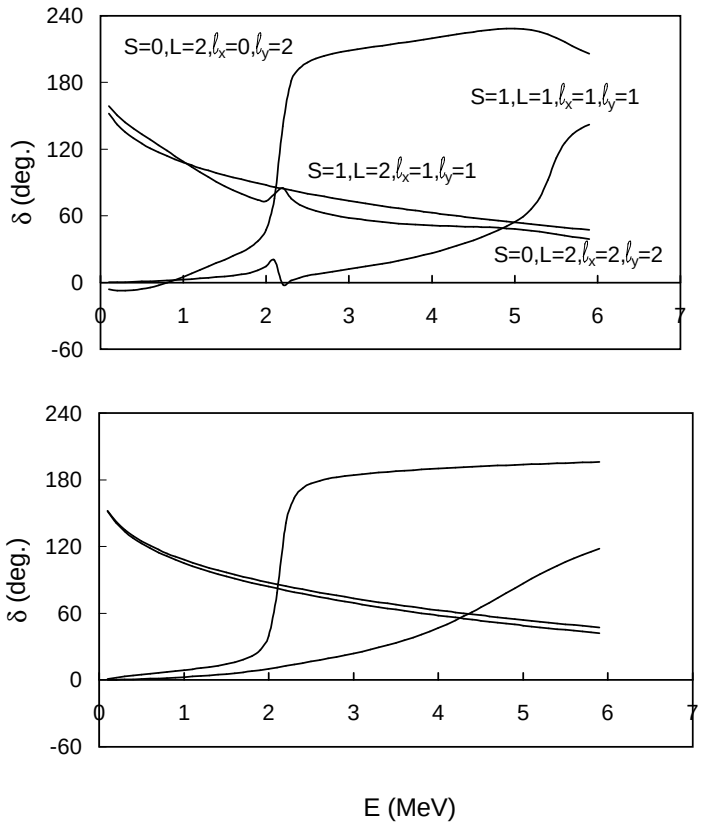

Fig. 3.2. Diagonal phase shifts (upper panel) and eigenphases (lower panel) for the α+n+n system ($J = 2^+, K_{max} = 2$).

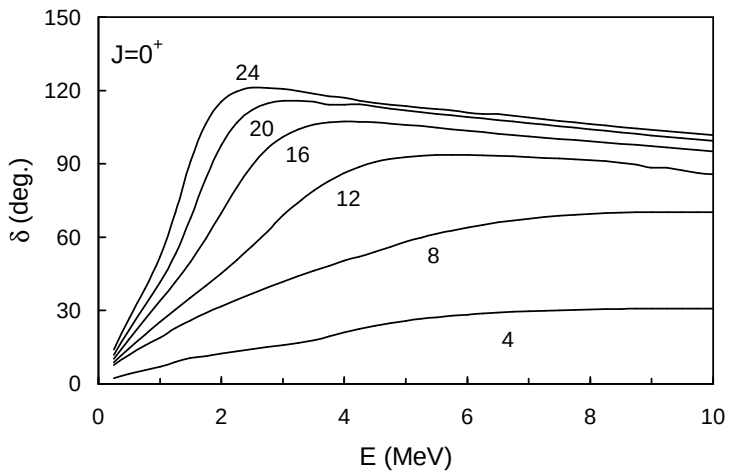

Fig. 3.3. Energy dependence of α+n+n eigenphases ($J = 0^+$) for different K_{max} values.

Figure 3.4 gives the eigenphases for $J = 0^+, 1^-, 2^+$ in ^{6}He and ^{6}Be (K_{max} is taken as 24, 19 and 16, respectively). As expected, the 2^+ phase shift of ^{6}He presents a narrow resonance. The theoretical energy (about 0.2 MeV) is however underestimated as the experimental value [153] is $E = 0.82$ MeV. In order to provide meaningful properties for this state, we have readjusted the scaling factor to $\lambda = 1.020$, which provides the correct energy. The 0^+ and 1^- phase shifts show broad structures near 1.5 MeV. Similar phase shifts have been obtained by Danilin *et al.* [154, 155] and by Thompson *et al.* [89] with other potentials.

In ^{6}Be, the ground state is found at $E = 1.26$ MeV with a width $\Gamma = 65$ keV [91]. These values are in reasonable agreement with experiment [153] ($E = 1.37$ MeV, $\Gamma = 92 \pm 6$ keV), the width being underestimated by the model due to the lower energy. Experimentally, a 2^+ state is known near $E = 3.0$ MeV with a width of $\Gamma = 1.16 \pm 0.06$ MeV. These properties are consistent with the theoretical 2^+ eigenphase, which presents a broad structure near $E \approx 4$ MeV. The largest Coulomb eigenphases ($J = 0^+$) are shown as dotted lines in Fig. 3.4. As expected, the Coulomb interaction plays a dominant role at low energies, but it cannot be completely neglected even near 10 MeV. Coulomb eigenphases for other spin values are very similar and therefore are not presented.

3.2.3. Application to ^{14}Be

As shown in previous works [117, 156, 157], a ^{12}Be+n+n three-body model can provide a realistic description of ^{14}Be. The spectroscopy of the ^{14}Be ground state has already been investigated in non-microscopic [117, 156–158] and microscopic [159] models. In Ref. [91] the three-body model was extended to ^{14}Be excited and continuum states.

The ^{13}Be ground state is expected to be a virtual s wave, with a large and negative scattering length ($a_s < -10$ fm) [160]. In addition, the existence of a

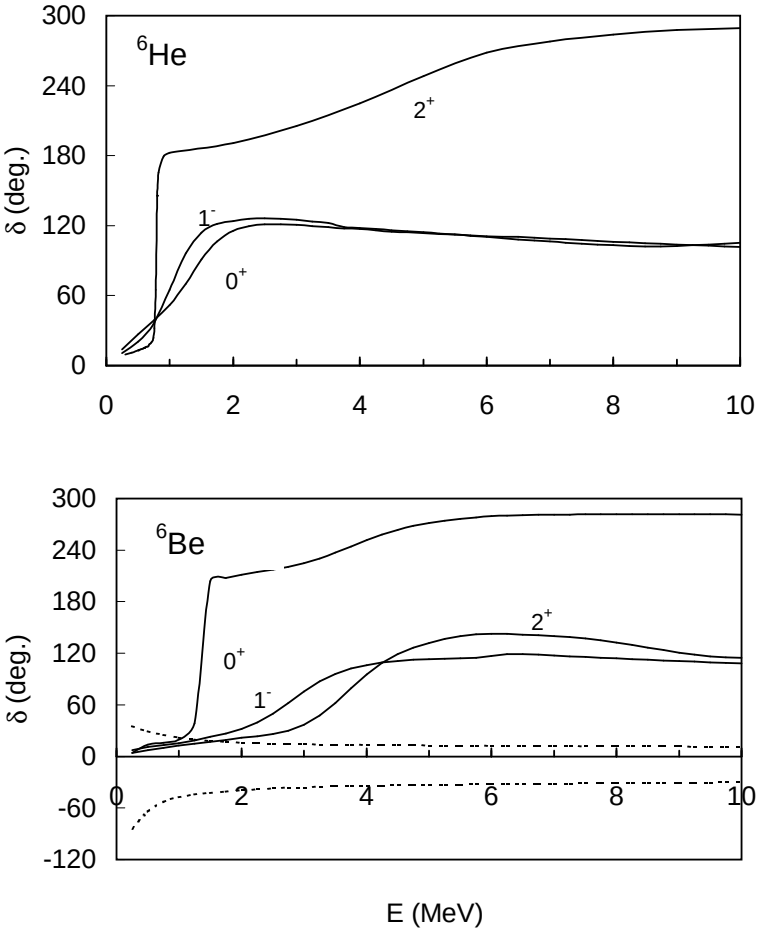

Fig. 3.4. Eigenphases of ^{6}He and ^{6}Be for different J values (solid lines). For ^{6}Be, dotted lines represent the largest Coulomb eigenphases for $J = 0^+$.

$5/2^+$ d-state near 2 MeV is well established. These properties can be reproduced by a ^{12}Be-n potential

$$V(r) = -\frac{V_0 + V_s\, \boldsymbol{\ell} \cdot \boldsymbol{s}}{1 + \exp((r - r_0)/a)}, \tag{3.46}$$

where $\boldsymbol{\ell}$ is the relative angular momentum and $\boldsymbol{s}$ the neutron spin. In Eq. (3.46), $r_0 = 2.908$ fm, $a = 0.67$ fm, $V_0 = 43$ MeV, $V_s = 6$ MeV. The range and diffuseness of the Woods-Saxon potential are taken from Ref. [157]. The amplitudes V_0 and V_s provide $E(5/2^+) = 2.1$ MeV, and $a_s = -47$ fm, which are consistent with the data. For the n-n potential, we use the Minnesota interaction, as for the ^{6}He study.

With these potentials, the ^{14}Be ground state is found at $E = -0.16$ MeV [91], which represents an underbinding with respect to experiment (-1.34 ± 0.11 MeV [161]). This calculation has been performed with $K_{max} = 24$, which ensures the convergence. The underbinding problem is common to all three-body approaches, and can be solved in two ways. (i) A renormalization factor $\lambda = 1.08$ provides a ground-state energy at -1.30 MeV, i.e. within the experimental uncertainties. This procedure leads to a slightly bound ^{13}Be ground state, which might influence the ^{14}Be properties. (ii) A three-body phenomenological term $V^{(123)}$, taken as in Ref. [89], i.e.,

$$V^{(123)}_{K\gamma,K'\gamma'}(\rho) = -\delta_{KK'}\delta_{\gamma\gamma'}\, V_3/[1 + (\rho/\rho_3)^2], \tag{3.47}$$

reproduces the experimental energy with an amplitude $V_3 = 4.7$ MeV (according to Ref. [89], we take $\rho_3 = 5$ fm). This potential is diagonal in (K, γ), and is simply added to the two-body term [see Eqs. (3.10), (3.11)]. In ^{6}He, it was shown that both readjustments of the interaction provide similar results [67]. However the renormalization factor is larger for ^{14}Be, and both methods will be considered in the following.

For $J = 0^+$, the calculations have been done with K_{max} up to 24. The energies obtained with renormalization or with the three-body potential are very similar. This confirms the conclusion drawn for the ^{6}He nucleus [67].

Spectroscopic properties of ^{14}Be are given in Ref. [91]. The r.m.s. radii of ^{14}Be have been determined with 2.57 fm as ^{12}Be radius. For the ground state, $\sqrt{< r^2 >} = 3.10$ fm or 3.14 fm, in nice agreement with experiment (3.16 ± 0.38 fm, see Ref. [162]). In all cases, the $S = 1$ component (denoted as $P_{S=1}$) is small ($< 5\%$). The decomposition in shell-model orbitals shows that the 0^+ state is essentially ($\approx 70\%$) $(2s_{1/2})^2$, with small $(2d_{3/2})^2$ and $(2d_{5/2})^2$ admixtures [91].

Regarding $J = 2^+$, the hypermomentum can take values up to $K_{max} = 16$, where the number of partial waves is 172. Going beyond $K_{max} = 16$ would require too large computer memories. For both potentials, the energy is below threshold, and the r.m.s. radius is close to 3 fm. A partial-wave analysis provides 19% of $S = 1$ admixture, a value much larger than in the ground state [91].

Three-body eigenphases are displayed in Fig. 3.5. As for the ^{14}Be spectroscopy the use of a three-body potential does not qualitatively change the phase shifts. The 1^- phase shift presents two jumps but they cannot be directly assigned to physical resonances. On the contrary, the 2^+ phase shift shows a narrow resonance near 2 MeV. For the sake of completeness, ^{12}O+p+p mirror phase shifts are also shown in Fig. 3.5. As expected, no narrow structure is found. A very broad 0^+ resonance shows up near 8 MeV, and should correspond to the ^{14}Ne ground state.

3.3. Conclusion

In this Chapter, we have extended the three-body formalism of Ref. [67] to unbound states. As for two-body systems, the Lagrange-mesh technique, associated with the R-matrix method, provides an efficient and accurate way to derive collision matrices and wave functions. Compared with two-body systems, three-body R-matrix approaches are more tedious, owing to the coupling

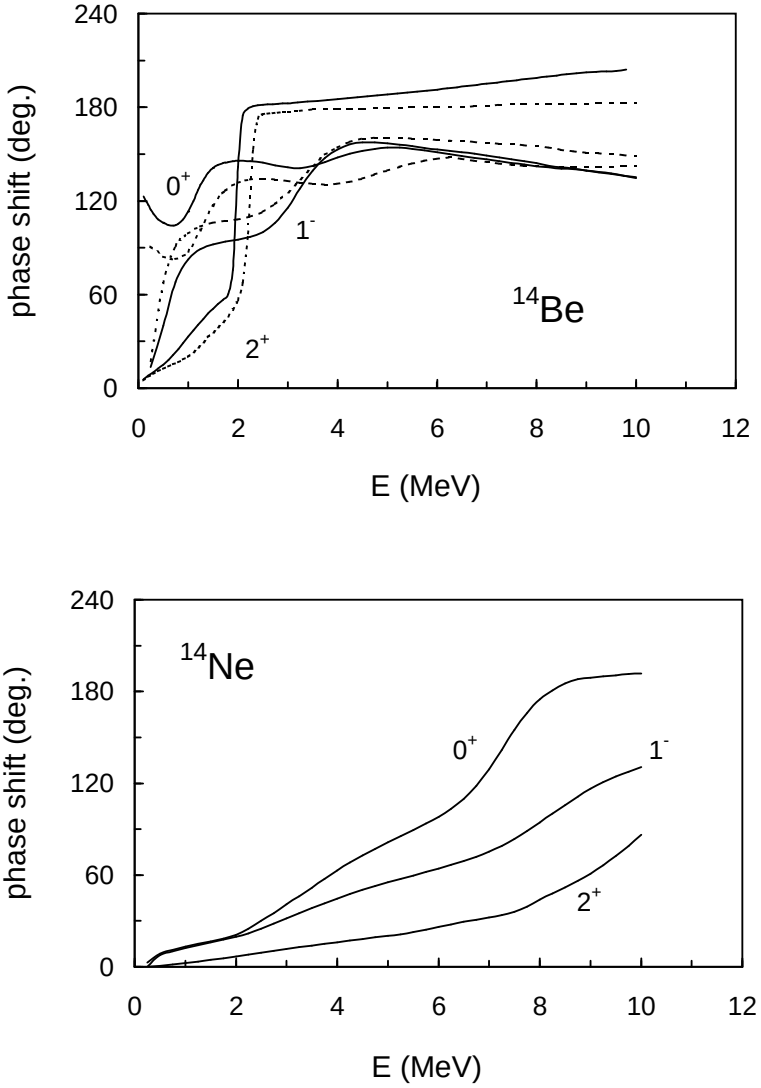

Fig. 3.5. Three-body ^{12}Be-n-n and ^{12}O-p-p eigenphases. Solid lines correspond to a renormalized core-nucleon potential, and dotted lines to a phenomenological three-body term.

potentials which extend to very large distances. This behaviour is inherent to the use of hyperspherical coordinates which provide three-body potentials behaving as $1/\rho^3$, even for short-range two-body interactions. This problem can be efficiently solved by using propagation techniques. Here, we propagate the wave function and the R matrix by using the Numerov algorithm. This formalism has been extended to charged systems.

The ^{6}He system has essentially been used as a test of the method, as most of its properties are available in the literature. The phase shift analyze has been performed for the $0^+, 1^-$ and 2^+ states of the ^{6}He, as well as of the ^{6}Be nucleus.

Application to three-body ^{12}Be+n+n states is new. The analyze of the ^{12}Be+n+n three-body phase shifts indicates the existence of a second narrow 2^+ resonance at $E_x \approx 3.4$ MeV. Our results is now confirmed by recent experimental study [163] with E_x =3.54(16) MeV.

A limitation of the method is the slow convergence of the phase shifts with respect to the maximum hypermomentum K_{max}. To achieve a full convergence, values up to $K_{max} = 20$ or more are necessary. This problem is even stronger for high spins, where the number of partial waves increases rapidly. A possible solution to this problem would be to apply the Feshbach reduction method [164] to scattering states. Another possible development would be to use a projection technique to remove Pauli forbidden states [87]. In that case, asymptotic potentials (3.15) are non local, which makes the calculation still heavier.

The present model offers an efficient way to investigate bound and unbound states. In exotic nuclei, most low-lying states are unbound, and a rigorous analysis requires scattering conditions. The inclusion of the Coulomb interaction still extends the application field, and is interesting even for non-exotic nuclei. In this context, an accurate analysis of unbound $\alpha+\alpha+\alpha$ states seems desirable in view of its strong interest in the triple-α reaction rate [165].

IV. ANALYSIS OF THE ^{6}He BETA-DECAY INTO THE ALPHA PLUS DEUTERON CONTINUUM IN A THREE-BODY MODEL

As was discussed in chapter 1, in this chapter we estimate the transition probabilities per time and energy units for the β decay of the ^{6}He halo nucleus into $\alpha+d$ continuum channel with the ^{6}He wave function in the $\alpha+n+n$ three-body cluster potential model [105]. [1] For the description of the structure of the ^{6}He and ^{6}Li nuclei, we use the hyperspherical harmonics method on a Lagrange mesh developed by the Belgian group (D. Baye, P. Descouvemont, etc.) [67, 166], which was used in the previous chapter for the three-body continuum studies of halo nuclei. The $\alpha+d$ scattering wave function is treated as factorized into a deuteron wave function and a nucleus-nucleus scattering state. We will choose several versions of the central interaction potential: a deep Gaussian potential [167] which fits both the s-wave phase shift and the binding energy of the ^{6}Li ground state (1.473 MeV), and potentials obtained by folding the $\alpha + N$ potential of Voronchev et al. [168]. For the sake of comparison we will also perform a calculation with a repulsive $\alpha + d$ potential which was used by the authors of Ref. [100].

4.1. Model

For the β decay process

$$^6\mathrm{He} \rightarrow \alpha + d + e + \bar{\nu}, \tag{4.1}$$

the transition probability per time and energy units is given by the equation

[1] This chapter is based on the results of Ref. [105, 106]

[169]

$$\frac{dW}{dE} = \frac{m_e c^2}{\pi^4 v \hbar^2} G_\beta^2 f(Q-E) B_{\mathrm{GT}}(E), \tag{4.2}$$

where m_e is the electron mass,

v and E are the relative velocity and energy in the center of mass system of the α and deuteron, and

$G_\beta = 2.996 \times 10^{-12}$ is the dimensionless β decay constant [170].

The Fermi integral $f(Q-E)$ depends on the kinetic energy $Q-E$, available for the electron and antineutrino. The mass difference Q between initial and final particles is 2.03 MeV. The Gamow-Teller reduced transition probability reads

$$B_{\mathrm{GT}}(E) = 12\lambda^2 \langle \Psi_{\alpha d}^{1;0}(E) | \sum_{j=1}^{2} t_{j-} s_{jz} | \Psi_{^6\mathrm{He}}^{0;1} \rangle^2, \tag{4.3}$$

where $\lambda = 1.268 \pm 0.002$ is the ratio of the axial-vector to vector coupling constants [171],

$\Psi_{\alpha d}^{1;0}(E)$ is the wave function of the final $\alpha + d$ system with total angular momentum $J = 1$ and isospin $T = 0$,

$\boldsymbol{t}_j$ and $\boldsymbol{s}_j$ are the isospin and spin operators, respectively, of particle j,

$\Psi_{^6\mathrm{He}}^{0;1}$ is the ^{6}He ground state wave function with $J = 0$ and $T = 1$,

particles 1 and 2 are the nucleons and 3 is the α cluster.

For the calculation of the β decay transition matrix elements to the ^{6}Li ground state, we replace the wave function $\Psi_{\alpha d}^{1;0}(E)$ in Eq. (4.3) by the wave function of the ^{6}Li ground state.

The ^{6}He ground state wave function contains components with total intrinsic spin $S = 0$ and 1. The total orbital momentum L is equal to S. For the scattering state, we assume a factorized expression into a deuteron ground state

wave function and an $\alpha + d$ scattering state derived from a potential model. We neglect the small D component of the deuteron. Since the total orbital momentum and parity are conserved, only the $l = 0$ partial scattering wave contributes. Hence, only the initial $L = S = 0$ component of ^{6}He can decay to $\alpha + d$. It is convenient to express the Gamow-Teller matrix element with the help of an effective wave function [101]

$$\Psi_{\text{eff}}(\boldsymbol{R}) = \int \Psi_d(\boldsymbol{r})\Psi_{^6\text{He}}(\boldsymbol{r}, \boldsymbol{R})d\boldsymbol{r}, \tag{4.4}$$

where $\boldsymbol{R} = \boldsymbol{r}_3 - \frac{1}{2}(\boldsymbol{r}_1 + \boldsymbol{r}_2)$ is the $\alpha + d$ relative coordinate,

$\boldsymbol{r} = \boldsymbol{r}_2 - \boldsymbol{r}_1$ is the deuteron relative coordinate.

In this expression, $\Psi_d(\boldsymbol{r})$ and $\Psi_{^6\text{He}}(\boldsymbol{r}, \boldsymbol{R})$ are the spatial parts of the deuteron and ^{6}He wave functions, respectively. The Gamow-Teller matrix element reads

$$B_{\text{GT}}(E) = 6\lambda^2 \left[\int \Psi_{\text{eff}}(\boldsymbol{R})\Psi_{\alpha d}(E, \boldsymbol{R})d\boldsymbol{R} \right]^2 . \tag{4.5}$$

The initial three-body wave function is expressed in hyperspherical coordinates. A set of Jacobi coordinates for the three particles with mass numbers $A_1 = 1$, $A_2 = 1$, and $A_3 = 4$ is defined as (see Eq. (2.2))

$$\boldsymbol{x} = \sqrt{\mu_{12}}\boldsymbol{r}, \qquad \boldsymbol{y} = \sqrt{\mu_{(12)3}}\boldsymbol{R}, \tag{4.6}$$

where the (dimensionless) reduced masses are given by $\mu_{12} = 1/2$ and $\mu_{(12)3} = 4/3$. Equations (5.6) define six coordinates which are transformed to the hyperspherical coordinates as

$$\rho^2 = x^2 + y^2, \qquad \alpha = \arctan(y/x), \tag{4.7}$$

where α varies between 0 and $\pi/2$ (see Eq. (3.2)). With the angular variables $\Omega_x = (\theta_x, \varphi_x)$ and $\Omega_y = (\theta_y, \varphi_y)$, equations (5.9) define a set of hyperspherical coordinates. This set of coordinates is known to be well adapted to the three-body Schrödinger equation.

With the notation $\Omega_5 = (\alpha, \Omega_x, \Omega_y)$, the wave function in the HHM reads (see chapter 4 and Ref. [67])

$$\Psi^{JM\pi}(\rho, \Omega_5) = \rho^{-5/2} \sum_{l_x l_y LSK} \chi^{J\pi}_{l_x l_y LSK}(\rho) \mathcal{Y}^{JM}_{l_x l_y LSK}(\Omega_5), \tag{4.8}$$

where l_x and l_y are the orbital momenta associated with the Jacobi coordinates $\boldsymbol{x}$ and $\boldsymbol{y}$, respectively,

$\chi^{J\pi}_{l_x l_y LSK}$ are hyperradial functions,

$\mathcal{Y}^{JM}_{l_x l_y LSK}$ are hyperspherical harmonics. The sums in Eq. (4.8) and in the following run over even K values only. Since only $l_x = l_y = L = S = 0$ contributes, let us define

$$Z_K(x, y) = (2/3)^{3/4} N_K \rho^{-5/2} \chi_{0000K}(\rho) P^{1/2,1/2}_{K/2}(\cos 2\alpha), \tag{4.9}$$

where N_K is a normalisation factor and

$P^{1/2,1/2}_{K/2}$ is a Jacobi polynomial [144] (see Ref. [67] for details).

The deuteron and α+d wave functions are factorized as $\Psi_d(\boldsymbol{r}) = r^{-1} u_d(r) Y_{00}(\hat{\boldsymbol{r}})$ and $\Psi_{\alpha d}(E; \boldsymbol{R}) = R^{-1} u_E(R) Y_{00}(\hat{\boldsymbol{R}})$, respectively. The radial scattering function u_E has the asymptotic behavior,

$$u_E(R) \underset{R\to\infty}{\longrightarrow} F_0(kR) \cos\delta_0(E) + G_0(kR) \sin\delta_0(E), \tag{4.10}$$

where k is the wave number of the relative motion,

F_0 and G_0 are Coulomb functions, and

$\delta_0(E)$ is the s-wave phase shift at energy E. After integration over angular parts, the reduced transition probability becomes

$$B_{\mathrm{GT}}(E) = 6\lambda^2 \left[\sum_K \int_0^\infty u_E(R) u_{\mathrm{eff}}^{(K)}(R) dR \right]^2 . \tag{4.11}$$

It involves the K-dependent effective functions

$$u_{\mathrm{eff}}^{(K)}(R) = R \int_0^\infty Z_K(x,y) u_d(r) r dr, \tag{4.12}$$

the sum of which forms the radial part of $\psi_{\mathrm{eff}}(\boldsymbol{R})$.

Some among the $\alpha + d$ potentials $V_{\alpha d}(R)$ we are using are obtained by folding an $\alpha + N$ potential $V_{\alpha N}(r)$. They are given by the equation

$$V_{\alpha d}(R) = \langle \Psi_d(\boldsymbol{r}) \mid V_{\alpha n}(|\boldsymbol{R} + \tfrac{1}{2}\boldsymbol{r}|) + V_{\alpha p}(|\boldsymbol{R} + \tfrac{1}{2}\boldsymbol{r}|) \mid \Psi_d(\boldsymbol{r}) \rangle, \tag{4.13}$$

where the integration is performed over the radial and angular parts of the variable $\boldsymbol{r}$.

4.2. Results and discussion

The initial $\alpha + n + n$ bound state is calculated as explained in Ref. [67]. The same nucleon-nucleon interaction is used, i.e.. the central Minnesota interaction [152] which reproduces the deuteron binding energy and fairly approximates the low-energy nucleon-nucleon scattering. This potential provides the deuteron wave function Ψ_d. The $\alpha + N$ potential is however different from the one employed in Ref. [67]. Here we employ the $\alpha + N$ potential of Voronchev et al. [168] with a multiplicative factor 1.035 in order to reproduce the ^{6}He binding energy. This change of interaction is motivated by the fact that we want to use the same interaction for the derivation of the $\alpha + d$ folding potential. The calculations are done with $\hbar^2/2m_N = 20.7342$ MeV fm^2.

Since the valence neutron and proton in the ^{6}Li nucleus belong to the $(0p_{3/2})$ spectrum, we use the p-wave $\alpha+N$ potential of Ref. [168] when deriving the $\alpha+d$ folding potential by using Eq. (4.13). The s-wave $\alpha+d$ folding potential derived from the $\alpha+N$ potential yields two bound states for ^{6}Li with $E_0 = -19.87$ MeV and $E_1 = -0.83$ MeV, respectively. The first one is forbidden by the Pauli principle and the second one is underbound compared with the experimental ground-state energy $E_{\rm exp} = -1.473$ MeV. The $\alpha+N$ potential of Kanada et al. [145] employed in Ref. [67] does not yield an $\alpha+d$ folding potential with a physical bound state in the s wave.

The numerical calculations of the Gamow-Teller matrix elements and of the transition probability for the β decay of the ^{6}He nucleus are done with $\alpha+d$ folding potentials, with a phenomenological Gaussian attractive potential V_a [167] and it's modification V_m, and with a Woods-Saxon repulsive potential [100]. The simple Gaussian potential $V_a(r) = V_0 exp(-\alpha_0 r^2)$ with parameters α_0=0.20 $fm^{-1/2}$ and V_0=-76.12 MeV, simultaneously provides the correct ^{6}Li binding energy (together with a forbidden state) and a fair fit of the low-energy experimental phase shifts. The modified potential V_m with the parameter values α_0=0.21 $fm^{-1/2}$ and V_0=-79.4 MeV yields the same phase shift and bound state energy, however it gives a different node position in the S-wave $\alpha+d$ scattering wave function due-to the Pauli forbidden state. Since the folding potential does not reproduce the ^{6}Li ground-state energy, we multiply the central part of the original $\alpha+N$ potential by factor $f_a = 1.068$. The corresponding folding $\alpha+d$ potential V_{f1} puts the physical state at $E_1 = -1.470$ MeV. The s-wave phase shifts for the different $\alpha+d$ potentials are compared in Fig. 4.1 with phase-shift analyses [172, 173]. The folding potential V_{f1} does not have the same quality of phase shift description as the simple Gaussian potential. Therefore, we also choose another factor $f_b = 1.15$ for the folding potential V_{f2}, which gives a stronger binding for the ^{6}Li ground state, $E_1 = -2.386$ MeV. From Fig. 4.1, one can see that the description of the $\alpha+d$ phase shift is poor for the

Woods-Saxon repulsive potential, which does not bind the ^{6}Li ground state.

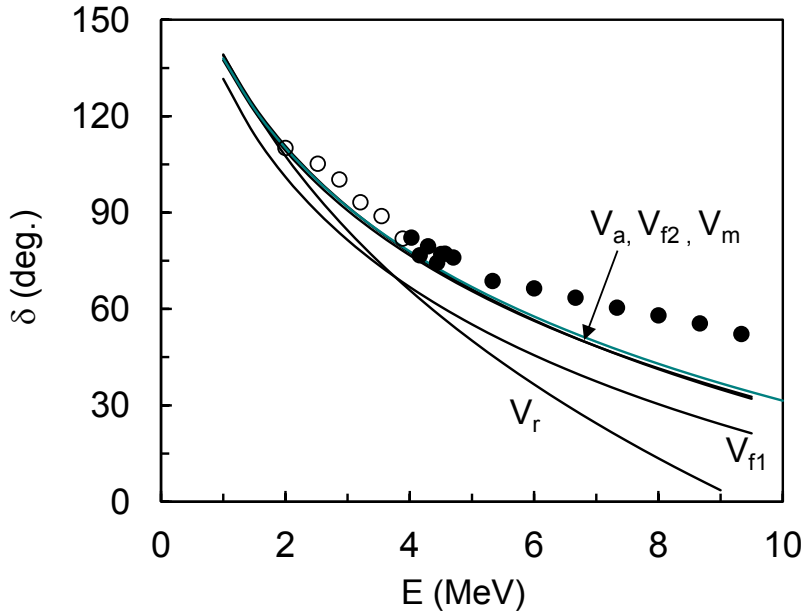

Fig. 4.1. s-wave phase shift obtained with different $\alpha + d$ potentials: folding potentials V_{f1} and V_{f2} (see text), attractive Gaussian potential V_a [167], and repulsive Woods-Saxon potential V_r [100]. The modified potential V_m is described in the text. Experimental data are from Refs. [172, 173].

The deuteron wave function is calculated over a Lagrange-Laguerre mesh involving 40 mesh points and a scaling parameter $h = 0.25$ (see Ref. [67] for details). A binding energy $E_d = 2.20176$ is obtained. The integration over r is done by using the corresponding Gauss-Laguerre quadrature formula with 40 mesh points. This ensures convergent numerical results for the transition probability with more than needed correct digits. The integration over variable R is performed with the simple trapezoidal rule with a step 0.05 fm. Later we show that with this choice of the step of the quadrature formula, convergent results

for the transition probability are obtained with 600 points, which corresponds to a maximal $\alpha + d$ relative distance $R_{\max} = 30$ fm.

In Fig. 4.2, we display the integrals

$$I_E^{(K)}(R) = \int_0^R u_{\text{eff}}^{(K)}(R')u_E(R')dR' \tag{4.14}$$

at the $\alpha + d$ relative energy $E = 1$ MeV for different K values. They are obtained by using the $\alpha + d$ potential of Ref. [167]. The Gamow-Teller matrix element is given by the limit

$$B_{\text{GT}}(E) = 6\lambda^2 \lim_{R\to\infty} \left[\sum_K I_E^{(K)}(R)\right]^2 . \tag{4.15}$$

From Fig. 4.2, one can see that at large R values the dominant contribution to $\sum_K I_E^{(K)}$ for all K values up to $K_{\max}$ comes from the $K = 2$ and $K = 8$ components. Although the $K = 0$ component is rather important around $R = 5$ fm, it is suppressed at large R values even more than the $K = 10$ component.

To understand this interesting effect, we display in Figs. 4.3 and 4.4 the different components of the effective wave function $u_{\text{eff}}^{(K)}(R)$. As is seen from these figures, for the relative distance from $R = 6$ fm up to 25 fm, the contribution of the $K = 8$ component is larger than the contributions of the $K = 4$ and 6 components. One can observe that $u_{\text{eff}}^{(0)}$ keeps a constant sign over the whole region while $u_{\text{eff}}^{(2)}$ changes sign at $R \approx 2$ fm. The full line represents the sum

$$u_{\text{eff}}(R) = \sum_{K=0}^{K_{\max}} u_{\text{eff}}^{(K)}(R). \tag{4.16}$$

In Fig. 4.3, we also show the $\alpha + d$ scattering s-wave function u_E for $E = 1$ MeV. It is important to note that this function keeps a constant sign in the interval 5-19 fm. This constant-sign interval is even broader for smaller values of E. Comparing the curves in Figs. 4.3 and 4.4, we observe that the product $u_{\text{eff}}^{(K)}(R)u_E(R)$ for $K = 0$ changes sign several times. The integral

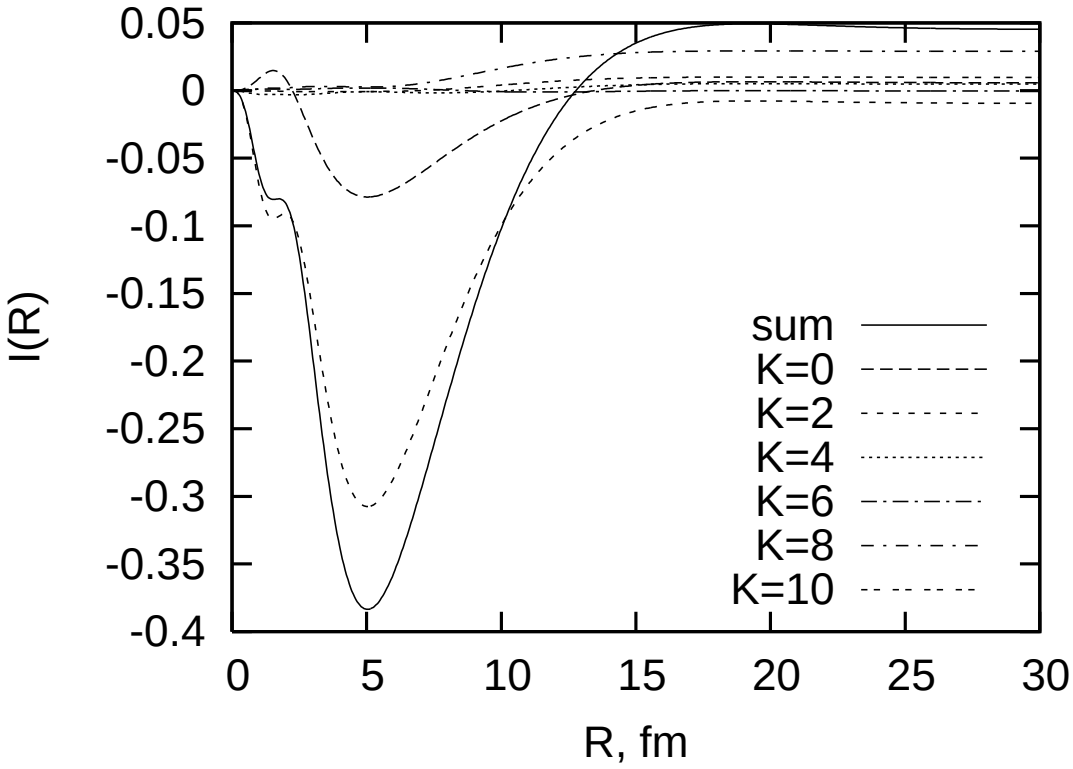

Fig. 4.2. Integrals $I_E^{(K)}(R)$ (Eq. 4.14) at the energy $E = 1$ MeV for the $\alpha + d$ potential of Ref. [167] and different K values with $K_{\max} = 24$ and $R_{\max} = 30$ fm.

$I_E^{(0)}$ is first positive, starts decreasing at the first zero of u_E, changes sign near 2 fm and increases again at the second zero of u_E. The combined effect of both zeros results in a cancellation between the internal and external parts of the corresponding integral $I_E^{(0)}$. These zeros at short distances are due to the existence of two (one physical and one forbidden) bound states in the potential. The cancellation would not occur so strongly with a single zero.

The combined effects of the zero of $u_{\text{eff}}^{(2)}$ and of the first zero of u_E is just a small plateau near 2 fm. The second zero of u_E gives a minimum near 5 fm. The result for the $K = 2$ component also yields an important cancellation, but not as strong as in the $K = 0$ case. The effective functions for $K = 4$ and 6 are very small in the region where u_E keeps a constant sign and lead to negligible

contributions.

A new situation appears for the $K = 8$ component. The effective wave function is much smaller than $K = 0$ or 2 but the cancellation is minimal. Hence it gives the second largest $I_E^{(K)}$ at infinity. The same mechanism applies for the smaller $K = 10$, 12, 14, ... components. The $K = 10$ integral still contributes significantly to the total sum.

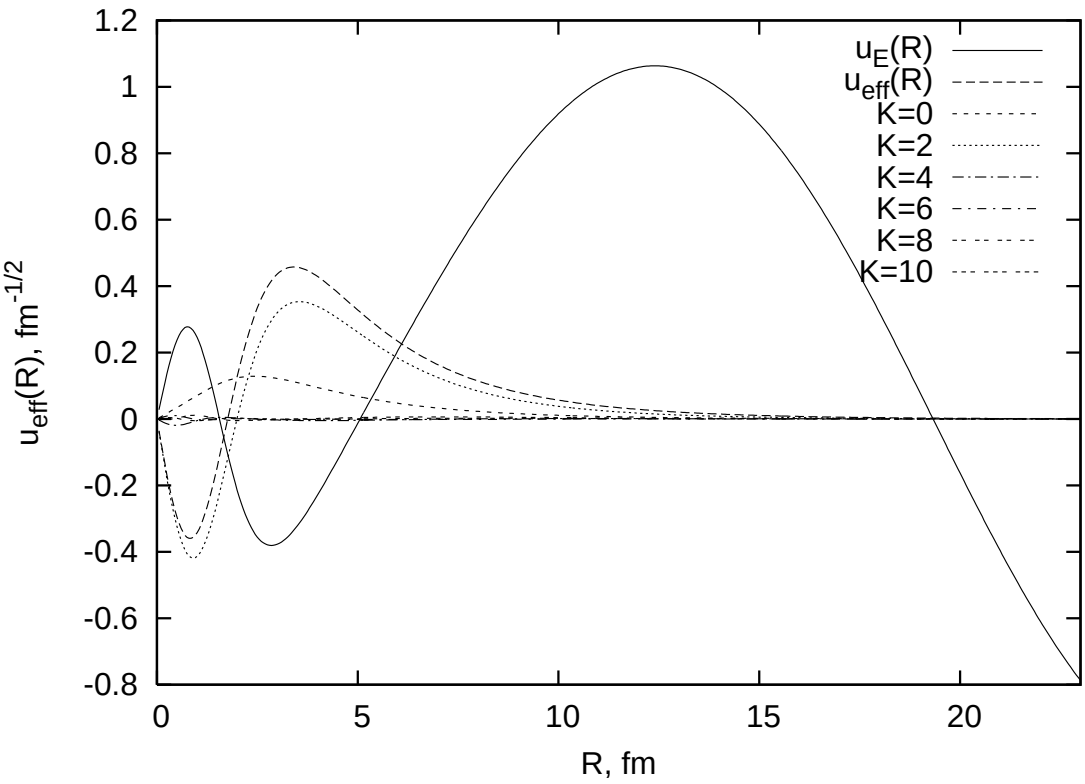

Fig. 4.3. Effective wave functions $u_{\rm eff}^{(K)}(R)$ [Eq. (4.12)] and $u_{\rm eff}(R)$ [Eq. (4.16)] for the $\alpha + d$ potential of Ref. [167] and different K values with $K_{\rm max} = 24$ and $R_{\rm max} = 30$ fm. The scattering wave function u_E at 1 MeV is also represented.

In Fig. 4.5, we display the integral function $I_E = \sum_K I_E^{(K)}$ at the energy $E = 1$ MeV for different potentials: folding potentials V_{f1} and V_{f2}, attractive potential V_a, repulsive Woods-Saxon potential V_r and the potential V_a^{S1} which is obtained by a pair of supersymmetric transformations from the initial potential

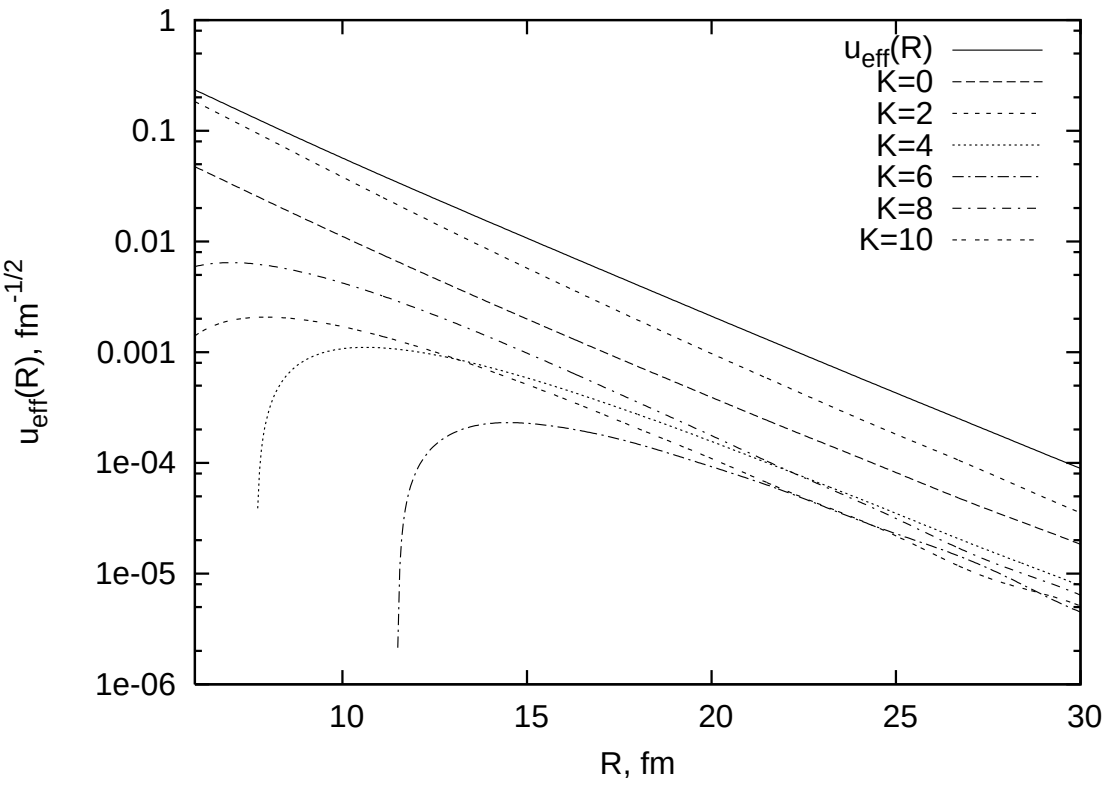

Fig. 4.4. Same as in Fig. 4.3 in logarithmic scale.

V_a [24]. The last potential V_a^{S1} has exactly the same ^{6}Li ground-state energy and the same s-wave phase shift as V_a but its scattering wave functions have one node less at small distances. The effective integral for the repulsive potential displays a strongly different behavior from the integrals for other potentials.

Thus, we find that the $K = 2$ and $K = 8$ components of the three-body hyperspherical wave function of the ^{6}He nucleus give dominant contributions to the integral $I_E(R)$ at large values of R and to the Gamow-Teller reduced transition probability $B_{\rm GT}(E)$. This finding contradicts the statement of the authors of Ref. [100], that the contributions of the $K = 0$ and 2 components are dominant. To show the convergence with respect to the value of maximal hypermomentum $K_{\rm max}$, we display in Fig. 4.6 the corresponding transition probabilities [Eq. (4.3)] for $K_{\rm max} = 2$, 16, 22 and 24 for the potential V_a. The calculation involves 600 integration mesh points with a step of 0.05 fm ($R_{\rm max} = 30$

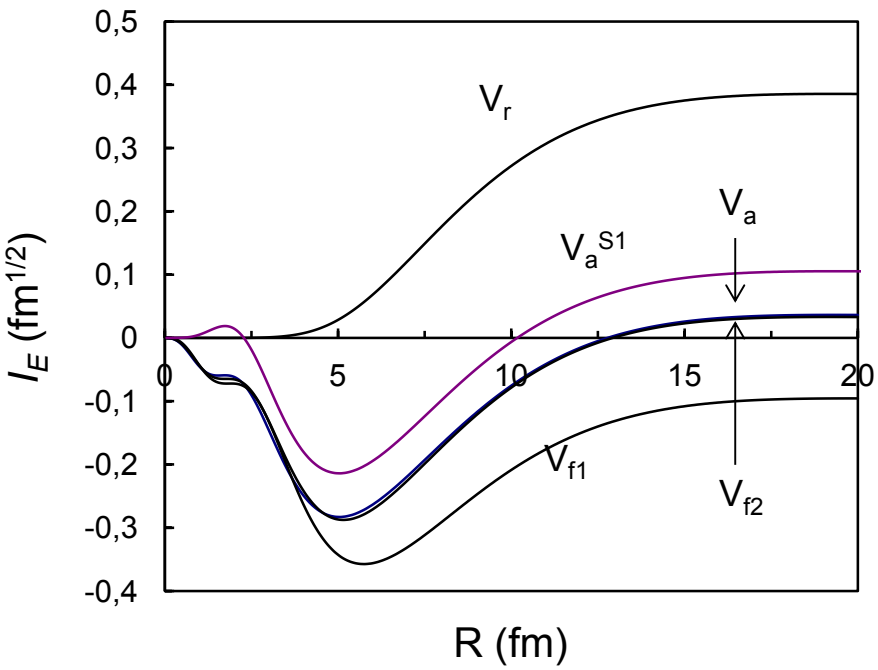

Fig. 4.5. Integrals $I_E(R)$ [Eq. (4.14)] at the energy $E = 1$ MeV for different $\alpha + d$ potentials calculated with $K_{\max} = 24$ and $R_{\max} = 30$ fm.

fm). From Fig. 4.6, we can see that the components with large K values still give contributions to the transition probability. They are especially important at lower energies. However, from the analysis of $I_E(R)$, we already found that the main contributions come from the $K = 2$ and $K = 8$ components.

Additionally, the convergence is faster for the repulsive potential V_r and for the folding potentials V_{f1} and V_{f2}. In the case of V_r, the transition probability for $K_{\max} = 16$ and $K_{\max} = 24$ shows almost the same features but has a larger value. However, even in this case, the choice $K_{\max} = 2$ of the authors of Ref. [100] is not realistic.

In Fig. 4.7, we display the transition probability dW/dE [Eq. (4.11)] obtained with the potential V_a and a fixed $K_{\max} = 24$ fm for different values of

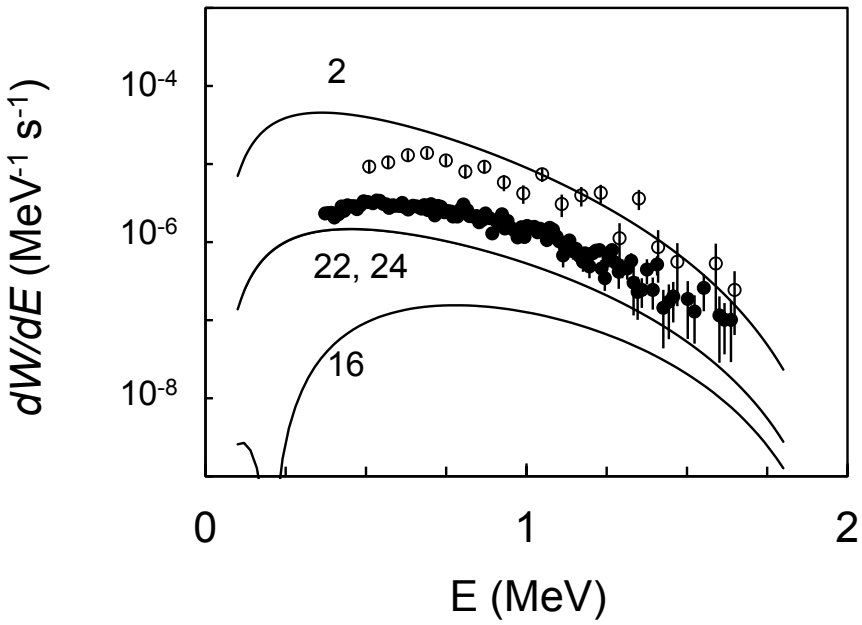

Fig. 4.6. Transition probability per time and energy units dW/dE of the ^{6}He β decay into the $\alpha + d$ continuum with the $\alpha + d$ potential V_a and $R_{\max} = 30$ fm for several values of $K_{\max}$. The experimental data Exp.1 and Exp.2 are from Ref. [93] and [94], respectively.

$R_{\max}$, i.e., 14 fm, 20 fm, 30 and fm. We can see here that convergent results are obtained only beyond $R_{\max} \approx 30$ fm, which means that the extended halo effects are very important in a correct treatment of the low transition probability dW/dE of the ^{6}He β decay into $\alpha + d$.

In Fig. 4.8, we display the transition probability for different potential models with the same $K_{\max} = 24$, and $R_{\max} = 30$ fm. One can see that a good description of experimental data is obtained with the attractive Gaussian potential V_a: the shape of the data is reproduced well, though the theoretical curve is below the data. We modified slightly the parameters of the potential V_a, while keeping the phase shift description (potential V_m in the Fig. 4.1), and obtain

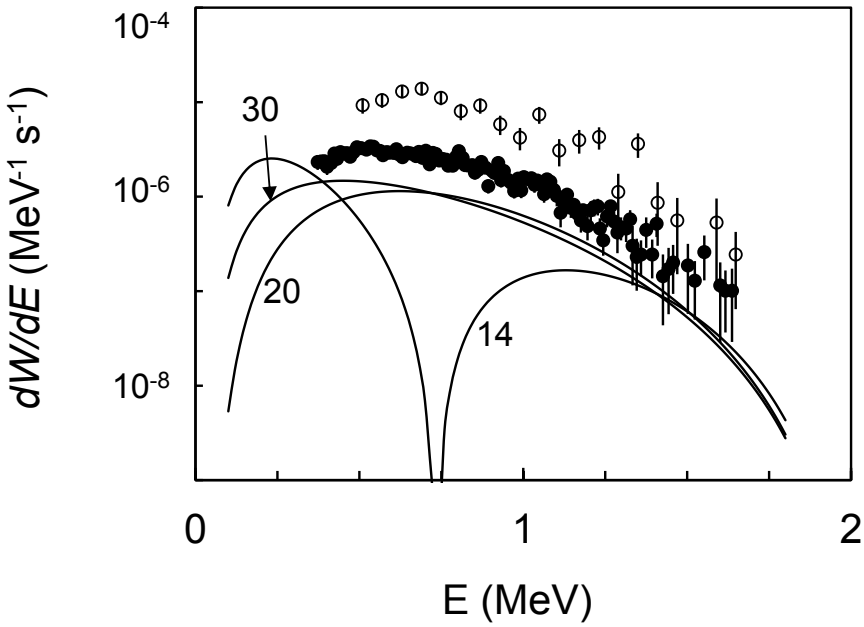

Fig. 4.7. Transition probability per time and energy units dW/dE of the ^{6}He β decay into the $\alpha + d$ continuum with the $\alpha + d$ potential V_a and $K_{\max} = 24$ for several values of $R_{\max}$. The experimental data Exp.1 and Exp.2 are from Ref. [93] and [94], respectively.

the best description of the beta-decay data. The worst results correspond to the repulsive Wood-Saxon potential, which does not give any bound state for ^{6}Li and for which the description of the s-wave phase shift at low energies is poor. The folding potentials V_{f1} and V_{f2} have intermediate behaviors. Potential V_{f1} overestimates the recent data while potential V_{f2} provides a better order of magnitude but its energy dependence disagrees with the experimental one. The success of the deep Gaussian potential could be attributed to the fact that it simultaneously reproduces both the ^{6}Li ground state binding energy and the s-wave phase shift at low energies. However the discussion of Figs. 4.2-4.4 indicates that an important ingredient is the existence of two nodes in u_{eff}. In order

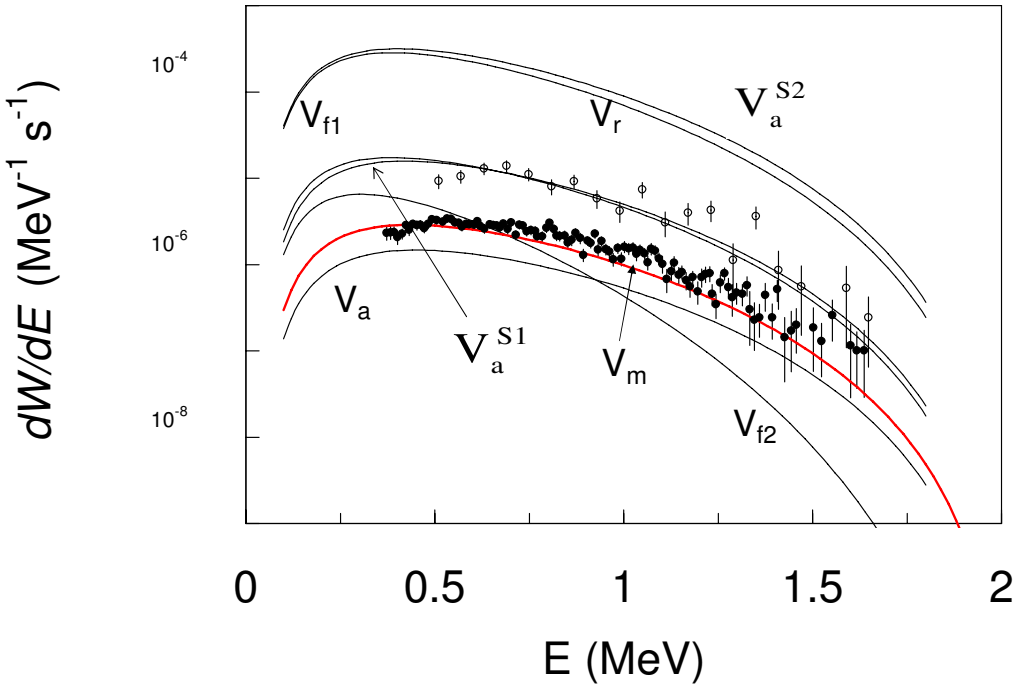

Fig. 4.8. Transition probability per time and energy units dW/dE of the ^{6}He β decay into the $\alpha + d$ continuum for different $\alpha + d$ potentials with $K_{\max} = 24$ and $R_{\max} = 30$ fm. The experimental data are as in Fig. 4.6.

to test this assumption, we remove the non-physical ground state of V_a by using a pair of supersymmetric transformations [24]. The resulting phase-equivalent potential V_a^{S1} yields a scattering wave functions which have one node less at small distances. The resulting dW/dE is about one order of magnitude larger and resembles the one obtained with the folding potential V_{f1} (see Fig. 4.8). Notice however that V_{f1} has two bound states but the phase shifts are not well reproduced. A second phase-equivalent potential V_a^{S2} is obtained by removing the ^{6}Li ground state from V_a^{S1} with another pair of transformations. This repul-

sive potential has still exactly the same phase shifts as V_a but no bound state. Its scattering wave functions have no node near the origin. The corresponding transition probability dW/dE is now very close to the one obtained with potential V_r. The comparaison emphasizes the crucial role played by the forbidden bound state, in addition to the physical ^{6}Li ground state, for reproducing the order of magnitude of the experimental data.

The total transition probabilities for different potentials are given in Table 4.1. The second row contains results corresponding to the experimental cutoff [94]. The values in the last column are derived from the most recent experimental branching ratios and from the ^{6}He half life [94]. As expected from the previous discussion, the result obtained with the Gaussian potential V_a falls within the experimental error bars. The other results are too large, especially with the repulsive potential.

Table 4.1.

Total transition probability per second W (in $10^{-6}s^{-1}$) for the β decay of ^{6}He into $\alpha + d$.

	V_a	V_{f1}	V_{f2}	V_r	V_m	Exp. [94]
$E > 0$ MeV	1.06	13.65	3.15	185	2.04	(2.2 ± 1.1)
$E > 0.37$ MeV	0.84	9.90	1.81	134	1.59	(1.5 ± 0.8)

We have also calculated the Gamow-Teller matrix elements for the β decay to the ^{6}Li ground state. The value $B_{\rm GT} = 4.489\lambda^2$ obtained with a three-body ^{6}Li wave function calculated under the same conditions and with the same nuclear potentials as for ^{6}He is about 5 % below the experimental value $B_{\rm GT}^{(\rm exp)} = 4.745\lambda^2$.

4.3. A comment on R-matrix fits

The R-matrix method has been extended by Barker [103] to the β decay of a halo nucleus. This method has been applied to analyze experimental results [94]. Like in other models, it is crucial in the R-matrix method to take care of the large extension of the halo. Without entering into details which are explained in Refs. [94, 103], this is achieved by introducing external corrections proportional to the integral

$$\hat{I}_E(a) = \int_a^\infty E_i(R) E_f(E,R) dR = \int_a^\infty \frac{u_i(R)}{u_i(a)} \frac{u_E(R)}{u_E(a)} dR, \tag{4.17}$$

where u_E is replaced by its asymptotic expression (4.10). In the model of Ref. [103], the asymptotic form of the two-body α+dineutron system is employed for u_i,

$$u_i^{\alpha+2n}(R) = \exp[-(2\mu_{(12)3}|E_B|/\hbar^2)^{1/2} R]. \tag{4.18}$$

However, three-body asymptotics are rather different from this expression. In Eq. (4.11), this role is played by the effective radial wave function u_{eff} defined by Eq. (4.16). In order to avoid the knowledge of three-body wave functions, we test here an expression,

$$u_i^{\alpha+n+n}(R) = \int_0^\infty u_d(r) \rho^{-5/2} \exp[-(2m_N|E_B|/\hbar^2)^{1/2} \rho] dr, \tag{4.19}$$

which is the projection of three-body asymptotics [67,174] on the deuteron wave function.

In Table 4.2, we present for different values of the channel radius the correction (4.17) calculated with $u_i^{\alpha+2n}$, $u_i^{\alpha+n+n}$, and u_{eff} at two typical energies. One observes that the integrals obtained with the two-body asymptotic expression

Table 4.2.

Correction integrals (4.17) in R-matrix fits: $I_E^{\alpha+2n}$, $I_E^{\alpha+n+n}$, and $I_E^{\rm eff}$ are calculated with $u_i^{\alpha+2n}$, $u_i^{\alpha+n+n}$, and $u_{\rm eff}$ [Eq. (4.16)], respectively, as a function of the channel radius a and of the relative energy E.

E (MeV)	a (fm)	$\hat{I}_E^{\alpha+2n}$	$\hat{I}_E^{\alpha+n+n}$	$\hat{I}_E^{\rm eff}$
0.5	4.0	−0.022	−1.546	−1.402
	4.5	0.232	0.427	0.669
	5.0	4.585	2.756	2.981
	5.5	6.285	4.897	5.059
	6.0	6.900	6.255	6.345
1.0	4.0	−2.478	−0.761	−1.153
	4.5	−4.379	−2.808	−3.143
	5.0	−5.672	−4.606	−4.830
	5.5	−5.892	−5.592	−5.707
	6.0	−4.768	−5.333	−5.365

(4.18) are rather far from the realistic values obtained with $u_{\rm eff}$, even for $a = 6$ fm. Hence, using this approximation in R-matrix fits may significantly distort the energy shape of the β delayed deuteron spectrum. A better approximation is given by the three-body asymptotic expression (4.19), especially at higher relative energies. However channel radii such as 4 fm or smaller should be avoided.

4.4. Conclusion

In the present Chapter, we studied the β decay process of the ^{6}He halo nucleus into the $\alpha + d$ continuum in the framework of a three-body model.

Three-body hyperspherical bound-state wave functions on a Lagrange mesh and two-body $\alpha+d$ scattering wave functions have been used. For the calculation of the transition probabilities per time and energy units of the β decay, several $\alpha+d$ potentials were tested: an attractive Gaussian potential [167] and it's slightly modified version with a deep forbidden bound state, folding potentials derived from the $\alpha + N$ p-wave potential of Ref. [168], and a repulsive potential [100].

The low experimental values result from a strong cancellation in the Gamow-Teller matrix element describing the transition to the continuum. This cancellation occurs between the internal and halo parts of the matrix element [101] and is thus very sensitive to the halo description. Reaching convergence is not easy: the two-body and three-body wave functions must extend up to 30 fm. From the analysis of the theoretical results we have found that converged results require the large value $K_{\max} = 24$ of the maximal hypermomentum. The dominant contributions to the transition probability come from $K = 2$, $K = 8$, and $K = 10$ components of the three-body hyperspherical wave function. The contribution of the $K = 0$ component is small due to an almost perfect cancellation of the internal and external parts of the Gamow-Teller matrix element.

The experimental transition probabilities per time and energy units [94] are well described with the deep Gaussian potential of Ref. [167] (energy dependence) and it's modified version (energy dependence and magnitude) which fairly reproduce the ^{6}Li binding energy and the s-wave $\alpha + d$ phase shifts. The quality of the agreement arises from the node structure of the initial and final wave functions in the internal part. With the help of phase-equivalent potentials derived with supersymmetric transformations, we have shown that the role of the forbidden state is also essential. We realize that the efficiency of the deep potential may be somewhat fortuitous but the existence of a good agreement with experiment shows which ingredients are crucial in the interpretation of the β delayed deuteron decay of ^{6}He.

Our results allow testing the validity of corrections necessary in the R-matrix

method [103]. We have shown that, in order to avoid some systematic bias in the integrals over the external region, the two-body asymptotics could usefully be replaced by three-body asymptotics.

Further progress must come from fully microscopic consistent descriptions of the bound and scattering states. The results obtained with a microscopic cluster model [104] still agree qualitatively with the most recent data [94] but overestimate them by about a factor of two. Progress may be expected from the possibility of calculating ^{6}He wave functions ab initio from realistic two- and three-body forces. However the present study shows that an accurate description of the β delayed deuteron emission will require very accurate bound-state wave functions up to distances as large as 30 fm and a development of consistent scattering wave functions. The accidental cancellation occurring in this process will make a successfull ab initio description particularly difficult.

V. GAMMA-DELAYED DEUTERON EMISSION OF THE ^{6}Li$(0^+;1)$ HALO STATE

In this chapter we study the M1-transitions from the ^{6}Li(0^+) isobar-analog state to the $\alpha + d$ continuum, and to the ^{6}Li(1^+) ground state [110]. [1] For the description of the ^{6}Li states, we use different two-body and three-body models. Three-body hyperspherical wave functions [63] are based on the Lagrange-mesh method and give an accurate solution of the three-body Schrödinger equation (see chapter 4 and Ref. [67] for details). They have been calculated by the Belgian group (D. Baye, P. Descouvemont, etc.). The $\alpha + d$ scattering wave function is factorized into a deuteron wave function and a nucleus-nucleus scattering state as was done in chapter 5. First we will develop the three-body model of the M1-transition process. The details of the model and matrix elements of the M1-transition operator in the three-body system are given in Appendices D and E. Then we describe the potentials and the corresponding two-body and three-body wave functions. At last we discuss the numerical results in comparison with the experimental data, and analyze the sensitivity with respect to the $\alpha + d$ potential.

5.1. Model

5.1.1. Three-body wave functions of ^{6}Li bound states

The ^{6}Li bound-state wave functions are defined in an $\alpha + n + p$ model using the hyperspherical coordinates [63]in the same way as was done in previous

[1] This chapter is based on the results of Refs. [106, 110]

chapters. A set of Jacobi coordinates for three particles with mass numbers $A_1 = 1$, $A_2 = 1$, and $A_3 = 4$ is defined as (see Eq. (2.2)

$$\boldsymbol{x} = \sqrt{\mu_{pn}}\,\boldsymbol{r}, \qquad \boldsymbol{y} = \sqrt{\mu_{\alpha d}}\,\boldsymbol{R}, \tag{5.1}$$

where the (dimensionless) reduced masses are given by $\mu_{pn} = 1/2$ and $\mu_{\alpha d} = 4/3$,

$\boldsymbol{r}$ and $\boldsymbol{R}$ are $p - n$ relative coordinate and the coordinate between α and d, respectively. Equations (5.1) define six coordinates which are transformed to the hyperspherical coordinates as (see Eq. (3.2))

$$\rho^2 = x^2 + y^2, \qquad \alpha = \arctan(y/x), \tag{5.2}$$

where α varies between 0 and $\pi/2$. With the angular variables $\Omega_x = (\theta_x, \varphi_x)$ and $\Omega_y = (\theta_y, \varphi_y)$, equations (5.2) define a set of hyperspherical coordinates which are known to be well adapted to the three-body Schrödinger equation.

We define $\gamma = (\ell_x, \ell_y, L, S)$ where ℓ_x and ℓ_y are the orbital momenta associated with the Jacobi coordinates $\boldsymbol{x}$ and $\boldsymbol{y}$, respectively. With the notation $\Omega_5 = (\alpha, \Omega_x, \Omega_y)$, a three-body wave function with spin J and parity π reads (see chapters 4, 5 and Ref. [67])

$$\Psi^{JM\pi}_{^6\mathrm{Li}}(\rho, \Omega_5) = \rho^{-5/2} \sum_{\gamma K} \chi^{J\pi}_{\gamma K}(\rho) \mathcal{Y}^{JM}_{\gamma K}(\Omega_5), \tag{5.3}$$

where $\mathcal{Y}^{JM}_{\gamma K}(\Omega_5)$ are the hyperspherical functions (including spin). The three-body wave functions contain components with total intrinsic spin $S = 0$ and $S = 1$. Because of the positive parity, $\ell_x + \ell_y$ is even and only even K values are involved.

5.1.2. $\alpha + d$ two-body wave functions

As it was done in Ref. [105] and in chapter 5 for the ^{6}He β decay, the scattering $\alpha + d$ wave functions are factorized into a deuteron ground-state wave

function, calculated with an appropriate NN potential, and an $\alpha+d$ wave function derived from a potential model. We neglect the small D component of the deuteron. In the $\alpha+d$ exit channel, only S waves are involved. Consequently, the final 1^+ wave function reads [110]

$$\Psi_{\alpha d}^{1M+}(E,\boldsymbol{r},\boldsymbol{R}) = \Psi_d(\boldsymbol{r})\,\Psi_{\alpha d}(E;\boldsymbol{R}). \tag{5.4}$$

The spatial part of the deuteron wave function is written as

$$\Psi_d(\boldsymbol{r}) = r^{-1}\,u_d(r)\,Y_{00}(\hat{\boldsymbol{r}}). \tag{5.5}$$

The S-wave component of the $\alpha+d$ relative motion wave function is factorized as [110]

$$\Psi_{\alpha d}(E;\boldsymbol{R}) = R^{-1}\,u_E(R)\,Y_{00}(\hat{\boldsymbol{R}}). \tag{5.6}$$

The normalization of the scattering wave function is fixed by the asymptotic behavior as

$$u_E(R) \underset{R\to\infty}{\longrightarrow} F_0(k_{\alpha d}R)\cos\delta_0(E) + G_0(k_{\alpha d}R)\sin\delta_0(E), \tag{5.7}$$

where F_0 and G_0 are the Coulomb functions,

$k_{\alpha d}$ is the wave number of the relative motion,

$\delta_0(E)$ is the s-wave phase shift at energy E.

The present two-body model can also be applied to $\alpha+d$ bound states. In that case, the scattering wave function $u_E(R)$ in Eq. (5.6) is replaced by an S-wave bound-state radial function.

5.1.3. Transition probability per time and energy units

For the M1 transition to the ground state, the gamma-width is calculated from [110]

$$\Gamma_\gamma(0^+\to 1^+) = \frac{16\pi}{9}\,k_\gamma^3\,|\langle\Psi_{^6\mathrm{Li}}^{1^+}||\mathcal{M}_1^M||\Psi_{^6\mathrm{Li}}^{0^+}\rangle|^2, \tag{5.8}$$

where k_γ is the wave number of the emitted photon. This definition involves bound-state wave functions on both sides.

With the normalization (5.7) of the scattering wave function, the M1 transition probability of the process

$$^6\mathrm{Li}(0^+) \rightarrow \alpha + d + \gamma, \tag{5.9}$$

per time and energy units, is given by reduced matrix elements between the initial bound state and the final scattering states as [110] (see Appendix 4)

$$\frac{dW_\gamma}{dE} = \frac{32\mu_{ad} m_N}{3\hbar^3 k_{\alpha d}} k_\gamma^3 \, |\langle \Psi^{1^+}_{\alpha d}(E) || \mathcal{M}^M_1 || \Psi^{0^+}_{^6\mathrm{Li}} \rangle|^2, \tag{5.10}$$

where m_N is the nucleon mass. The maximum $\alpha + d$ energy is $Q = 2.089$ MeV. The M1 differential gamma-width per energy unit to continuum states is expressed as

$$\frac{d\Gamma_\gamma(0^+ \rightarrow \alpha + d)}{dE} = \hbar \, \frac{dW_\gamma}{dE}, \tag{5.11}$$

and the total width is deduced by integration over the energy.

The M1 operator contains orbital and spin-dependent components. For a general three-body system, it reads, in Jacobi coordinates [67]

$$\mathcal{M}^M_{1\mu}(\boldsymbol{x}, \boldsymbol{y}) = \mu_N \sqrt{\frac{3}{4\pi}} [A_x \ell_{x,\mu} + A_y \ell_{y,\mu} + A_{xy} (\boldsymbol{x} \times \boldsymbol{p_y} + \boldsymbol{y} \times \boldsymbol{p_x})_\mu + \sum_{i=1}^{3} g_s(i) \boldsymbol{s}_{i\mu}], \tag{5.12}$$

where $\mu_N = e\hbar/m_N c$ is the nuclear magneton,

$g_s(i)$ their gyromagnetic factors,

$\boldsymbol{s}_i$ are the spins of the three particles.

Coefficients A_x, A_y and A_{xy} are related to the mass and charge numbers as

$$A_x = \frac{Z_2 A_1^2 + Z_1 A_2^2}{A_1 A_2 A_{12}}, A_y = \frac{(Z_1 + Z_2) A_3^2 + Z_3 A_{12}^2}{A A_{12} A_3}, A_{xy} = \sqrt{\frac{A_1 A_2 A_3}{A_{12}^2 A}} \left(\frac{Z_1}{A_1} - \frac{Z_2}{A_2} \right), \tag{5.13}$$

where A_{12} is the reduced mass of the $1+2$ system; in the present case it is denoted as μ_{pn}. Variables $\boldsymbol{p_x}$ and $\boldsymbol{p_y}$ are the momenta associated with the Jacobi coordinates $\boldsymbol{x}$ and $\boldsymbol{y}$, respectively. The matrix elements of the M1 operator between hyperspherical functions are given in appendix 5.

5.2. Results and discussion

5.2.1. Conditions of the calculations

Three-body wave functions of the 1^+ and 0^+ states

The initial 0^+ wave function is calculated in an $\alpha + n + p$ three-cluster model, using hyperspherical coordinates, as explained in Ref. [67]. The same model is applied to the ^{6}Li ground state. In both cases, the Coulomb $\alpha + p$ interaction is included, and is taken as a point-sphere potential parameterized as $V_C(r) = 2e^2 \mathrm{erf}(r/R_C)$ with a radius $R_C = 1.2$ fm. Two-body forbidden states are removed by using the Orthogonalising Pseudopotential method [135]. The central Minnesota interaction [152] describes the $n+p$ system. It is adjusted on the deuteron binding energy and reproduces fairly well nucleon-nucleon phase shifts at low energies. For the $\alpha+N$ nuclear interaction we employ the potential of Voronchev *et al.* [168], slightly renormalized by a scaling factor (1.008 for 1^+ and 1.043 for 0^+) to reproduce the experimental energies with respect to the three-body threshold (-3.70 MeV for the ground state, and -0.13 MeV for the

0^+ state). We truncate the hypermomentum expansion to $K_{max} = 20$ which ensures a good convergence of the energies.

The matter r.m.s. radius of the ground state (with 1.4 fm as α radius) is found as $\sqrt{< r^2 >} = 2.25$ fm, a value slightly lower than the experimental value (2.32 ± 0.03 fm [162]) (note however that a significantly larger radius, 2.54 ± 0.03 fm, was found in Ref. [175]). For the excited 0^+ level, we find $\sqrt{< r^2 >} = 2.56$ fm, which is close to the ^{6}He radius. This large value confirms the halo structure of this state [176]. The ground state is essentially $S = 1$ (96.0%). The $S = 0$ component is 84.4% for ^{6}Li(0^+) and 82.1% for ^{6}He. The ^{6}Li(0^+) and ^{6}He hyperradial wave functions are plotted in Fig. 5.1 for the dominant $K = 0, 2$ hypermoments.

According to charge symmetry the short-range parts of the ^{6}He and ^{6}Li(0^+) analog levels should be very close to each other. This is confirmed by Fig. 5.1. On the contrary, the halo components of both wave functions are expected to differ significantly: the charges of the halo nucleons are different, and the binding energy of ^{6}Li(0^+) is much lower. Consequently, the asymptotic decrease of the wave function is slower, and matrix elements involving this long-range part should be different from their analogs in ^{6}He.

$\alpha + d$ scattering states

In the following we use the same $\alpha + d$ potentials from Chapter IV (the phase shifts are given Fig. 4.1): the attractive Gaussian potential of Ref. [167] V_a, two folding potentials V_{f1} and V_{f2}, and a potential V_a^{S1}, obtained from a supersymmetric transformation [24] from the deep potential V_a. The last potential gives the same phase shifts and the same ground-state energy as the initial potential V_a, but the forbidden state is removed and the role of the Pauli principle is simulated by a short-range core. It is used in order to test the influence of the short-range part of the $\alpha + d$ wave functions, and in particular

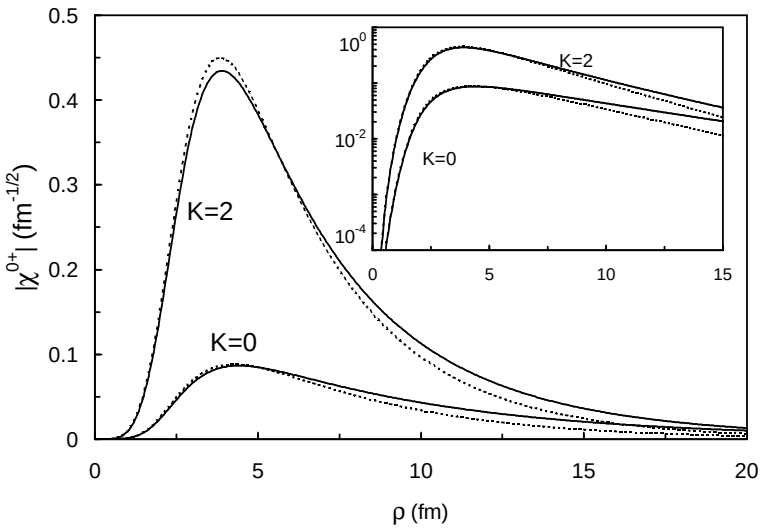

Fig. 5.1. Hyperradial wave functions for ^{6}Li(0^+) (solid lines) and ^{6}He (dashed lines) corresponding to $S = L = 0, K = 0, 2$. The insert shows the same plot in a logarithmic scale.

of the node location.

The folding potential V_{f1} yields the correct binding energy for ^{6}Li, however the quality of the S-wave phase shift is poor. The folding potential V_{f2} describes the S-wave phase shift accurately (see Fig. 4.1), but overestimates the binding energy of the ^{6}Li ground state (-2.386 MeV).

In all cases, the $\alpha + d$ Coulomb potential is chosen as in Ref. [167], i.e. as a bare Coulomb potential.

5.2.2. $M1$ properties of bound states

A test of three-body wave functions is provided by M1 spectroscopic properties, which are well known experimentally [153]. In Table 5.1, we present the calculated values of the magnetic moment and of the B(M1) in ^{6}Li. Separate contributions are given for the orbital and spin terms of the M1 operator [see Eq. (5.12)]. In both cases, the contribution of the orbital term is small since the

dominant component in the ground-state wave function is an S wave. The main contribution to the M1 matrix element comes from the spin term. The present matrix element corresponds to $B(M1) = 7.9$ W.u., or $\Gamma_\gamma = 7.5$ eV, which are in good agreement with experiment (8.62 ± 0.18 W.u. and 8.19 ± 0.17 eV, respectively). The results are also close to those of Kukulin *et al.* [177] who use different variants of a three-body model. These matrix elements can also be

Table 5.1.

Contributions (in μ_N) of the orbital (L) and spin (S) components to the M1 matrix elements. The three-body model is used for the 0^+ state. Experimental data are taken from [153].

	(L)	(S)	Sum	Exp.
Three-body model for 1^+				
$\mu(^6\mathrm{Li})$	0.02	0.84	0.86	0.82
$\langle \Psi^{1^+}_{^6\mathrm{Li}} \| \mathcal{M}^M_1 \| \Psi^{0^+}_{^6\mathrm{Li}} \rangle$	0.13	2.04	2.17	2.28
Two-body model for 1^+				
$\mu(^6\mathrm{Li})$	0	0.88	0.88	0.82
$\langle \Psi^{1^+}_{^6\mathrm{Li}} \| \mathcal{M}^M_1 \| \Psi^{0^+}_{^6\mathrm{Li}} \rangle$	0.04	1.53	1.57	2.28

obtained with a 2-body description of the ^{6}Li ground state. In that case we use the potential V_a to generate the wave functions. Since components with $L \neq 0$ are small in the ground-state wave function, the two-body model is expected to be a good approximation. The 1^+ magnetic moment in the two-body model is a simple sum of the proton and neutron magnetic moments. In this case, both approaches provide similar results, in good agreement with experiment. However the rms radius in the two-body model is $\sqrt{< r^2 >} = 2.11$ fm, lower than experiment and than the three-body value. In addition, the M1 transition matrix element (see Table 5.1) provides $\Gamma_\gamma = 3.9$ eV, i.e. an underestimate of

the experimental value. These results suggest that the short-range part of the two-body description is too simple. However, transitions to the continuum are more sensitive to the long-range part of the $\alpha - d$ wave functions.

5.2.3. M1-transition to the $\alpha + d$ continuum: effective wave functions and their integrals

Since the $\alpha + d$ relative motion is described by S waves, the first and second orbital terms of the M1 transition operator (5.12) do not contribute to the reduced matrix elements for transitions to the $\alpha + d$ continuum. The orbital and spin terms yield nonzero matrix elements only for the $\ell_x = \ell_y = L = S = 1$ and $\ell_x = \ell_y = L = S = 0$ components of the three-body wave function, respectively. As it will be shown further, the main contribution comes from the spin part of the transition operator. The P-wave hyperspherical components give small corrections to the process since the 0^+ state is essentially $S = 0$.

In order to analyze the γ decay process to the continuum, we introduce effective wave functions and their integrals, in analogy with the β decay study of the ^{6}He halo nucleus into the $\alpha + d$ continuum [105]. We restrict the presentation to the dominant spin part. For the initial 0^+ state, let us define the effective wave function with hypermomentum K

$$u_{\text{eff}}^{(K)}(R) = \left(\frac{A-2}{A}\right)^{3/4} R \int dr\, \phi_K^{00}(\alpha)\, \frac{\chi_{0000K}^{0^+}(\rho)}{\rho^{5/2}} r u_d(r), \tag{5.14}$$

and the effective integrals

$$I_E^{(K)}(R) = \int_0^R dR'\, u_E(R') u_{\text{eff}}^{(K)}(R'), I_E(R) = \sum_K I_E^{(K)}(R), \tag{5.15}$$

where ρ and α depend on (r, R), as given in Eq. (5.2). The normalization factor in Eq. (5.14) arises from the Jacobian between the $(\boldsymbol{R}, \boldsymbol{r})$ and $(\boldsymbol{x}, \boldsymbol{y})$ coordinates. The reduced matrix elements of the M1 operator (spin part) are then directly proportional to $I_E(R)$ (see Appendix 5).

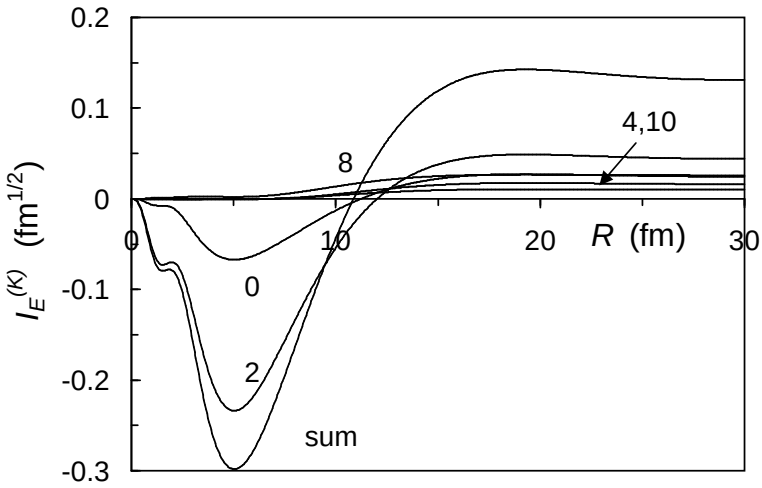

Fig. 5.2. Integrals $I_E^{(K)}(R)$ [Eq. (5.15)] at $E = 1$ MeV for the $\alpha + d$ potential V_a and different K values (labels).

In the following, we analyze two properties: the convergence of the hypermomentum expansion, and the sensitivity of the effective integrals with respect to the $\alpha + d$ potential. Let us start with the influence of $K_{\max}$. In Fig. 5.2 we show the integrals $I_E^{(K)}(R)$ calculated at $E = 1$ MeV with potential V_a, for different K-values. The dominant contribution at large R values comes from the $K = 0, 2, 8$ components in the ^{6}Li(0^+) wave function. The components $K = 4$ and $K = 10$ give smaller and comparable effects to the process. The contributions of other components are small and not visible at the scale of the figure. Similar results were obtained for the β decay of ^{6}He [105]. In Ref. [105] it was shown that the $K = 4$ and $K = 6$ contributions are affected by cancellation effects, which do not occur for $K \geq 8$. The situation is therefore very close to the ^{6}He(0^+) beta-decay [105] into the $\alpha + d$ continuum which confirms the halo structure of the ^{6}Li(0^+) state, suggested by its large r.m.s. radius.

In the second step, we analyze the sensitivity of the effective integrals with respect to the potential. In Fig. 5.3, these integrals are shown at $E = 1$ MeV. The potentials V_a and V_{f2}, which provide similar phase shifts and wave functions, give results close to each other. This is due to the similar node positions near 5 fm of the corresponding scattering wave functions. The folding potential V_{f1}, owing to a poor phase-shift description, yields a scattering wave function with an inner node shifted to the right (about 0.7 fm), and therefore provides a different integral.

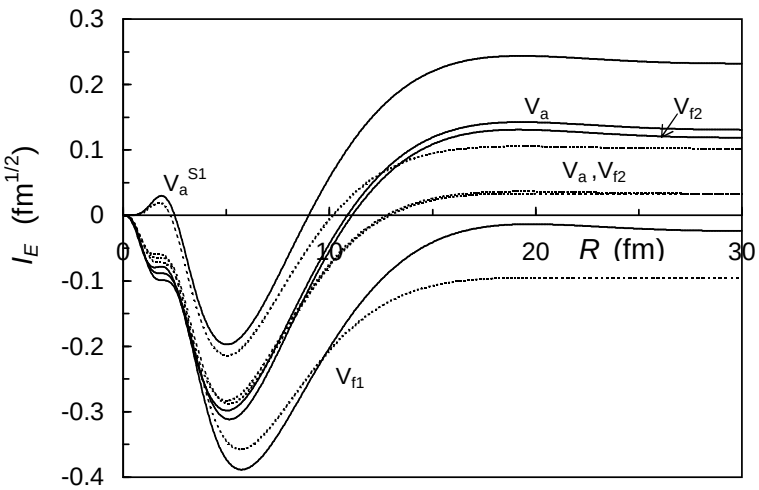

Fig. 5.3. Effective integrals $I_E(R)$ [Eq. (5.15)] at $E = 1$ MeV for different $\alpha + d$ potentials (solid lines). Dotted lines represent the equivalent integrals for the ^{6}He β decay [105].

In Fig. 5.3, we also show as dotted lines, for each potential, the effective integrals obtained for the ^{6}He β decay [105] (notice that in Ref. [105], the factor $((A-2)/A)^{3/4} = 0.74$ in the effective wave function was missing). In that work, we have shown that a node in the $\alpha + d$ continuum wave functions is responsible for a nearly perfect cancellation effect in the β decay matrix element. This is illustrated in Fig. 5.3: for the recommended potential V_a, the internal contribution to the matrix element is about -0.30 whereas the external term is about $+0.35$. The final result is therefore much lower than each component

individually. This phenomenon yields a strong sensitivity of the β spectrum with respect to the $\alpha + d$ potential.

Coming back to the γ decay of the ^{6}Li analog level (solid lines in Fig. 5.3), the internal parts of the matrix elements are very close to their ^{6}He counterparts up to about 10 fm. However, as the long-range parts of the wave functions are different in both nuclei, the external contribution to the γ decay matrix element is significantly larger (about +0.42 for V_a). Consequently, a cancellation effect still occurs, but is less important. If we disregard potential V_{f1} which does not reproduce the $\alpha + d$ phase shifts, and hence the correct location of the nodes in the continuum wave functions, all potentials provide the same sign for the matrix element.

5.2.4. M1-transitions to the $\alpha + d$ continuum: transition probabilities

In Table 5.2 we give the contributions of different K values to the M1 reduced matrix element into the $\alpha + d$ continuum. As we noted above, the orbital and spin parts of the M1 transition operator yield nonzero matrix elements only with the $\ell_x = \ell_y = L = S = 1$ (P-wave) and $\ell_x = \ell_y = L = S = 0$ (S-wave) components of the three-body wave function, respectively. As expected from the previous analysis, the dominant contributions come from the $K = 0, 2$ and 8 components. Additionally, the contribution of the orbital part of the M1 transition operator is strongly suppressed (2% at most).

To analyze the convergence with respect to the upper bound $R_{\max}$ [see Eq. (5.15)], we display in Fig. 5.4 the differential width $d\Gamma_\gamma/dE$ for several values of $R_{\max}$ (potential V_a is used). From Fig. 5.4, one can see that $R_{\max} = 10$ fm is far from sufficient. Achieving a precise convergence requires larger values ($\sim 25 - 30$ fm), as in the beta-decay calculations of the ^{6}He halo nucleus into

Table 5.2.

Contribution of different ^{6}Li(0^+) hypermomenta to the M1 reduced matrix elements for transitions into the $\alpha + d$ continuum (in $10^{-3}\mu_N$) for the orbital (L) and spin (S) terms at several energies

	$E = 0.5$ MeV		$E = 1$ MeV		$E = 1.5$ MeV	
K	(L)	(S)	(L)	(S)	(L)	(S)
0	0	-56.9	0	-54.2	0	-46.4
2	0.5	-85.9	0.6	-104.9	0.4	-115.6
4	3.1	-36.3	4.5	-31.0	5.2	-21.0
6	1.5	-11.4	2.1	-4.9	2.2	1.4
8	-1.2	-51.1	-1.6	-61.6	-1.7	-61.3
10	-0.3	-22.2	-0.3	-23.1	-0.3	-20.0
> 10	0.3	-21.2	0.4	-14.5	0.4	-7.3
Sum	3.9	-285.0	5.7	-294.2	6.2	-270.2

the $\alpha+d$ continuum [105]. This is not surprising as the halo structure of ^{6}Li(0^+) is even more pronounced (see Fig. 5.1).

In Fig. 5.5, we display the differential width $d\Gamma_\gamma/dE$ for several $\alpha+d$ potentials. Contributions from three-body components up to $K_{\max} = 20$ are taken into account with the maximal relative distance $R_{\max} = 30$ fm. The folding potential V_{f1} shows a picture strongly different from the other ones, with even a sharp minimum at about $E = 0.8$ MeV. This potential gives a poor description of the $\alpha + d$ phase shift (see Ref. [105]) and hence a shifted node position for the $\alpha + d$ scattering wave function. This results in a strong cancellation effect as explained in the previous section. The folding potential V_{f2} and the deep potential V_a give close results and the supersymmetric potential V_a^{S1} slightly overestimates them.

The integrated γ widths (from $E = 0$ up to $Q = 2.089$ MeV) are given in

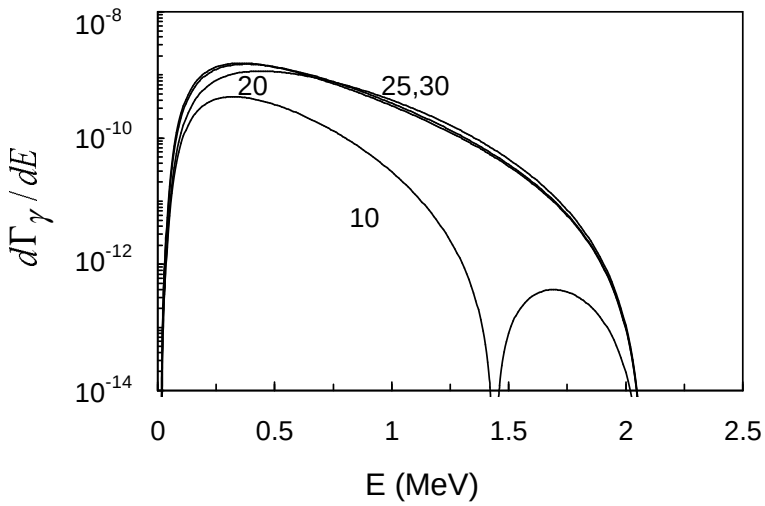

Fig. 5.4. Differential width for M1 transitions into the $\alpha + d$ continuum with the $\alpha + d$ potential V_a for several values of $R_{\max}$ (in fm).

Table 5.3 for the different potentials. The Gaussian potential V_a simultaneously reproduces both the ^{6}Li ground state binding energy and the S-wave phase shift at low energies. Additionally, the S-wave scattering wave function of this potential has two nodes at short distances (one due to the ground state, and one due to the Pauli forbidden state). The nearly phase-equivalent potential V_{f2}, which also has a forbidden bound state (and hence two nodes at short distances) gives similar results.

The influence of the nodes in the scattering wave function can be tested by using potential V_a^{S1}. The non-physical ground state of V_a is removed by using a supersymmetric transformation [24]. The resulting phase-equivalent potential V_a^{S1} has exactly the same ^{6}Li ground-state energy and the same S-wave phase shift as V_a but its scattering wave functions have one node less at small distances. The corresponding width of the M1 transition is about two times larger (see Table 5.3). In the ^{6}He β decay process, this potential strongly overestimates the data [105]. Notice that a very different result is obtained with the folding potential V_{f1}, which has two bound states, but does not reproduce

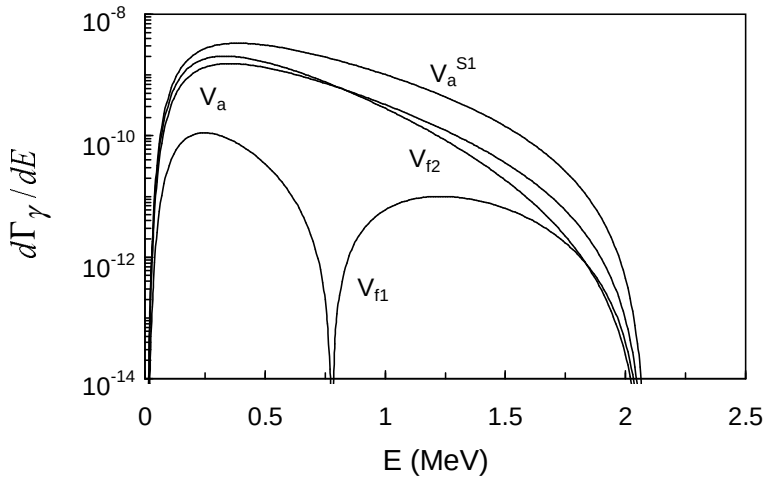

Fig. 5.5. Differential width for M1 transitions into the $\alpha + d$ continuum for several potentials.

the $\alpha + d$ phase shifts and the ^{6}He delayed β decay. The shape and magnitude of the transition width and probability are strongly different from the result for V_a.

Table 5.3.

Integrated γ widths for different potentials, and branching ratio $BR = \Gamma_\gamma(0^+ \to \alpha + d)/\Gamma_\gamma(0^+ \to 1^+)$ (we use the theoretical value $\Gamma_\gamma(0^+ \to 1^+) = 7.5$ eV).

potential	Γ_γ (meV)	BR
V_a	0.90	1.2×10^{-4}
V_{f1}	0.04	5.3×10^{-6}
V_{f2}	1.08	1.4×10^{-4}
V_a^{S1}	2.27	3.0×10^{-4}

Considering the V_a and V_{f2} potentials, which are consistent with the data on ^{6}He β decay, we deduce a recommended branching ratio of 1.3×10^{-4} by

averaging both values. A previous estimate [108] of the branching ratio $\Gamma_\gamma(0^+ \to \alpha + d)/\Gamma_\gamma(0^+ \to 1^+)$ provides 0.8×10^{-4}. This value is close to our results obtained with potential V_a [167], and is also similar to the branching ratio observed in the β decay of ^{6}He [94]. Such a branching ratio should be observable experimentally.

5.3. Conclusion

In the present chapter, we have studied the M1 transition process from the ^{6}Li(0^+) halo state into the $\alpha + d$ continuum and into the ^{6}Li(1^+) ground state. Our goal was twofold: (i) to determine the energy distribution of the γ width for the decay into the continuum, and to analyze its sensitivity with respect to the $\alpha+d$ potential; (ii) to compare the results of M1- process study with the results of the chapter 4 on the ^{6}He β delayed decay. This comparison is a good tool to test charge symmetry in exotic nuclei. The ^{6}Li$(0^+, 1^+)$ states are defined in the three-body hyperspherical formalism. The experimental magnetic moment of the ground state and γ width of the $0^+, T = 1$ state are reproduced with a good accuracy.

We have shown that the spin-dependent term of the M1 transition operator gives the essential part of the matrix elements. In order to test the influence of the ^{6}Li bound-state wave functions, we have also used the supersymmetric transform [24] instead of the Orthogonalising Pseudopotential method for the removal of forbidden states in the three-body wave functions. The results are very similar to the present ones, and were therefore not shown.

In the M1 transition probability, the $K = 0$ and $K = 2$ components of the three-body wave function provide about 50% of the matrix elements; consequently, higher hypermomenta play an important role. The same conclusion holds in the ^{6}He β decay into the $\alpha+d$ continuum, where large K values cannot

be neglected.

M1 transitions to the continuum provide a good probe of the halo structure in the ^{6}Li(0^+) state. The comparison with the ^{6}He β decay shows that the inner parts of the matrix elements are very close to each other, as expected from charge symmetry. However, the halo parts are different, owing to the different binding energies, and different charges of the halo nucleons. In ^{6}Li, the binding energy is lower, and therefore the asymptotic decrease of the wave function is slower. Consequently the halo contribution is larger in the γ decay matrix element, and even represents the dominant part. This leads to the conclusion that charge-symmetry breaking is rather strong in these processes. The nearly perfect cancellation effect between short-range and halo contributions observed in ^{6}He β decay is less important here, and the sensitivity with respect to the potential is therefore weaker. Several $\alpha + d$ potentials were tested. The sensitivity is still important (about a factor of 2), but lower than in the ^{6}He β delayed decay.

The present branching ratio of about 1.3×10^{-4} is consistent with the value of Ref. [108], where the authors use a simplified model. This value is based on potential V_a which reproduces the ^{6}Li binding energy, the α+d low-energy phase shifts, and provides good results for the ^{6}He β decay. It is therefore expected to have the same quality for the ^{6}Li γ decay. An experimental measurement seems to be possible with current facilities, and would provide, in combination with the data on ^{6}He β decay, an important step in a better understanding of the halo structure in isobaric analog states.

VI. BETA-DECAY OF THE ^{11}Li NUCLEUS INTO ^{9}Li AND DEUTERON WITHIN A THREE-BODY MODEL

As we have shown in chapter 4, the low value of the branching ratio of the ^{6}He beta-decay into the deuteron continuum channel is the result of a strong cancellation between contributions of the "internal" and "halo" parts of the Gamow-Teller matrix element [101, 105]. [1] It was shown that the cancellation requires that the $\alpha+d$ potential contains a forbidden state below the ^{6}Li ground state in order to have the correct node structure of the scattering wave function. The cancellation is so strong in the Gamow-Teller matrix element for ^{6}He that it requires an almost perfect balance between the internal and halo parts, which should be fortuitous. A similar effect is thus not expected for other halo nuclei possessing a β delayed deuteron decay branch such as ^{11}Li:

$$^{11}\mathrm{Li} \rightarrow \ ^{9}\mathrm{Li} + d + e^{-} + \tilde{\nu}_{e}. \tag{6.1}$$

In section 6.1., the β decay model for the ^{11}Li two-neutron halo nucleus into the $^{9}\mathrm{Li} + d$ continuum is summarized. The potentials and the corresponding three-body hyperspherical and two-body scattering wave functions are described in section 6.2. The properties of the Gamow-Teller matrix element are studied in section 6.3. In section 6.4., we discuss the obtained numerical results and compare them with experimental information. Development of the model in view of new data will be done in section 6.5. Conclusions are given in section 6.6.

[1] This chapter is based on the results of Refs. [123, 124]

6.1. Model

The initial wave function is expressed as a bound-state wave function of the three-body $^9\mathrm{Li} + n + n$ system with local $^9\mathrm{Li} + n$ and nn interactions. It was calculated by the Belgian group (D. Baye, P. Descouvemont, etc.). The spin of the core is neglected. The total orbital momentum L of the three particles is assumed to be equal to the total spin S of the neutrons as for ^{6}He [105]. Jacobi coordinates, i.e. the relative coordinate $\boldsymbol{r}$ between the neutrons and the coordinate $\boldsymbol{R}$ of their center of mass with respect to the ^{9}Li core, are necessary to calculate the overlap with the final scattering state. These coordinates are conveniently replaced by hyperspherical coordinates which involve five angular variables Ω_5 and the hyperradius ρ. The wave function is expanded over hyperspherical harmonics depending on Ω_5 and on the hypermomentum K, as was done in previous chapters 4-6. The coefficients in this expansion depend on the hyperradial coordinate ρ and are expanded in Lagrange functions [166] (see Ref. [67] and chapter 4 for details).

For the final scattering state, we assume an expression factorized into the deuteron ground-state wave function depending on r and a $^9\mathrm{Li} + d$ scattering wave function depending on R derived from a potential model. We neglect the small D component of the deuteron.

The transition probability per time and energy units is given by [169]

$$\frac{dW}{dE} = \frac{m_e c^2}{\pi^4 v \hbar^2} G_\beta^2 f(Q-E) B_{\mathrm{GT}}(E), \tag{6.2}$$

where m_e is the electron mass,

v and E are the relative velocity and energy in the center of mass system of ^{9}Li and deuteron,

$G_\beta = 2.996 \times 10^{-12}$ is the dimensionless β decay constant [170]. The Fermi integral $f(Q-E)$ depends on the kinetic energy $Q-E$, available for the electron

and antineutrino. The mass difference Q between initial and final particles is given in MeV by

$$Q = 3.007 - S_{2n} \tag{6.3}$$

as a function of the two-neutron separation energy of the halo nucleus. With the ^{11}Li value $S_{2n} = 300 \pm 19$ keV from the atomic mass evaluation [111], Q is equal to 2.71 ± 0.02 MeV. However according to a recent remeasurement, the ^{11}Li two-neutron separation energy becomes $S_{2n} = 376 \pm 5$ keV [112] leading to $Q = 2.63$ MeV. We shall first use the standard value and then consider the importance of this modification.

Since the total orbital momentum and parity are conserved, only the $l = 0$ partial scattering wave contributes. Hence, only the initial $L = S = 0$ component of ^{11}Li described with a spin 0 core can decay to $^{9}\mathrm{Li} + d$. In order to allow the use of a complex optical potential for describing the scattering states, we generalize the formula of Refs. [101, 105]. The final state is described by an ingoing scattering wave. At energy E, a partial wave $u^{(-)}_{E,l}$ of an ingoing scattering wave function is related to a partial wave $u^{(+)}_{E,l}$ of an outgoing scattering wave function by

$$u^{(-)}_{E,l}(R) = (-1)^l u^{(+)*}_{E,l}(R). \tag{6.4}$$

The outgoing radial scattering wave functions

$$u^{(+)}_{E,l}(R) = e^{i\delta_l} u_{E,l}(R) \tag{6.5}$$

are normalized asymptotically according to

$$u_{E,l}(R) \underset{R\to\infty}{\longrightarrow} \cos\delta_l(E) F_l(kR) + \sin\delta_l(E) G_l(kR), \tag{6.6}$$

where $\delta_l(E)$ is the l-wave phase shift at energy E,

F_l and G_l are Coulomb functions [144],

and k is the wave number of the relative motion,. The subscript $l = 0$ is understood in the following.

The reduced transition probability can be written as

$$B_{\mathrm{GT}}(E) = 6\lambda^2 \left| e^{i\delta_0} I_E(\infty) \right|^2, \tag{6.7}$$

where $\lambda = -1.25$ [171]. The phase in front of I_E does not play any role if the potential is real. The integral

$$I_E(R) = \int_0^R u_E(R') u_{\mathrm{eff}}(R') dR' \tag{6.8}$$

depends on a cutoff radius R over the relative coordinate between the core and the center of mass of the nucleons. Only its value at infinity is physically relevant but it will help us to understand the physics of the decay process. This integral involves scattering wave functions $u_E(R)$ and depends thus on the $^9\mathrm{Li} + d$ relative energy E. This integral also involves an effective wave function

$$u_{\mathrm{eff}}(R) = R \sum_K \int_0^\infty Z_K(r, R) u_d(r) r dr, \tag{6.9}$$

where $u_d(r)$ is the deuteron radial wave function depending on the relative coordinate r of the two nucleons. The sum runs over the values of the hypermomentum K in the expansion of the initial bound state. The function $Z_K(r, R)$ is the radial part of the K component with all angular momenta equal to zero in the expansion of the initial wave function. Its expression is given by Eqs. (3) and (14) in Ref. [105]) where however a normalization factor $[(A-2)/A]^{3/4}$ is missing. The results of Ref. [105]) must be modified accordingly. In the following, we also make use of partial integrals $I_E^{(K)}(R)$ obtained from Eq. (6.8) with the different terms in Eq. (6.9). The sum of the $I_E^{(K)}(R)$ is $I_E(R)$.

6.2. Potentials

The deuteron wave function u_d was calculated with the central Minnesota interaction [152] (see Ref. [67] for details). An energy $E_d = -2.202$ MeV was obtained.

The $^9\mathrm{Li}+n+n$ wave function was calculated with the $^9\mathrm{Li}+n$ potential P2 of Ref. [118] and the nn Minnesota interaction with exchange parameter $u=1$. In order to fit the binding energy of ^{11}Li, the P2 interaction is multiplied by a parameter [117]. The values 0.992 and 0.9965 provide $S_{2n}=0.307$ and 0.376 MeV, respectively. The s-wave scattering length is then slightly modified from -25.4 fm to -19.0 or -22.2 fm, respectively. Potential P2 contains a forbidden state in the s wave which is eliminated with the pseudopotential method [135]. Forbidden states need not be eliminated in two-body systems as they do not affect scattering properties. Their presence leads to more realistic wave functions for the relative motion. In three-body systems however, forbidden states must be eliminated because otherwise they would unrealistically contribute to the binding energy. The pseudopotential moves them to a high energy without affecting the other properties of the two-body potentials.

A $^9\mathrm{Li}+d$ optical potential has been obtained by fitting elastic scattering data at a c.m. energy of 3.86 MeV [178]. The real part of this potential does not display any resonance below the Coulomb barrier. Such a resonance has been observed in several channels at the excitation energy 18.15 ± 0.15 MeV [97], i.e. at the c.m. energy 0.25 ± 0.15 MeV above the $^9\mathrm{Li}+d$ threshold. As shown below, this resonance is crucial to explain the order of magnitude of the β delayed deuteron decay of ^{11}Li. The potential of Ref. [178] is thus not useful here. Its real part provides three bound states. When the depth of its real part is reduced from 104.6 MeV to 89 MeV, the upper bound state becomes a resonance near the experimental value. However the agreement with the elastic scattering experiment is then lost.

We approximate the $^9\mathrm{Li}+d$ potential by expressions based on simple physical arguments derived from a microscopic cluster model interpretation. (i) At short distances, ^{9}Li and deuteron can form a bound state in the s wave. This bound state has the same parity as the ^{9}Li core, i.e. a negative parity. We thus impose to the potential to reproduce the energy of the $1/2^-$ excited state of ^{11}Be at

an excitation energy of 0.320 MeV. This means that our potentials will have a bound state near -17.6 MeV. (ii) In the microscopic cluster model, the $^9\mathrm{Li} + d$ system possesses a forbidden state in the s wave. The role of such a state can be simulated by a potential deep enough to contain an unphysical bound state below the physical bound state in order to simulate the correct node structure of the scattering wave function. (iii) The ^{11}Be nucleus displays a resonance around 0.25 MeV above the $^9\mathrm{Li} + d$ threshold. As in Ref. [121], we consider

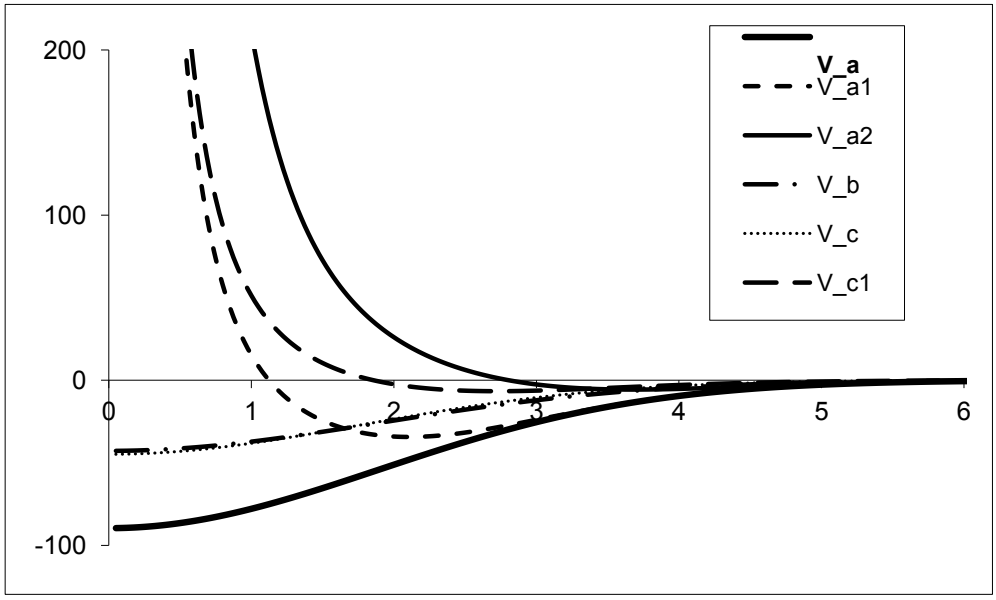

Fig. 6.1. Potential V_a and phase-equivalent potentials V_{a1} and V_{a2} (full lines); potential V_b (dashed line); potential V_c and phase-equivalent potentials V_{c1} (dotted lines).

simple Gaussian potentials parametrized as

$$V(R) = -V_0 \exp(-\alpha R^2). \tag{6.10}$$

The choice of a Gaussian form factors restricts the number of parameters. A Coulomb term $3e^2\,\mathrm{erf}(\beta r)/r$ with $\beta = 0.71$ fm^{-1} (scaled from 0.75 fm^{-1} in the

$\alpha + d$ case) is added to all potentials. The Coulomb barrier is located between 0.55 and 0.6 MeV.

Potential V_a with $\alpha = 0.14$ fm^{-2} and $V_0 = 89.5$ MeV (see Fig. 6.1) has a bound state at energy -17.63 MeV and a forbidden state at -52.42 MeV. The width of the Gaussian form factor has been chosen in such a way that the potential also verifies criterion (iii). The corresponding phase shift is displayed as a full line in Fig. 6.2. A resonance appears at about 0.33 MeV with a width of about 0.1 MeV. The spin and parity of this resonance should be $3/2^-$. Its width is smaller than the experimental width derived in Ref. [97] which however largely exceeds the Wigner limit and is therefore questionable.

In the ^{6}He case, a forbidden state plays a crucial role in the reproduction of the experimental order of magnitude. In order to study the role of the forbidden state here, we perform pairs of supersymmetric transformations [24] in order to remove it from V_a while keeping the other bound state and the s-wave resonance and phase shift. The resulting phase-equivalent potential denoted as V_{a1} exhibits a strong repulsive core (see Fig. 6.1). The physical bound state of V_{a1} is then removed by another pair of transformations leading to the phase-equivalent potential V_{a2} without any bound state. Both potentials V_{a1} and V_{a2} provide the same s-wave phase shift as V_a in Fig. 6.2.

We also consider other Gaussian potentials. Potential V_b with the same range as V_a but $V_0 = 42.7$ MeV has its ground state at -17.63 MeV. This potential possesses a weakly bound state near -0.184 MeV in place of a resonance. Potential V_c is quite similar to V_b but differs from it by the fact that it possesses a resonance at 0.28 MeV in addition to a bound state at -17.66 MeV, with $\alpha = 0.161$ MeV and $V_0 = 44.8$ MeV. Removing the bound state leads to the phase-equivalent potential V_{c1} with a repulsive core. These potentials are compared in Fig. 6.1 and their phase shifts are displayed in Fig. 6.2. One observes that the phase shift of potential V_c has the same shape as the phase shift of V_a and also displays the expected resonance but at a lower energy. On the

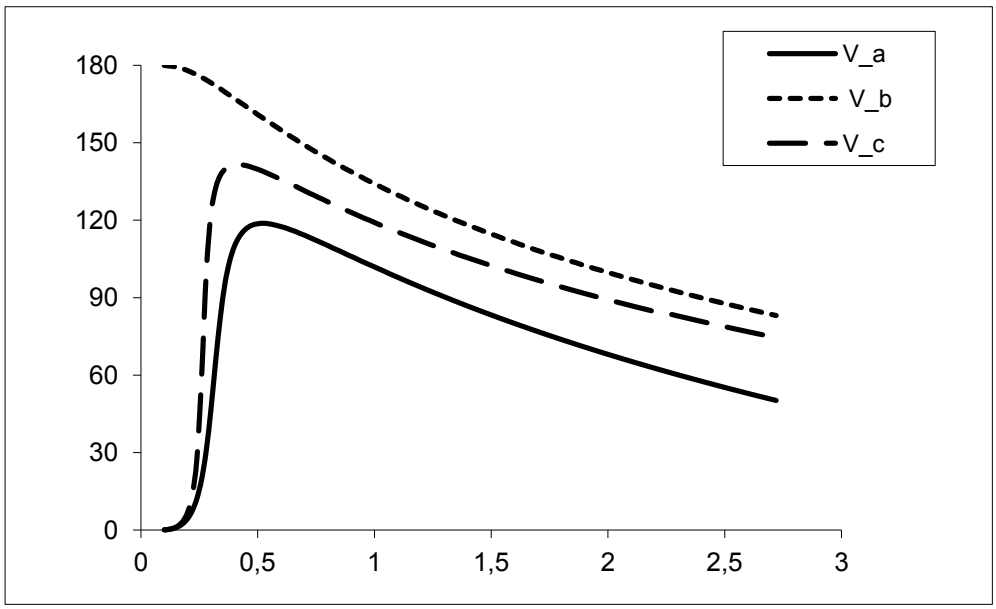

Fig. 6.2. s**-wave** ^{9}**Li** $+ d$ **phase shifts obtained with potentials** V_a **(and** V_{a1}**,** V_{a2}**, full line),** V_b **(dashed line) , and** V_c **(and** V_{c1}**, dotted line).**

contrary, the phase shift of potential V_b is monotonic.

These potentials are compatible with the elastic scattering data of Ref. [178] if some surface absorption is added. Without absorption, even the order of magnitude of the cross section is incorrect beyond 70 degrees. We use the simple optical potential

$$V_{\rm opt}(R) = -(V_0 + iW_0\sqrt{\alpha}R)e^{-\alpha R^2}, \tag{6.11}$$

where the imaginary part is proportional to the derivative of the real part.

6.3. Gamow-Teller integrals

The integrals $I_E^{(K)}(R)$ calculated with potential V_a are displayed in Fig. 6.3

as a function of R for different K values at energy 1 MeV. The convergence of $\sum_K I_E^{(K)}(R)$ is reached for $K_{\max} = 20$. Partial waves $K = 2$, 0, and 4 are strongly dominant, although the cumulated contribution of all higher partial waves is not negligible. Contrary to the ^{6}He case, no important cancellation is encountered here because the dominant contributions have the same sign.

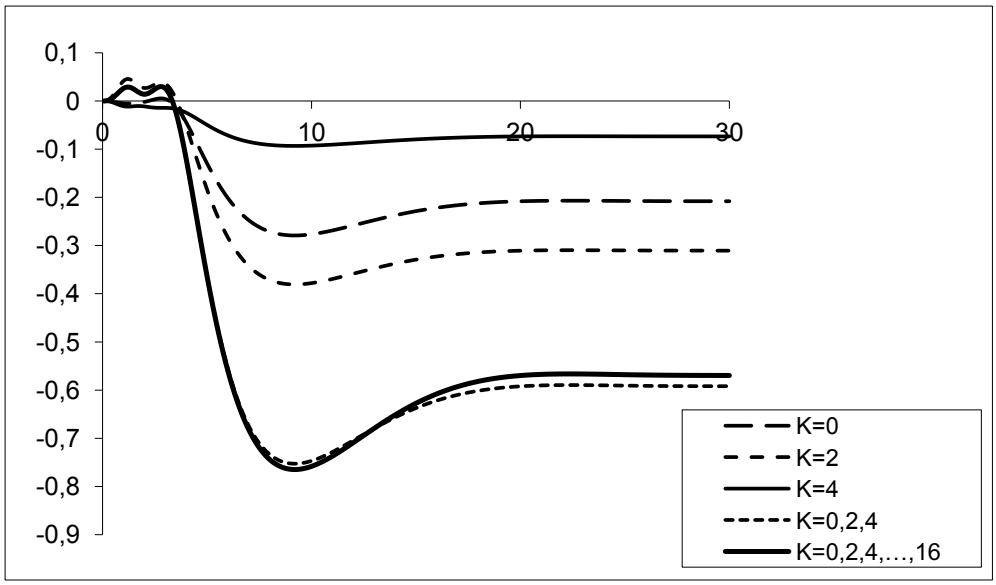

Fig. 6.3. Partial integrals $I_E^{(K)}(R)$ for $K = 0$, 2, and 4 at the energy $E = 1$ MeV for potential V_a. The sum of the three components $K = 0$, 2, and 4, (dotted line) and the converged sum $I_E(R) = \sum_K I_E^{(K)}(R)$ [Eq. (6.8)] (lowest full line) are also displayed.

In Figs. 6.4, 6.5 the integrals $I_E(R)$ are compared for the different potentials considered at two energies: the near-resonance energy 0.3 MeV and a typical non-resonant energy 1 MeV. As shown by Eq. (6.8), the integral I_E displays a minimum or a maximum every time either u_E or u_{eff} vanishes. Its behavior depends on the node structure of the scattering wave function and thus on the

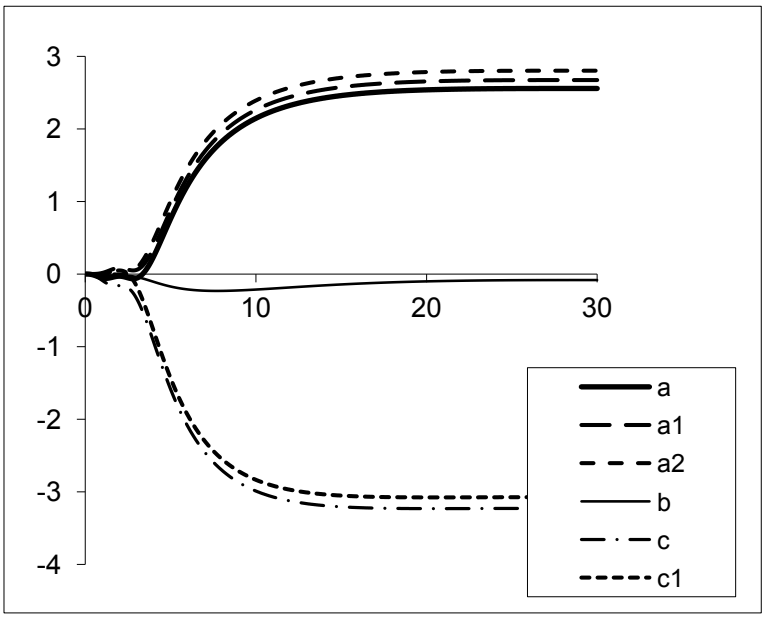

Fig. 6.4. Integrals $I_E(R)$ [Eq. (6.8)] at $E = 0.3$ MeV, for various potentials.

depth of the potential. At both energies, all curves present an extremum near 2 fm which corresponds to the unique node of u_{eff}. They present one to three additional nodes corresponding to the possible bound states and resonance of the potential. However, in spite of their different numbers of bound states and thus of nodes, potentials V_a, V_{a1}, and V_{a2} do not give very different results at both energies. In all three cases, the amplitude of the integral starts to increase beyond 3 fm and reaches a plateau near 20 fm. At 1 MeV, it presents a maximum near 9 fm. This maximum is at the same location for V_a, V_{a1}, and V_{a2} because phase-equivalent potentials have the same asymptotic behavior and thus the same nodes beyond the potential range. This situation must be contrasted with the ^{6}He case where the cancellation enhances tiny differences and where phase-equivalent potentials provide very different results [105].

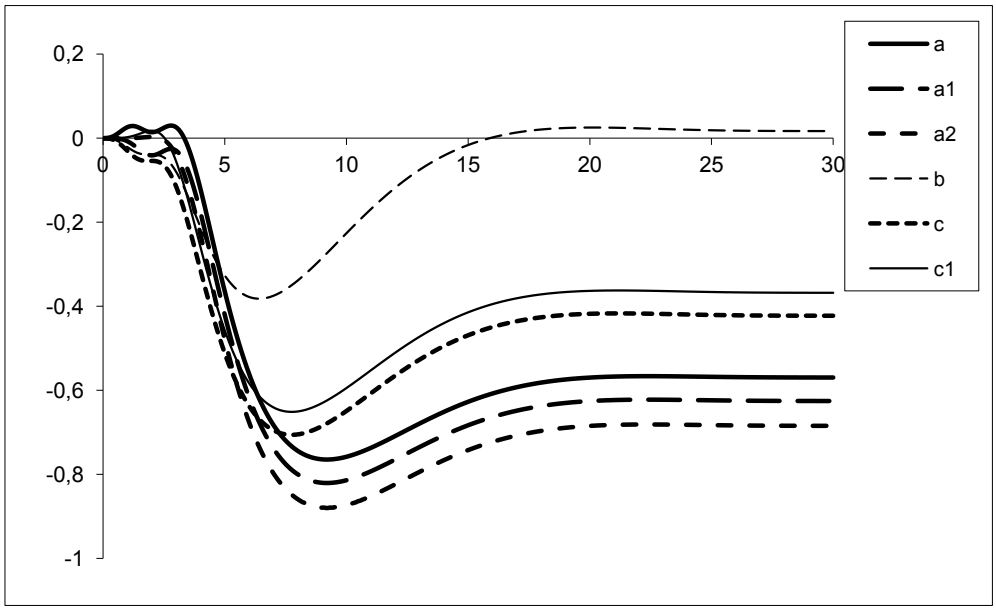

Fig. 6.5. Integrals $I_E(R)$ [Eq. (6.8)] at (a) $E = 0.3$ MeV and (b) 1 MeV, for various potentials.

The results for potential V_c which satisfies the same physical conditions as V_{a1} are very similar because the scattering wave function has the same number of nodes and similar locations of these nodes. At 0.3 MeV, the integrals have opposite signs for V_a and V_c beyond 4 fm because the resonance is below 0.3 MeV for V_c while it is above for V_a. They have the same sign and similar magnitudes at 1 MeV.

On the contrary, the results obtained with V_b are very different, even off resonance, because the scattering wave function has nodes at quite different locations. In particular its node near 8 fm at 0.3 MeV or 6 fm at 1 MeV leads to a cancellation similar to that of the ^{6}He case. We shall see in the next section that this type of result is ruled out by experiment. It is important to realize that V_b has the same physical bound state as V_{a1} and V_c near -17.6 MeV. However,

V_b does not reproduce the resonance (see Fig. 6.2).

6.4. Transition probability per time and energy units

The transition probability per time and energy units given by Eq. (6.2) is plotted in Fig. 6.6 as a function of the relative $^9\mathrm{Li} + d$ energy E for the different potentials. For the potentials displaying a resonance, the results are qualitatively very similar. The shape of the curve does not depend much on the resonance location. On the contrary, potential V_b provides results with a much smaller order of magnitude. The same situation is observed with other potentials that do not possess a resonance. The total transition probabilities per time unit (integrated from 0 or from some cutoff to Q) corresponding to the various potentials are compared with the experimental value in Table 6.1. This value is calculated from the experimental branching ratio $\mathcal{R}$ by

$$W_{\mathrm{exp}} = \mathcal{R} \ln 2/t_{1/2} \approx 81.5\,\mathcal{R}\ \mathrm{s}^{-1}, \tag{6.12}$$

where $t_{1/2}$ is the ^{11}Li ground-state half life 8.5 ms. The experimental branching ratio is $(1.5 \pm 0.2) \times 10^{-4}$ [97]. The results at various cutoff values in Table 6.1 will be useful for comparison with the new experiment.

All potentials except V_b provide the right order of magnitude but overestimate the experimental value of Ref. [97] by a factor larger than 3. Results of successive phase-equivalent potentials differ by about 10 %. The main difference between V_a and V_c arises in the cutoff dependence which is sensitive to the resonance location.

Table 6.1 also indicates the role of a larger two-neutron separation energy S_{2n}. This introduces a modification of the Q value and of the ^{11}Li wave function. Except for V_b, the transition probabilities are slightly reduced, by about 20 %.

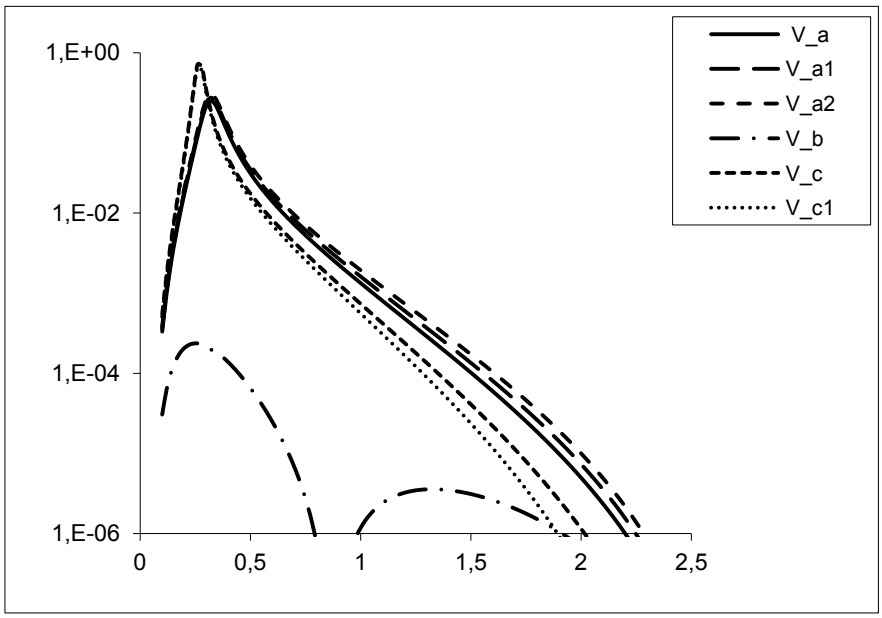

Fig. 6.6. Transition probability per time and energy units dW/dE of the ^{11}Li β decay into the ^{9}Li $+ d$ continuum as a function of the relative ^{9}Li $+ d$ energy E calculated with various ^{9}Li $+ d$ potentials.

This effect is rather weak and does not modify the discussion. The V_b variation emphasizes the high sensitivity to weak modifications when a cancellation occurs, like in the ^{6}He case.

Let us study the role of the main uncertainties in our theoretical description. The first uncertainty concerns the energy location of the resonance. The location of the peak in Fig. 6.6 affects the total transition probability. In Table 6.2, we study the dependence of the transition probability on the resonance energy E_r. To this end, we slightly vary the depth V_0 in potential V_a. This leads to a small violation of our criterion (i), i.e. the energy E_{BS} of the physical bound state is somewhat modified, but this modification remains acceptable in view of our other simplifying assumptions. As shown by Table 6.2, W is locally

Table 6.1.

Total transition probability per second W (in 10^{-3} s^{-1}) for the β decay of ^{11}Li into ^{9}Li $+ d$. For each value of the two-neutron separation energy S_{2n} (in MeV), the rows correspond to various cutoffs.

S_{2n}	cutoff	V_a	V_{a1}	V_{a2}	V_b	V_c	V_{c1}	Exp.
0.307	$E > 0$	38.1	42.1	46.7	0.0718	59.7	54.1	12 ± 2 [97]
	$E > 0.3$	31.0	34.3	38.2	0.0392	22.0	19.7	
	$E > 0.5$	4.7	5.4	6.2	0.0096	2.7	2.3	
0.376	$E > 0$	31.5	34.9	39.0	0.1014	50.8	45.8	12 ± 2 [97]
	$E > 0.3$	25.7	28.6	32.1	0.0622	19.0	17.0	
	$E > 0.5$	4.0	4.6	5.3	0.0185	2.4	2.1	

quite sensitive to the resonance energy and a slightly higher location would lead to smaller values. A higher location of the resonance also reduces the cutoff dependence.

Another effect, not encountered in the ^{6}He case, arises from the fact that several channels are open below the ^{9}Li $+ d$ channel, the lowest one being the ^{10}Be$+n$ channel. Transfer towards these channels is possible at all energies but should be rather weak below the Coulomb barrier. Therefore we restrict the discussion to small values of W_0 in Eq. (6.11) (this parameter should probably depend on energy but we neglect this effect here). One observes in Fig. 6.7 that the role of the resonance is strongly reduced even by a weak absorption. On the contrary, the results above 1 MeV are not much affected. The energy dependence of dW/dE becomes weaker when absorption increases.

The total transition probabilities per second W calculated with potential (6.11) in Eq. (6.7) are displayed in Table 6.3 with α and V_0 as in potential V_a for several fixed values of the surface absorption constant W_0. One observes

Table 6.2.

Dependence of the total transition probability per second W (in 10^{-3} s^{-1}) on the resonance energy E_r (in MeV) calculated with a Gaussian potential with $\alpha = 0.14$ fm^{-2} as a function of its depth V_0 (in MeV) for various cutoffs. The forbidden state energy E_{FS} and the physical bound state energy E_{BS} are also displayed.

V_0	E_{FS}	E_{BS}	E_r	W		
				$E > 0$	$E > 0.3$	$E > 0.5$
90.8	−53.44	−18.26	0.25	47.5	10.7	2.1
90.1	−52.89	−17.92	0.30	42.1	24.6	3.3
89.5	−52.42	−17.63	0.35	38.1	31.0	4.7
89.0	−52.02	−17.38	0.40	35.2	31.0	6.2
88.5	−51.63	−17.15	0.46	32.5	29.6	8.0

that a much small absorption leads to a strong reduction of the transition probability. As explained by Fig. 6.7, absorption leads to a weaker dependence on the cutoff.

6.5. Development of the model in view of new data

In this section we use the results of the analysis done above, for the explanation of new data [98]. First, in Fig. 6.8 we compare the theoretical energy dependent transition probability calculated with the potential Eq. (6.11) with a real part V_a, with the new data.

As we see in the Fig. 6.8, the energy dependence of the data is not reproduced

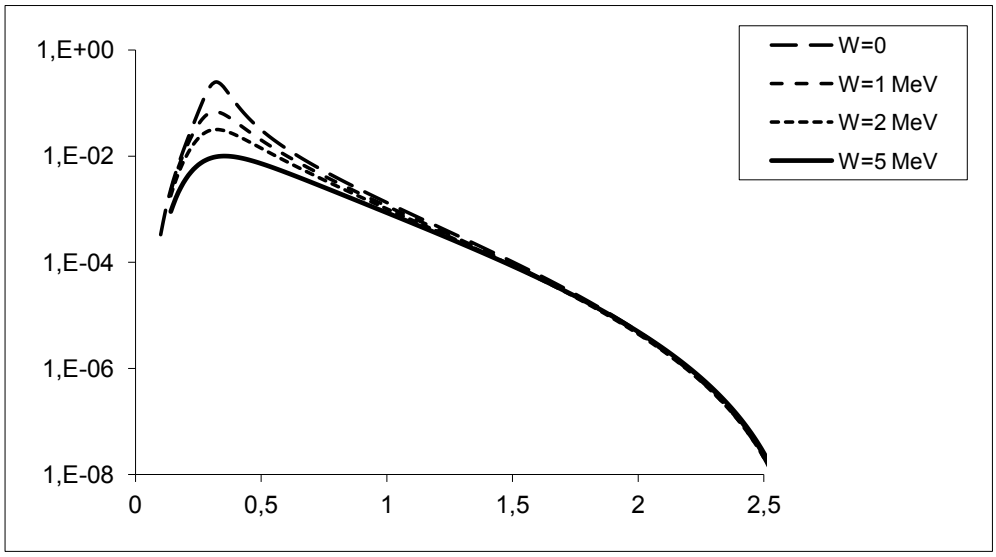

Fig. 6.7. Transition probability per time and energy units dW/dE of the ^{11}Li β decay into the ^{9}Li $+ d$ continuum as a function of the relative ^{9}Li $+ d$ energy E calculated with various values of the surface absorption strength W_0 (in MeV) in Eq. (6.11).

with the optical potential (6.11) based on the parameters of V_a. The absorbtion with the parameter $W = 5$ MeV reduces the probability around the resonance, but does not influence the tail. Thus, according to the results of above analysis, the only way to explain the new data is to move the resonance location to the right, which must reduce essentially the transition probability.

Now we take a slighly narrower and deeper potential $V_n(R)$ with $\alpha = 0.17$ fm^{-2} and $V_0 = 100.1$ MeV. As shown in Fig. 6.8, potential V_a locates a resonance around 0.3 MeV with a width of about 0.1 MeV, but such a resonance does not appear in the new data [98]. Potential V_n moves the resonance to a higher energy, around 0.7 MeV (see Fig. 6.9). This leads to an automatic increase of

Table 6.3.

Dependence of the total transition probability per second W (in 10^{-3} s^{-1}) on the surface absorption strength W_0 (in MeV), calculated with potential V_a as real part for various cutoffs.

W_0	$E > 0$	$E > 0.3$	$E > 0.5$
0	38.1	31.0	4.7
1	16.7	13.0	3.5
2	9.9	7.8	2.7
5	4.4	3.6	1.8

its width.

The transition probability per time and energy units calculated with Eqs. (6.2)-(6.4) is displayed in Fig. 6.10. The dashed curve corresponds to V_n with $W_0 = 0$. The broad resonance visible in Fig. 6.9 leads to a slow decrease of dW/dE around 1 MeV, different from the fast decrease obtained with V_a in Fig. 6.8. A non-zero value of W_0 is used to simulate the absorption to the various open channels. The results (full curve) are now in fair agreement with the two sets of data points obtained with two different techniques of measurement in Ref. [98], i.e. detection of decays of the ^{9}Li core (triangles) or detection of the emitted deuteron (squares).

The total transition probability per second W calculated with V_n is 13.3 for $W_0 = 0$ and 7.3 for $W_0 = 5$ MeV in units of 10^{-3} s^{-1}. These values remain essentially unchanged with the experimental cutoff $E > 0.2$ MeV. The result with absorption compares well with the values of Ref. [98], 10.6±1.0 (^{9}Li decays) and 8.8 ± 1.9 (deuteron emissions) in the same units.

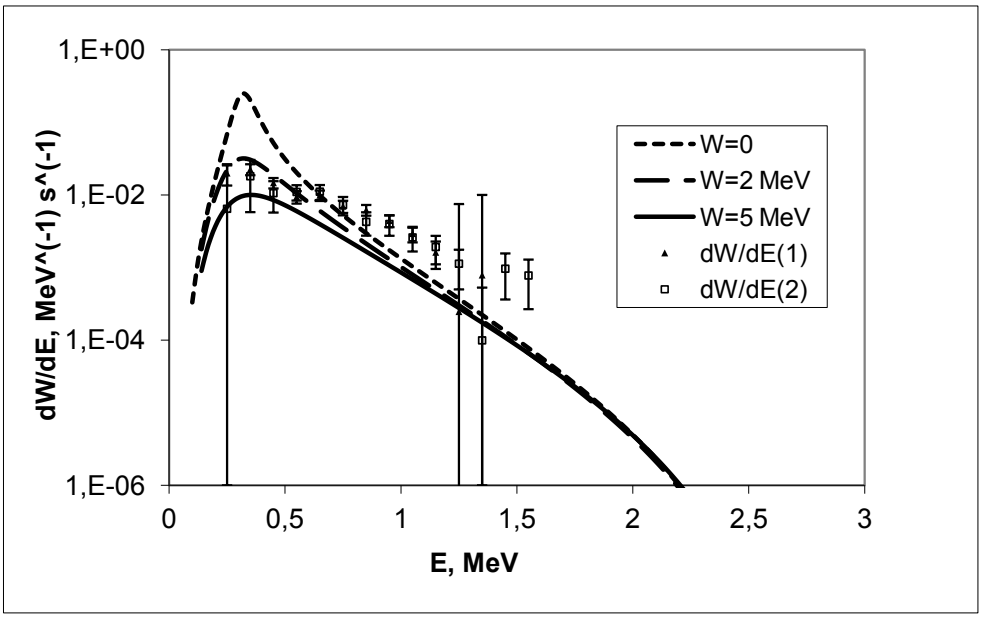

Fig. 6.8. Transition probability per time and energy units dW/dE of the ^{11}Li β decay into the ^{9}Li $+ d$ continuum as a function of the relative ^{9}Li $+ d$ energy E calculated with various values of the surface absorption strength W_0 (in MeV) in Eq. (6.11) with the real part V_a.

6.6. Conclusion

In the present Chapter, we studied the β decay process of the ^{11}Li halo nucleus into the ^{9}Li $+ d$ continuum in the framework of a three-body model. Three-body hyperspherical bound-state wave functions on a Lagrange mesh and two-body ^{9}Li $+ d$ scattering wave functions have been used. For the calculation of the β decay transition probabilities per time and energy units, several ^{9}Li $+ d$ potentials were employed.

Some ^{9}Li $+ d$ potentials are physically inspired by a microscopic cluster

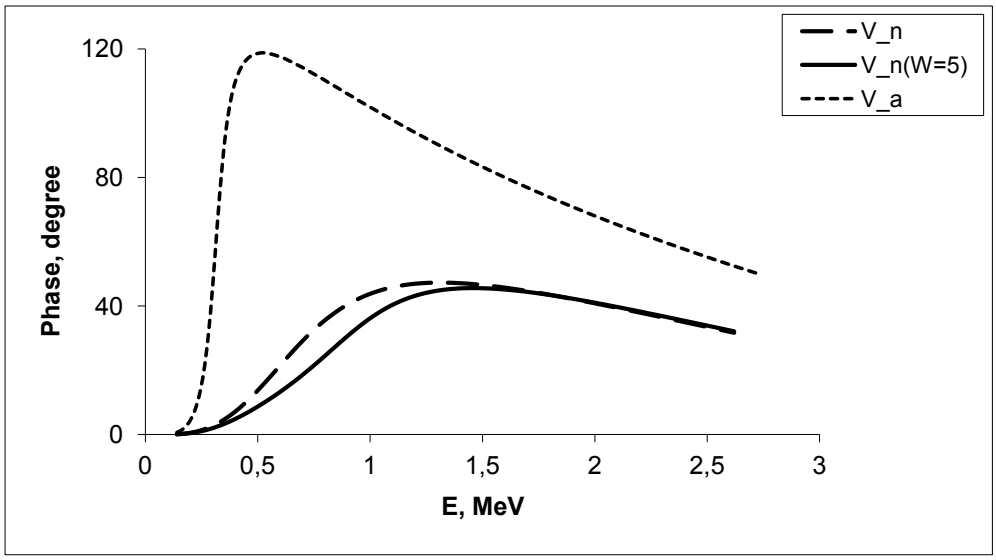

Fig. 6.9. Phase shift δ_0 with potentials V_a (full line) and V_n (dashed line) with $W_0 = 0$, and real part of phase shift δ_0 for V_n with $W_0 = 5$ MeV (dotted line).

picture and involve a forbidden state and a physical bound state simulating the $1/2^-$ excited state of ^{11}Be. A resonance occurs in the s wave at about the experimental energy. For potentials of this family, the transition probability per time unit is weakly sensitive to the potential choice. However a potential without this resonance fails to reproduce even the order of magnitude of the transition probability. The high sensitivity of the delayed β decay of ^{6}He due to a cancellation in the Gamow-Teller matrix element does not occur here. This is emphasized by using phase-equivalent potentials differing by their number of bound states: they give very different results for ^{6}He and very similar results for ^{11}Li.

The theoretical result is strongly sensitive to the location of the resonance.

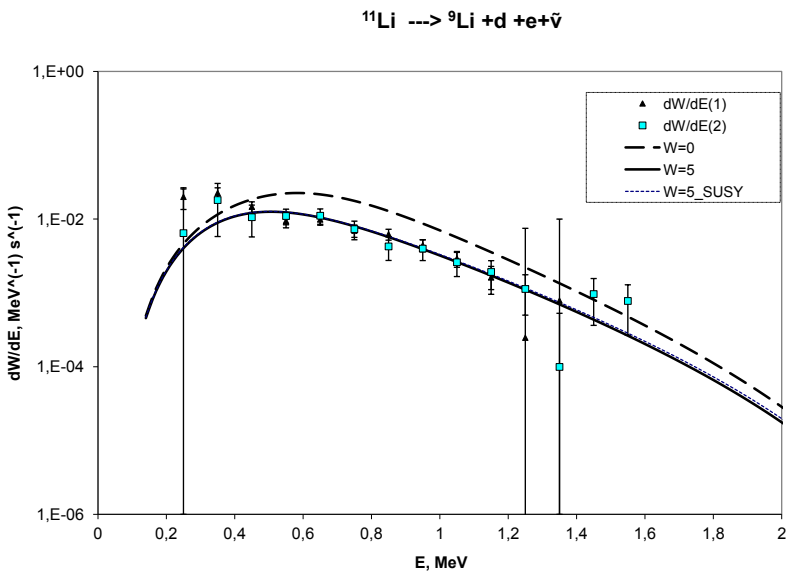

Fig. 6.10. Transition probability per time and energy units dW/dE of the ^{11}Li β decay into the ^{9}Li $+ d$ continuum as a function of the relative ^{9}Li $+ d$ energy E calculated with various values of the surface absorption strength W_0 (in MeV) in Eq. (6.11) with the real part V_n.

It is also sensitive to the ^{11}Li separation energy (about 20 % if S_{2n} is increased by about 70 keV).

The overestimation of the transition probability can be reduced by modifying the resonance location and by introducing absorption removing flux from the ^{9}Li $+ d$ final channel.

The new experimental data of Ref. [98] was reproduced within a developed three-body model. The resonance in the s wave phase shifts is present at a higher energy, around 0.7 MeV and it is very broad.

VII. A UNIQUE DECAY PROCESS: BETA-DELAYED EMISSION OF A PROTON AND A NEUTRON BY THE ^{11}Li HALO NUCLEUS

In this chapter we study the unique decay process:

$$^{11}\mathrm{Li} \rightarrow \ ^{9}\mathrm{Li} + n + p + e^{-} + \tilde{\nu}_e \tag{7.1}$$

[1] The ^{11}Li nucleus is described in a ^{9}Li+n+n three-body model [67] as in previous chapters and our studies of the deuteron delayed emission [105, 123]. It's wave function has been calculated by the Belgian group (D. Baye, P. Descouvemont, etc.) The ^{9}Li+n+p final state is in the three-body continuum of ^{11}Be. The calculation of wave functions in this continuum is much more complicated than in the three-body continuum of ^{6}He [91, 154] (see chapters 4 and 5). The construction of three-body scattering states for ^{9}Li+n+n would already be more difficult than for α+n+n because of the poor knowledge of the ^{9}Li+n interaction. The study of the ^{9}Li+n+p continuum is worse for several reasons.

(i) The halo nucleons are not identical and the wave functions have about twice as much components at the same level of truncation in an expansion in hyperspherical harmonics.

(ii) The presence of a Coulomb interaction between the ^{9}Li core and the proton requires a more complicated treatment than in the neutral case.

(iii) The structure of the continuum wave functions is more complicated since one can expect a larger number of bound states to which they must be orthogonal. For these reasons, the technique that we have developed [91] can not provide a converged calculation with our present computer capabilities. Since an evaluation of the branching ratio would be necessary to guide future

[1] This chapter is based on the results of Ref. [125]

experiments, we shall simplify the study by describing the continuum with three-body Coulomb waves. This approximation should be accurate enough to estimate the order of magnitude of the branching ratio and the shape of the energy distribution.

In section 7.1., we present general formulas for the decay probability per time unit for the β delayed np emission. In section 7.2., we evaluate the branching ratio and discuss its origin. Concluding remarks are presented in section 7.3.

7.1. Decay probability for β delayed np emission

7.1.1. General expression of decay probability

In this section, we establish the general expression for the β decay probability distribution for a three-body final state in the continuum. The initial nucleus with mass number A is described as a three-body bound state of a core and two nucleons. This state with angular momentum J_i, projection M_i, and parity π_i is expressed in hyperspherical coordinates. The spin, isospin and parity of the core are neglected. Three-body scattering states are discussed in Ref. [91] and used in Ref. [179].

Let us follow the notation in Ref. [179] and denote the three particles as 1, 2, and c (for the core). Let $\boldsymbol{k}_{12}$ be the relative wave vector between particles 1 and 2 and $\boldsymbol{k}_{c(12)}$ be the relative wave vector between the center of mass of those particles and the core. When the spin of the core c is neglected, the outgoing scattering states can be denoted as $\Psi^{(+)}_{\boldsymbol{k}_{12}\boldsymbol{k}_{c(12)}M_1M_2}$, where M_1 and M_2 are the projections of the spins of particles 1 and 2. These states are assumed to be normalized with respect to $\delta(\boldsymbol{k}_{12}-\boldsymbol{k}'_{12})\delta(\boldsymbol{k}_{c(12)}-\boldsymbol{k}'_{c(12)})\delta_{M_1M'_1}\delta_{M_2M'_2}$.

The distribution of decay probability per time unit can be written as

$$\frac{dW}{d\boldsymbol{k}_{12}d\boldsymbol{k}_{c(12)}} = \frac{1}{2\pi^3}\frac{m_e c^2}{\hbar}G_\beta^2\frac{f(Q-E)}{2J_i+1}\sum_{M_i}\sum_{M_1M_2}\left(|M_{\mathrm{F}}|^2 + \lambda^2\sum_{\mu}|M_{\mathrm{GT}\mu}|^2\right), \quad (7.2)$$

where $G_\beta \approx 2.996 \times 10^{-12}$ is the dimensionless β decay constant,

$\lambda \approx -1.268$ is the ratio of the axial-vector to vector coupling constants,

and E is the total energy of the nuclear fragments.

The Fermi integral $f(Q-E)$ depends on the kinetic energy $Q-E$ available for the electron and antineutrino with

$$Q = (m_n - m_p - m_e)c^2 - S_{2n}. \quad (7.3)$$

The Fermi and Gamow-Teller matrix elements are respectively given by

$$M_{\mathrm{F}}(E) = \langle\Psi^{(-)}_{\boldsymbol{k}_{12}\boldsymbol{k}_{c(12)}M_1M_2}|\sum_{j=1}^{2}t_{j-}|\Psi^{J_iM_i\pi_i}\rangle \quad (7.4)$$

and

$$M_{\mathrm{GT}\mu}(E) = 2\langle\Psi^{(-)}_{\boldsymbol{k}_{12}\boldsymbol{k}_{c(12)}M_1M_2}|\sum_{j=1}^{2}t_{j-}s_{j\mu}|\Psi^{J_iM_i\pi_i}\rangle \quad (7.5)$$

where $\boldsymbol{t}_j$ and $\boldsymbol{s}_j$ are the isospin and spin of particle j, and

$\mu = -1,\ 0,\ +1$ labels the tensor components of the spin.

If one integrates expression 8.2 over all directions, the distribution of probability as a function of the total center-of-mass energy $E < Q$ of the three particles is given by

$$\frac{dW}{dE} = \frac{1}{2\pi^3}\frac{m_e c^2}{\hbar}G_\beta^2 f(Q-E)\left(\frac{dB(\mathrm{F})}{dE} + \lambda^2\frac{dB(\mathrm{GT})}{dE}\right). \quad (7.6)$$

The Fermi and Gamow-Teller strengths appearing in this expression are given for σ = F or GT by

$$\frac{dB(\sigma)}{dE} = \int \frac{d\boldsymbol{k}_{12} d\boldsymbol{k}_{c(12)}}{2J_i+1} \delta\left(E - \frac{\hbar^2 k_{12}^2}{2\mu_{12}} - \frac{\hbar^2 k_{c(12)}^2}{2\mu_{c(12)}}\right) \sum_{M_i} \sum_{M_1 M_2} \sum_{\mu} |M_{\sigma\mu}|^2 \quad (7.7)$$

where μ_{12} is the reduced mass of particles 1 and 2, and

$\mu_{c(12)}$ is the reduced mass of the core c and the system 1+2.

The total transition probability per time unit W is obtained by integrating Eq. (7.6) from zero to Q. The branching ratio can than be derived as

$$\mathcal{R} = W t_{1/2} / \ln 2, \quad (7.8)$$

where $t_{1/2} \approx 8.75$ ms is the half life of ^{11}Li.

7.1.2. Bound-state and scattering three-body wave functions

In hyperspherical coordinates, the three-body wave function of a bound state is defined as

$$\Psi^{JM\pi}(\rho, \Omega_{5\rho}) = \rho^{-5/2} \sum_{\gamma K} \chi_{\gamma K}^{J\pi}(\rho)\ \mathcal{Y}_{\gamma K}^{JM}(\Omega_{5\rho}), \quad (7.9)$$

where ρ is the hyperradius,

$\Omega_{5\rho}$ represents the five hyperangles, and

$\mathcal{Y}_{\gamma K}^{JM}(\Omega_{5\rho})$ is a hyperspherical harmonics (see chapters 4 and Ref. [67]).

The symbol K corresponds to the hypermomentum quantum number and γ is a shorthand notation for $l_x l_y LS$,

where L is the total orbital momentum,

S is the total spin, and

l_x and l_y are the orbital momenta for the relative motions corresponding to the Jacobi coordinates between particles 1 and 2 and between the core and the center of mass of 1+2, respectively.

The parity of these relative motions is given by $\pi = (-1)^{l_x+l_y} = (-1)^K$, which implies that K must be either even or odd. The hyperradial wave functions are expanded as

$$\chi^{J\pi}_{\gamma K}(\rho) = \sum_{i=1}^{N} c^{J\pi}_{\gamma K i} f_i(\rho) \tag{7.10}$$

in terms of N Lagrange functions f_i (see [67] for definitions). Since the hyperspherical harmonics and the Lagrange functions are orthonormal, the wave functions are normed if

$$\sum_{\gamma K} \sum_{i=1}^{N} \left(c^{J\pi}_{\gamma K i}\right)^2 = 1. \tag{7.11}$$

In the present approximation of ^{11}Li with a 0^+ core, particles 1 and 2 are neutrons. The effective angular momentum and parity are $J^\pi = 0^+$. The isospin is $T = 1$ for the halo neutrons. Since they are identical, antisymmetry imposes $(-1)^{l_x} = (-1)^S$.

The final states of the decay are three-body scattering states. It is convenient to replace the projections M_1 and M_2 by the total spin S of nucleons 1 and 2 and its projection ν. With a zero-spin core, S is the channel spin. The ingoing scattering states read [179]

$$\begin{aligned}\Psi^{(-)}_{\boldsymbol{k_{12}}\boldsymbol{k_{c(12)}}S\nu} &= \frac{1}{(2\pi)^3\rho^{5/2}}\left(\frac{A}{A_c}\right)^{3/4} \sum_{JMl_{x\omega}l_{y\omega}L_\omega K_\omega} (L_\omega S\, M-\nu\, \nu|JM) \\ &\times\ \mathcal{Y}^{L_\omega M-\nu\,*}_{l_{x\omega}l_{y\omega}K_\omega}(\Omega_{5k}) \sum_{\gamma K}(-1)^K \mathcal{Y}^{JM}_{\gamma K}(\Omega_{5\rho})\chi^{J\pi *}_{\gamma K(\gamma_\omega K_\omega)}(\rho), \end{aligned} \tag{7.12}$$

where $A_c = A - 2$ is the core mass number. This formula differs from [179] because of a different normalization. The normalization for the hyperradial partial waves is [91]

$$\chi^{J\pi}_{\gamma K(\gamma_\omega K_\omega)}(\rho) \underset{\rho\to\infty}{\longrightarrow} i^{K_\omega+1}(\frac{2\pi}{k})^{5/2}$$

$$\times \quad \left[H^-_{\gamma K+2}(k\rho)\delta_{\gamma\gamma_\omega}\delta_{KK_\omega} - U^{J\pi}_{\gamma K,\gamma_\omega K_\omega} H^+_{\gamma K+2}(k\rho)\right]. \quad (7.13)$$

where the wave number k is given by $\sqrt{2m_N E/\hbar^2}$,

m_N is the nucleon mass,

and $U^{J\pi}_{\gamma K,\gamma_\omega K_\omega}$ is an element of the infinite-dimensional collision matrix.

The subscript ω refers to the entrance channel. Let us recall here that, in a three-body scattering state, there is in principle an infinity of degenerate entrance channels.

For charged systems, one has

$$H^\pm_{\gamma K+2}(x) \;=\; G_{K+\frac{3}{2}}(\eta_{\gamma K}, x) \pm iF_{K+\frac{3}{2}}(\eta_{\gamma K}, x), \quad (7.14)$$

where $G_{K+3/2}$ and $F_{K+3/2}$ are the irregular and regular Coulomb functions, respectively [146]. The Sommerfeld parameters $\eta_{\gamma K}$ are given by

$$\eta_{\gamma K} = Z^{J\pi}_{\gamma K,\gamma K}\frac{m_N e^2}{\hbar^2 k}, \quad (7.15)$$

where $Z^{J\pi}_{\gamma K,\gamma K}$ is a diagonal element of the effective-charge matrix and depends thus on the channel. One usually neglects non-diagonal terms of this matrix [142].

In the neutral case $\eta_{\gamma K} = 0$, Eq. (7.14) reduces to an expression independent

of γ,

$$H^{\pm}_{\gamma K+2}(x) = \pm i \left(\frac{\pi x}{2}\right)^{1/2} \left[J_{K+2}(x) \pm i Y_{K+2}(x)\right], \tag{7.16}$$

where $J_n(x)$ and $Y_n(x)$ are Bessel functions of first and second kind, respectively.

7.1.3. Reduced transition probabilities

For ^{11}Li, with the spin of the core neglected, we assume $J_i = M_i = 0$. The final state is a three-body ^{9}Li+n+p scattering state 7.12. Selection rules restrict this state to its 0^+ and 1^+ components for the Fermi and Gamow-Teller transitions, respectively. In the present approximation, the properties of the final state only depend on the total spin S and isospin T of the two nucleons. For the nucleons in the ^{9}Li+n+p continuum of ^{11}Be, the isospin is given by $(-1)^{l_x+S+T} = -1$. For $S = 0$, l_x even corresponds to $T = 1$ and l_x odd to $T = 0$. For $S = 1$, l_x even corresponds to $T = 0$ and l_x odd to $T = 1$. The number of channels is thus about the double of the number of channels in the ^{9}Li+n+n continuum of ^{11}Li.

The sum over M_1 and M_2 in Eq. (7.5) can be replaced by a sum over the channel spin equal to S and its projection ν. If one replaces the wave vectors $\boldsymbol{k}_{12}$ and $\boldsymbol{k}_{c(12)}$ by their hyperspherical counterparts k and Ω_{5k} [179], the reduced transition probabilities can be written as

$$\frac{dB(\sigma)}{dE} = \tfrac{1}{2}E^2 \left(\frac{2m_N}{\hbar^2}\right)^3 \sum_{S\nu\mu} \int d\Omega_{5k} |M_{\sigma\mu}|^2, \tag{7.17}$$

where $\mu = 0$ for F and $\mu = -1, 0, 1$ for GT.

After integration over $\Omega_{5\rho}$, the matrix elements can be written as

$$M_{\sigma\mu} = \frac{\sqrt{2}}{(2\pi)^3} \sum_{l_{x_\omega} l_{y_\omega} L_\omega K_\omega} (L_\omega S\, \mu{-}\nu\, \nu | J\mu) \mathcal{Y}^{L_\omega \mu-\nu *}_{l_{x_\omega} l_{y_\omega} K_\omega}(\Omega_{5k}) I^{J\pi}_{l_{x_\omega} l_{y_\omega} L_\omega S K_\omega}(\sigma), \quad (7.18)$$

where the spherical harmonics depend on the hyperangles characterizing the wave vectors, i.e. they depend on the directions of emission of the core and nucleons, and on the repartition of the total energy E between these particles [179].

The expressions $I^{J\pi}_{l_{x_\omega} l_{y_\omega} L_\omega S K_\omega}(\sigma)$ are one-dimensional integrals over the hyperradius ρ. After integration over Ω_{5k} and summation over the projections μ and ν, the reduced transition probabilities simplify as

$$\frac{dB(\sigma)}{dE} = \frac{2J+1}{(2\pi)^6} E^2 \left(\frac{2m_N}{\hbar^2}\right)^3 \sum_{l_{x_\omega} l_{y_\omega} L_\omega S K_\omega} \left| I^{J\pi}_{l_{x_\omega} l_{y_\omega} L_\omega S K_\omega}(\sigma) \right|^2 . \quad (7.19)$$

Let us list the possible cases. For the Fermi operator, the scattering-state partial wave has $J = 0$ and $\pi = +1$. One obtains for $S = 0$,

$$I^{0^+}_{l_{x_\omega} l_{y_\omega} 00 K_\omega}(\mathrm{F}) = \sum_{l_x \text{ even}} \sum_K \int_0^\infty \chi^{0^+}_{l_x l_x 00 K (l_{x_\omega} l_{y_\omega} 00 K_\omega)}(\rho) \chi^{0^+}_{l_x l_x 00 K}(\rho) d\rho, \quad (7.20)$$

and for $S = 1$,

$$I^{0^+}_{l_{x_\omega} l_{y_\omega} 11 K_\omega}(\mathrm{F}) = \sum_{l_x \text{ odd}} \sum_K \int_0^\infty \chi^{0^+}_{l_x l_x 11 K (l_{x_\omega} l_{y_\omega} 11 K_\omega)}(\rho) \chi^{0^+}_{l_x l_x 11 K}(\rho) d\rho. \quad (7.21)$$

For the Gamow-Teller operator, the scattering-state partial wave has $J = 1$ and $\pi = +1$. One obtains for $S = 0$,

$$I^{1^+}_{l_{x_\omega} l_{y_\omega} 10 K_\omega}(\mathrm{GT}) = \sqrt{\frac{1}{3}} \sum_{l_x \text{ odd}} \sum_K \int_0^\infty \chi^{1^+}_{l_x l_x 10 K (l_{x_\omega} l_{y_\omega} 10 K_\omega)}(\rho) \chi^{0^+}_{l_x l_x 11 K}(\rho) d\rho, \quad (7.22)$$

and for $S = 1$,

$$I^{1^+}_{l_{x_\omega} l_{y_\omega} L_\omega 1 K_\omega}(\mathrm{GT}) = -\sum_{l_x \text{ even}} \sum_K \int_0^\infty \chi^{1^+}_{l_x l_x 01 K (l_{x_\omega} l_{y_\omega} L_\omega 1 K_\omega)}(\rho) \chi^{0^+}_{l_x l_x 00 K}(\rho) d\rho$$

$$-\sqrt{\frac{2}{3}} \sum_{l_x \text{ odd}} \sum_K \int_0^\infty \chi^{1^+}_{l_x l_x 11 K (l_{x_\omega} l_{y_\omega} L_\omega 1 K_\omega)}(\rho) \chi^{0^+}_{l_x l_x 11 K}(\rho) d\rho. \quad (7.23)$$

Because of the properties of Lagrange functions, the integrals are simply given by

$$\int_0^\infty \chi^{J^\pi}_{\gamma K (\gamma_\omega K_\omega)}(\rho) \chi^{0^+}_{\gamma K}(\rho) d\rho \approx \sum_i (h\lambda_i)^{1/2} c^{0^+}_{\gamma K i} \chi^{J\pi}_{\gamma K (\gamma_\omega K_\omega)}(h x_i), \quad (7.24)$$

where x_i and λ_i are the zeros and weights of the Gauss quadrature associated with the Lagrange functions and h is a scaling factor providing mesh points $\rho_i = h x_i$ adapted to the extension of the physical system.

7.1.4. Coulomb-wave approximation

As mentioned in the introduction, we shall use a simpler approximation based on three-body Coulomb functions. In the pure Coulomb case, the scattering partial waves are approximated as

$$\chi^{J\pi}_{\gamma K (\gamma_\omega K_\omega)}(\rho) = 2 i^K (2\pi/k)^{5/2} F_{K+3/2}(\eta_{\gamma K}, k\rho) \delta_{\gamma \gamma_\omega} \delta_{K K_\omega}. \quad (7.25)$$

With this approximation, the reduced transitions probabilities become

$$\frac{dB(\mathrm{F})}{dE} = \frac{4m_N}{\pi k\hbar^2}\sum_{l_{x_\omega}}\sum_{K_\omega}\left|\int_0^\infty F_{K_\omega+3/2}(\eta_{\gamma_\omega K_\omega}, k\rho)\chi^{0^+}_{\gamma_\omega K_\omega}(\rho)d\rho\right|^2 \tag{7.26}$$

where γ_ω represents here $l_{x_\omega}l_{x_\omega}SS$ with $(-1)^S = (-1)^{l_{x_\omega}}$, and

$$\frac{dB(\mathrm{GT})}{dE} = 3\frac{dB(\mathrm{F})}{dE}. \tag{7.27}$$

The F and GT reduced transition probabilities are then proportional.

7.2. Results and discussion

7.2.1. Q value and Fermi integral

With the separation energy $S_{2n} = 376 \pm 5$ keV [112] of ^{11}Li, the Q value for the β delayed np emission is quite small,

$$Q \approx 0.404 \text{ MeV}. \tag{7.28}$$

Moreover, the wave number is also small,

$$k < 0.14 \text{ fm}^{-1}. \tag{7.29}$$

This will affect the behavior of wave functions at small distances.

In Fig. 7.1, the Fermi integrals $f(Q-E)$ for the emission of the different hydrogen isotopes are compared. The emitted electron being much faster than the heavy particles, the charge $Z = 4$ is used in the electron attraction by the final nuclear system. The Q values are 2.63 and 4.82 MeV for ^{2}H and ^{3}H, respectively. Both processes have been observed experimentally. In spite of

a much larger Fermi integral, the branching ratio for tritons [120, 180] is not larger than for deuterons [96, 97]. The emission of deuterons can be fairly well described in a model where the ^{9}Li+d resonance observed in the model of [105] is shifted to about 0.8 MeV and an absorption towards other open channels is included [124]. To our knowledge, no model description of the β delayed triton emission is available. The difficulty comes from the fact that this decay can not be described in a three-body model.

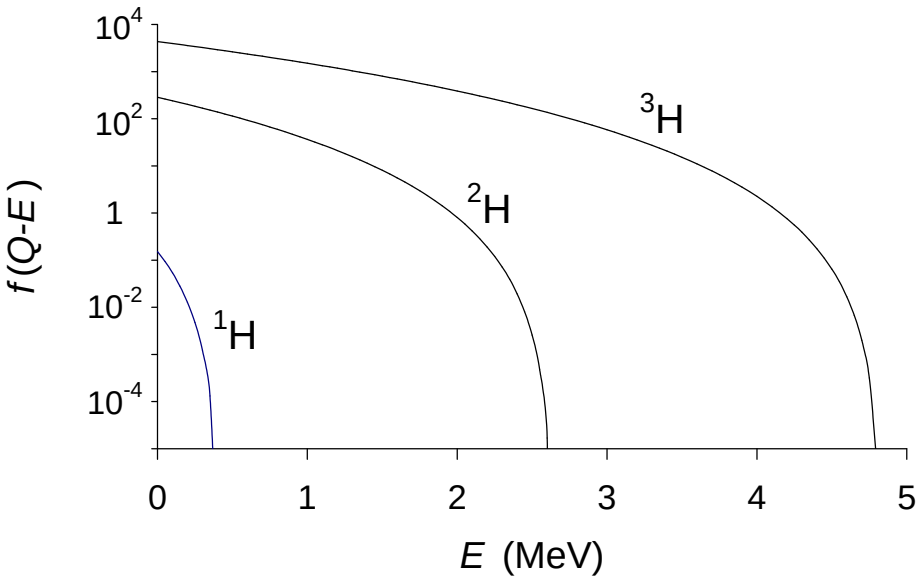

Fig. 7.1. Fermi integral $f(Q-E)$ as a function of the total energy E of the emitted nuclear fragments for the hydrogen isotopes ^{1}H, ^{2}H, and ^{3}H.

The Fermi integral for β delayed proton-neutron decay is much smaller than the other ones because of the limited phase space. The branching ratio can thus be expected to be much smaller than for the other β delayed emissions.

7.2.2. Bound-state and Coulomb wave functions

The ^{11}Li ground state is obtained as a bound state in a ^{9}Li+n+n model.

The Minnesota force is used as nucleon-nucleon interaction [152]. The ^{9}Li-neutron interaction is the P2 interaction of [118], downscaled by a factor 0.97 to approximate the experimental binding energy. The s and $p3/2$ forbidden states are eliminated by supersymmetric transformations [24]. The sum over partial waves in the wave function Eq. (7.9) is restricted to $K \leq K_{\max} = 20$. This wave function involves 66 components. The hyperradial functions Eq. (7.10) are expanded over a Lagrange-Laguerre basis with integrals calculated with the corresponding Gauss-Laguerre quadrature, as explained in [67]. The calculation is performed with $N = 40$ basis functions and mesh points and the mesh is scaled with a factor $h = 0.4$ (see [67] for definitions). The resulting energy is -0.391 MeV, close to the experimental value. We use the experimental Q value Eq. (7.28) in the calculation of Fermi integrals.

Because of the low values Eq. (7.29) of the wave number k, the hyperradial scattering wave functions should be small at distances where the integrals Eq. (8.9-7.24) are significant. They become smaller and smaller with increasing hypermomentum K. For this reason, the sum in Eqs. (8.7) or (7.26) is strongly dominated by $K = 0$. The $K = 0$ component of the ground state thus plays a crucial role. One should however not expect to use a low value of $K_{\max}$ because the convergence of this $K = 0$ component is slow [67].

For the three-body scattering states, we use approximations based on Coulomb waves. Let us first evaluate the effective charges entering the Sommerfeld parameter. Because of the $K = 0$ dominance in expression Eq. (7.26), we can restrict ourselves to this value and average the Coulomb potential over the $K = 0$ hyperspherical harmonics. The Coulomb potential is simply

$$V_C = \frac{3e^2}{|\boldsymbol{r}_c - \boldsymbol{r}_1|}, \tag{7.30}$$

where subscript 1 corresponds here to the proton. Using the hyperradius ρ and

the hyperangle α [67], the $K = 0$ average can be written as

$$\begin{aligned}\frac{Z^{0^+}_{00,00}e^2}{\rho} &= \sqrt{\mu_{c1}}\left\langle Y^{00}_{00}\left|\frac{3e^2}{\rho\cos\alpha}\right|Y^{00}_{00}\right\rangle \\ &= \sqrt{\mu_{c1}}\frac{3e^2}{\rho}\frac{16}{\pi}\int_0^{\pi/2}\sin^2\alpha\cos\alpha d\alpha, \end{aligned} \tag{7.31}$$

where $\mu_{c1} = A_c/(A_c + 1)$ is the reduced mass of the core and the proton and $\gamma = 0$ represents $l_x = l_y = L = S = 0$. Hence, the effective charge reads

$$Z^{0^+}_{00,00} = \frac{48}{\pi\sqrt{10}} \approx 4.83. \tag{7.32}$$

To simplify a calculation dominated by $K = 0$, we shall use this effective value for all partial waves.

7.2.3. Distribution of decay probability per time unit

Various approximations of the distribution of decay probability per time unit for the β delayed np decay of ^{11}Li are displayed in Fig. 7.2. With the effective charge Eq. (7.32), one obtains the lower dashed curve giving the total probability $W = 5.1 \times 10^{-10}$ s^{-1} and thus the branching ratio $\mathcal{R} = 6.5 \times 10^{-12}$. These results can be contrasted with a plane-wave calculation ($\eta_{00} = 0$) which leads to the upper dashed curve giving $W = 3.8 \times 10^{-8}$ s^{-1} and $\mathcal{R} = 4.8 \times 10^{-10}$. The Coulomb-wave calculation is pessimistic because it neglects an enhanced probability of presence of the emitted nucleons at short distances due to the attractive nuclear interaction. The plane-wave calculation overestimates the probability of presence of the emitted proton at short distances because of the missing Coulomb repulsion by the nucleus. Both calculations neglect a possible absorption towards other open channels affecting the final wave function.

However, it is difficult to figure out whether one of these cases is a better approximation. Hence we turn to a slightly different approach. For a better but

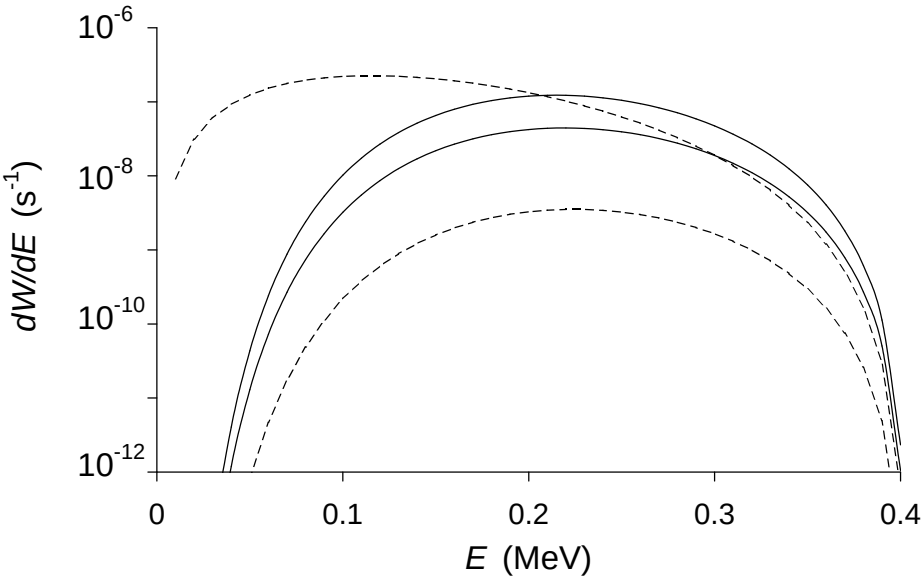

Fig. 7.2. Distribution of decay probability per time unit for the β delayed np decay of ^{11}Li: plane wave (upper dashed curve), Coulomb wave with effective charge Eq (7.32) (lower dashed curve), and shifted Coulomb waves with $a = 10$ (lower full curve) and 15 fm (upper full curve).

still simple approximation based on Coulomb functions, we have considered the eigenstates of the ^{9}Li+n+p system. With $K_{\max} = 20$, its wave functions involve 121 components. The conditions of the calculation are the same as for ^{9}Li+n+n except for the additional Coulomb interaction Eq. (7.30) between ^{9}Li and p and a reduced symmetry. The ^{9}Li+p relative motion only requires the elimination of an s forbidden state.

We obtain four bound states at -12.027, -3.944, -0.876, and -0.786 MeV with respect to the ^{9}Li+n+p threshold. Even the lowest bound state is far above the experimental ground-state energy -20.14 MeV. The state at -0.876 is the isobaric analog of the ^{11}Li ground state. The lowest positive-energy state

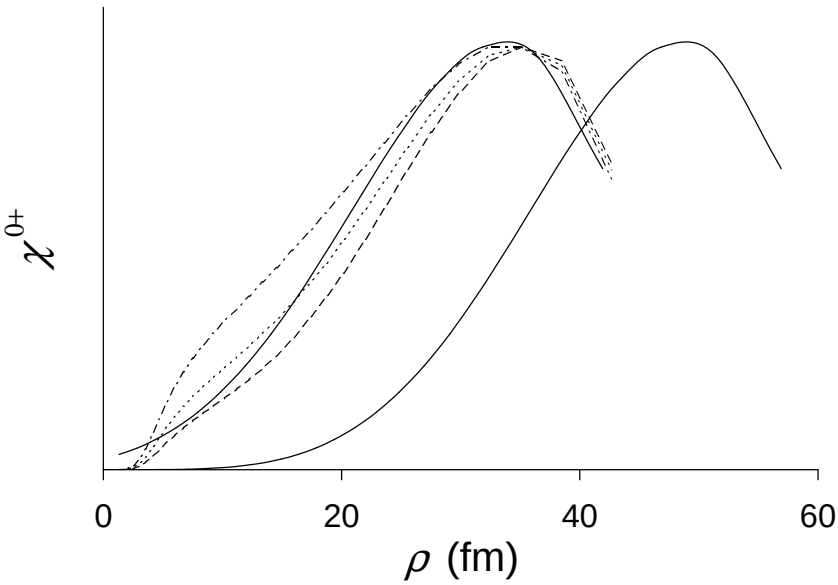

Fig. 7.3. $K = 0$ **components of the lowest positive-energy pseudostate near 0.4 MeV for** $K_{\max} = 12$ **(dashed line), 16 (dotted line), and 20 (dash-dotted line) normalized to the** $K = 0$ **Coulomb wave with** $Z^{0+}_{00,00} = 4.83$ **(right full line); same Coulomb wave shifted by 15 fm (left full line).**

is located at 0.379 MeV. It must not be considered as a resonance but rather as a pseudostate, a bound-state approximation of a scattering state at this energy. Its wave function will be useful to construct a better exploratory approximation.

The $K = 0$ components of the lowest positive-energy state located near 0.4 MeV obtained with $K_{\max} = 12$, 16, and 20 are displayed in Fig. 7.3. The energies do not vary much with $K_{\max}$ but the wave function is not yet converged. The amplitudes of the three curves are normalized to the $K = 0$ Coulomb wave Eq. (7.25) corresponding to the charge Eq. (7.32) (right full line). One observes a significant shift between the pseudostate and the Coulomb wave. As a simple qualitative approximation, we shift the Coulomb wave by 15 fm towards shorter distances (left full line). The resulting curve simulates the general behavior of the pseudostate. A shift by 10 fm would also be plausible.

We thus simulate the $K = 0$ component of the scattering state with the

shifted Coulomb functions

$$\chi^{J\pi}_{\gamma K(\gamma_\omega K_\omega)}(\rho) = 2i^K (2\pi/k)^{5/2} F_{K+3/2}[\eta_{\gamma K}, k(\rho + a)]\delta_{\gamma\gamma_\omega}\delta_{KK_\omega} \tag{7.33}$$

with $a = 10$ and 15 fm.

These functions do not vanish at the origin but this drawback has little influence, i.e. a smaller influence than other approximations. The results are displayed as full curves in Fig. 7.2: the lower curve corresponds to $a = 10$ fm and the upper curve corresponds to $a = 15$ fm. Their maximum is slightly shifted towards higher energies. The most probable total energies E are located between 0.15 and 0.3 MeV and the most probable total energies of the proton and neutron should approximately lie in the same interval since the ^{9}Li core is heavier. This approximation corresponds to $0.6 \times 10^{-8} < W < 1.8 \times 10^{-8}$ s^{-1} and $0.8 \times 10^{-10} < \mathcal{R} < 2.2 \times 10^{-10}$.

7.3. Conclusion

In this Chapter, we evaluate the order of magnitude of the branching ratio for the β delayed np emission by ^{11}Li, a very exotic decay process, unique among nuclei with known two-neutron separation energies. We have established the theoretical formulas for the Fermi and Gamow-Teller transitions leading to three-body final states.

An accurate model calculation is made very difficult by the need of three-body scattering states involving three different particles, two of them charged, at very low energies and by our lack of knowledge of physical properties of this three-body continuum and of absorption effects in the final three-body channel. To circumvent these difficulties in an exploratory calculation, we have made several simplifying approximations. Simple models of the final state involving a plane wave and a pure Coulomb wave provide likely upper and lower bounds

of the branching ratio, respectively. We think that more reasonable estimates of the branching ratio and of the energy distribution of the decays are obtained with shifted three-body Coulomb functions.

The obtained branching ratio should be comprised between 6×10^{-12} and 5×10^{-10} with more plausible values between 0.8×10^{-10} and 2.2×10^{-10}. The most probable total energies of the proton and neutron should lie between 0.15 and 0.3 MeV. In any case, the branching ratio is much smaller than for the deuteron and triton channels, i.e. $(1.3 \pm 0.13) \times 10^{-4}$ [98] and $(0.93 \pm 0.08) \times 10^{-4}$ [180], respectively. It is even much smaller than for the hindered deuteron decay of ^{6}He, $(2.6 \pm 1.3) \times 10^{-6}$ [94]. The main cause of this smallness is the small Q value of the process which leads to a limited phase space. The observation of this β delayed decay mode, if it is possible, will thus require high radioactive beam intensities and long measurement times to reach a significant enough number of ^{11}Li decays.

If this unique decay process is studied experimentally, a better model calculation will become necessary, with a full calculation of the three-body ^{9}Li+n+p continuum wave functions, using the formalism developed in Sec. 7.1. This study should be performed with ^{9}Li+n and ^{9}Li+p optical potentials in order to take absorption effects into account.

VIII. BETA-DELAYED EMISSION OF A PROTON BY A ONE-NEUTRON HALO NUCLEUS

In this chapter we study the beta-decay process of one-neutron halo nuclei ^{11}B, ^{19}C, and ^{31}Ne in the two-body potential model. [1] As was indicated in chapter 2, the β decay of the bound halo neutron may occur, under the condition of energy conservation

$$S_{\rm n} < (m_n - m_p - m_e)c^2 \approx 0.782 \text{ MeV}, \tag{8.1}$$

where $S_{\rm n}$ is the neutron separation energy of the decaying nucleus and

m_n, m_p and m_e are the neutron, proton and electron masses, respectively. The initial halo nucleus is treated as a core+neutron bound state. The final states are described as core+proton continuum. We will estimate transition probabilities and branching ratios for these processes.

8.1. Decay probability for β delayed proton emission

The β decay of the halo neutron releases the resulting proton from the core. The distribution of decay probability per time unit as a function of the energy $E < Q$ of the relative motion of the two particles is given by

$$\frac{dW}{dE} = \frac{1}{2\pi^3}\frac{m_e c^2}{\hbar} G_\beta^2 f(Q-E)\left(\frac{dB(\mathrm{F})}{dE} + \lambda^2 \frac{dB(\mathrm{GT})}{dE}\right), \tag{8.2}$$

[1] This chapter is based on the results of Ref. [126]

where $G_\beta \approx 2.996 \times 10^{-12}$ is the dimensionless β decay constant and $\lambda \approx -1.268$ is the ratio of the axial-vector to vector coupling constants. The Fermi integral $f(Q-E)$ depends on the kinetic energy $Q-E$ available for the electron and antineutrino with

$$Q = (m_n - m_p - m_e)c^2 - S_\mathrm{n}. \tag{8.3}$$

The total decay probability per time unit W is obtained by integrating Eq. (8.2) from zero to Q. The branching ratio can than be derived as

$$\mathcal{R} = W t_{1/2}/\ln 2, \tag{8.4}$$

where $t_{1/2}$ is the half life of the halo nucleus.

In the present model, the halo nucleus is described as a two-body core+neutron system in its ground state with total angular momentum J_i resulting from the coupling of the orbital momentum l_i of the relative motion and the neutron spin $s = 1/2$. The spin of the core is assumed to be zero. The parity of the initial state is $(-1)^{l_i}$. The radial wave function is denoted as $u_{il_iJ_i}$ with the normalization $\int_0^\infty |u_{il_iJ_i}(r)|^2 dr = 1$. It is obtained from a potential V_i adjusted to reproduce the experimental neutron separation energy S_n.

The final scattering state of the core and the proton is a distorted wave with wave vector $\boldsymbol{k}$. Because of selection rules, only some partial waves with total angular momentum J_f resulting from the coupling of the orbital momentum l_f and the proton spin s are allowed. The radial wave functions $u_{kl_fJ_f}$ for a wave number $k = \sqrt{2\mu E/\hbar^2}$ where μ is the core-proton reduced mass are obtained with a potential V_f describing the core+proton system. They are normalized according to $\int_0^\infty u_{kl_fJ_f}(r) u_{k'l_fJ_f}(r) dr = \delta(k-k')$. The potential V_f is usually poorly known when the core is unstable.

Within this model, the Fermi reduced decay probability is given by

$$\frac{dB(\mathrm{F})}{dE} = \frac{1}{\hbar v} \left| I_{l_i J_i J_i} \right|^2 \tag{8.5}$$

and the Gamow-Teller reduced decay probability by

$$\frac{dB(\mathrm{GT})}{dE} = \frac{6}{\hbar v} \sum_{J_f} (2J_f + 1) \left\{ \begin{array}{ccc} J_f & s & l_i \\ s & J_i & 1 \end{array} \right\}^2 \left| I_{l_i J_i J_f} \right|^2 \tag{8.6}$$

with the relative velocity $v = \hbar k/\mu$ and the radial integrals

$$I_{l J_i J_f} = \int_0^\infty u_{k l J_f}(r) u_{i l J_i}(r) dr. \tag{8.7}$$

If the final wave function does not depend on J_f, the Gamow-Teller term simplifies as

$$\frac{dB(\mathrm{GT})}{dE} = 3 \frac{dB(\mathrm{F})}{dE}. \tag{8.8}$$

The reduced decay probability can then also be written as

$$\frac{dW}{dE} = W_n \frac{f(Q-E)}{f_n} \frac{dB(\mathrm{F})}{dE}, \tag{8.9}$$

where W_n is the free-neutron β decay probability per second and f_n is the corresponding Fermi integral.

With respect to a free neutron, the decay probability is affected in two ways. First, the ratio $f(Q-E)/f_n$ is small due to the reduction of phase space, since $f_n \equiv f(Q+S_\mathrm{n})$. It becomes extremely small when E tends to Q. The β delayed proton emission is favoured by very small separation energies S_n. Second, the reduced decay probability Eq. (8.5) appearing in Eq. (8.9) is proportional to

the square of a radial integral Eq. (8.7). Because of the Coulomb repulsion and the smallness of the Q value, the scattering waves are small and, when E tends to zero, tend to zero as $k^{1/2}\exp(-\pi\eta)$ [181], where $\eta = Z_c e^2/\hbar v$ is the Sommerfeld parameter. They become thus smaller with increasing charge Z_c of the core. They also become smaller with increasing orbital momentum. Hence, at given Q value, we expect the decay probability to be largest for the lightest halo nuclei and for the halo neutron in the s wave.

8.2. Results and discussion

Before making explicit calculations, we have to specify the choice of potentials. The Fermi strength is proportional to the square of an overlap integral Eq. (8.7) between the initial and final radial wave functions. In order to have a realistic overlap, it is useful to have a correct node structure for these wave functions. Indeed, the presence of nodes leads to an integrand that changes sign one or several times and thus to a reduction of the overlap. Spectroscopic factors can also affect the size of the Fermi strength but given the limited knowledge on these quantities, we choose to ignore them in the present exploratory study. Finally, absorption in the core+proton optical potential might also play a role. However, the energies of the states after decay are lower than, or comparable to, the energy of the Coulomb barrier. Absorption should be weak and can safely be neglected.

Hence, we shall use real potentials V_i and V_f which should be deep enough to provide a realistic node structure of the initial and final radial wave functions. To keep the model simple we only use central Woods-Saxon potentials with range $r_0 A_c^{1/3}$ where A_c is the mass number of the core. The depth is adapted to the separation energy for the core+n system. The same form factor with an additional point-sphere Coulomb potential is employed for the final core+p

elastic scattering. Because of the small energies, the phase shifts are small and the sensitivity to V_f is weak. Now let us consider explicit cases.

The best documented case is ^{11}Be. Its $1/2^+$ ground state has a separation energy of about 501 keV [182] and its half life is 13.8 s [183]. The halo neutron is described by an s wave. The parameters of the Woods-Saxon potential are taken as $r_0 = 1.2$ fm, $a = 0.6$ fm and $V_{i0} = 62.52$ MeV [184]. In the s wave, this potential possesses one unphysical forbidden state. The same parameters are used for the final potential except V_{f0}. The ^{11}B nucleus has a proton separation energy $S_\mathrm{p} \approx 11.228$ MeV [111]. Its lowest $1/2^+$ state is located at the excitation energy $E_x \approx 6.79$ MeV. In the s wave, $V_{f0} = 84.1$ MeV is adjusted so that the potential possesses one forbidden state and one bound state fitted to the energy $E_x - S_\mathrm{p} \approx -4.52$ MeV with respect to the ^{10}Be+p threshold. Bound and scattering states should thus have a reasonable node structure.

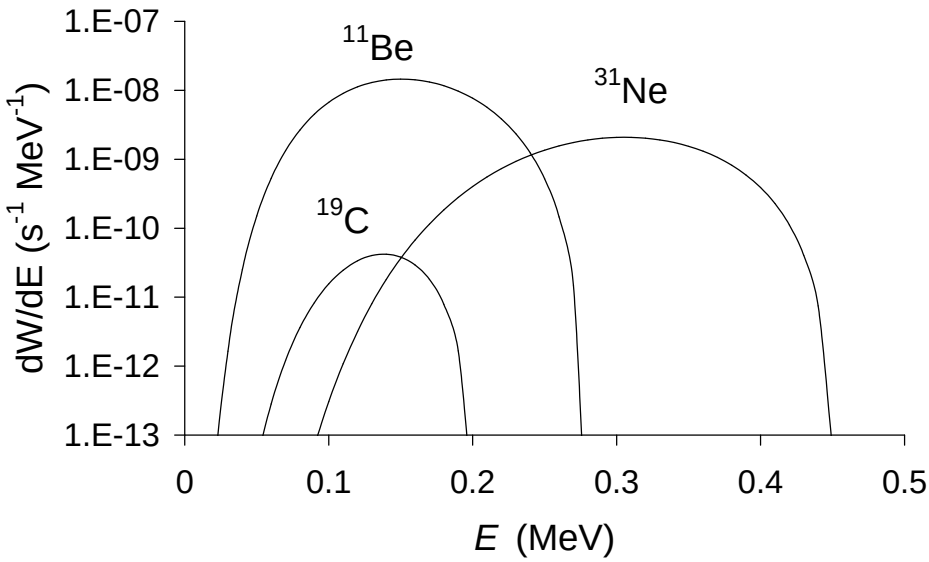

Fig. 8.1. Distribution of decay probability per second for the β delayed np decay of ^{11}Be, ^{19}C and ^{31}Ne.

The Q value Eq. (8.3) is small, 0.281 MeV. The distribution of decay probability is displayed in Fig. 8.1. The most probable energies of the relative motion

are in the interval 0.1-0.2 MeV. The total decay probability 1.5×10^{-9} s^{-1} leads to a branching ratio 3.0×10^{-8}. Recent experiments [185, 186] have confirmed the possibility of this decay. However, the experimental branching ratio was unexpectedly high: $(8.4 \pm 0.6) \times 10^{-6}$. As was explained in Ref. [185, 186] this is possible if the decay proceeds through a new single-particle resonance in ^{11}B.

The ^{19}C $1/2^+$ ground state has a separation energy of 580 ± 90 keV [111] and a half life $t_{1/2} = 46.2$ ms [183]. As a simple picture, we consider a neutron in the s wave with one forbidden state and no spectroscopic factor. The parameters of the Woods-Saxon potential are $r_0 = 1.25$ fm, $a = 0.62$ fm and $V_{i0} = 41.42$ MeV giving a Q value of 202 keV. For the final ^{18}C+p system, the s wave possesses one forbidden state. We assume a possible $1/2^+$ bound state near $E_x = 2.1$ MeV [187]. With $S_\mathrm{p} \approx 16.35$ MeV [111], we take $V_{f0} = 77.2$ MeV which gives a bound state at -14.2 MeV. The distribution of decay probability is displayed in Fig. 8.1. It is much smaller than for ^{11}Be because of the larger charge of the core and the smaller Q value. The total decay probability 2.7×10^{-12} s^{-1} leads to a branching ratio 1.8×10^{-13}.

A candidate for delayed proton emission is ^{31}Ne. Its neutron separation energy is poorly known: 0.33 ± 1.07 MeV [111]. Its half life is $t_{1/2} = 3.4$ ms [183]. This nucleus belongs to an island of inversion where its ground state should be an intruder state. Its one-neutron removal cross section [188] is too large for agreeing with the quantum numbers $0f7/2$ of the naive shell model. The ground state could be described with a $1p3/2$ orbital [189] although a $2s1/2$ orbital has also been considered [190]. Here we assume a p wave ground state at -0.33 MeV giving $Q = 0.45$ MeV. It can be reproduced with the parameters $r_0 = 1.25$ fm, $a = 0.75$ fm and $V_{i0} = 48.86$ MeV [189]. This potential has one forbidden state in the p wave. Little is known about the ^{30}Ne+p scattering. One can also expect an intruder $3/2^-$ state in the vicinity of the ground state. Hence we choose $V_{f0} = 90.0$ MeV which provides a forbidden state and a bound state at -16.1 MeV, not far above $-S_\mathrm{p} \approx -17.7$ MeV.

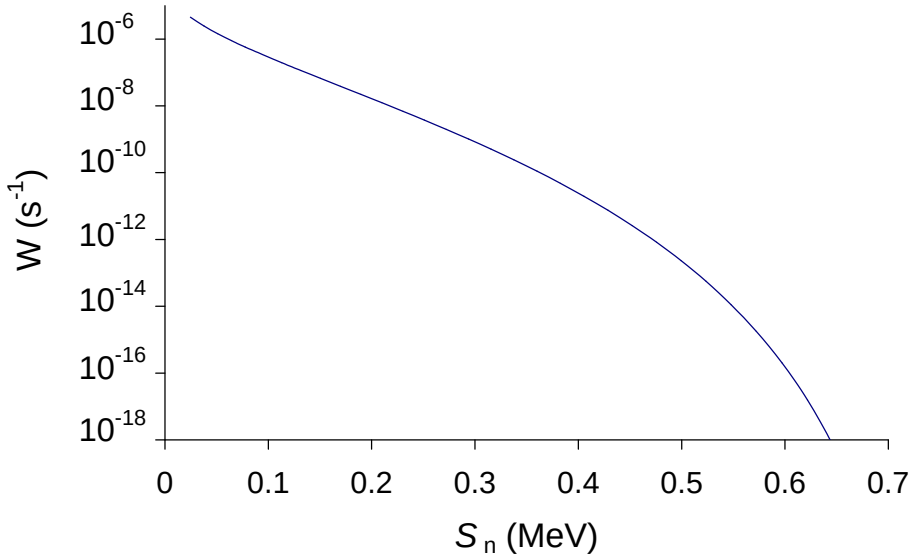

Fig. 8.2. Decay probability per second for the β delayed np decay of ^{31}Ne as a function of the separation energy $S_{\rm n}$.

The distribution of decay probability is displayed in Fig. 8.1. It is smaller than for ^{11}Be because of the larger charge of the core and the higher orbital momentum, but these effects are partly compensated by the larger Q value. The most probable energies E lie between 0.25 and 0.35 MeV. The total decay probability 3.3×10^{-10} s^{-1} leads to a branching ratio 1.6×10^{-12}. For an s ground state with two forbidden states ($V_{i0} = 69.27$ MeV), the decay probability $W \approx 1.6 \times 10^{-9}$ would be five times larger.

The separation energy of ^{31}Ne is quite uncertain. The one-neutron removal cross section can be interpreted as arising from $S_{\rm n} \approx 0.6$ MeV but this assumption is weakened by the lack of knowledge of spectroscopic factors [189]. Hence we display in Fig. 8.2 the dependence of the decay probability on the separation energy $S_{\rm n}$. One observes that it varies very strongly. If $S_{\rm n}$ is around 0.6 MeV, the decay probability is reduced by about six orders of magnitude. On the contrary, the decay probability can be larger by five orders of magnitude if the separation energy is very small.

Finally, let us note that an estimate of the order of magnitude (in general

within a factor of two) can be obtained with the simple approximation

$$I_{lJ_iJ_f} = C\sqrt{\frac{2}{\pi}} \int_a^\infty F_l(\eta, kr) e^{-\kappa r} dr \tag{8.10}$$

where $a = 5$ fm,

F_l is a regular Coulomb function,

$\kappa = \sqrt{2\mu S_n/\hbar^2}$. Under the same conditions as in Fig. 8.1, the asymptotic normalization constant C is 0.83, 0.96, 0.69 fm$^{-1/2}$ for ^{11}Be, ^{19}C, ^{31}Ne, respectively.

8.3. Conclusion

As a summary, we have evaluated the order of magnitude of the decay probability per second for the β delayed proton emission by one-neutron halo nuclei. The best candidate for observing such a decay is ^{11}Be in spite of its not very small separation energy. Because of a longer lifetime, the branching ratio is larger by two orders of magnitude than for the $n - p$ delayed decay of ^{11}Li [125]. The observation of this β delayed decay mode of ^{11}Be thus requires high radioactive beam intensities and long measurement times. Resent experiments have confirmed these predictions. However, the measured branching ratio was by two order of magnitude higher than expected. This can be understood if the decay proceeds through a new single-particle resonance in ^{11}B.

The neutron separation energies of the other candidates, ^{19}C and ^{31}Ne, are less well known and the decay probabilities are thus more uncertain. We have shown that the decay probability varies strongly with the neutron separation energy. A very small $S_{\rm n}$ would be advantageous for the study of this decay mode. This advantage however decreases when the charge of the core increases.

CONCLUSIONS

In the present dissertation, effective potential models have been applied to study the bound and continuum structure of light Borromean nuclei, including exotic halo systems, and the beta- and M1-transition processes of the halo nuclei into two-body and three-body continuum channels.

The obtained results have confirmed that the nuclear potential models are able to reproduce experimental data with a good accuracy if they describe the underlying microscopic features, and if the parameters of the potential are chosen in a consistent way. The most important cluster-cluster potential models have been examined: potentials with a strong repulsive core at short distances and, alternatively, deep potential models containing Pauli-forbidden states in the lower partial waves and yielding a node at short distances in the scattering wave function, a property of the microscopic cluster models. Thus, by comparing the results of the application of wave functions, obtained with different potential models, we have examined the importance of the microscopic description of the electromagnetic and weak processes with light nuclei, including exotic halo nuclei.

Conclusions of the dissertation work:

1) An extremely high sensitivity of the energies of the compact 0_1^+ and 2_1^+ states of the ^{12}C nucleus to the description of the two body $\alpha\alpha$ Pauli forbidden states was established.

2) For the first time the R-matrix approach has been developed for the study of the three-body continuum structure of light nuclei in the frame of the hyperspherical harmonics method on a Lagrange-mesh basis in combination with the propagation technique. It is found that the R-matrix, calculated at the boundary of the internal region, must be propagated up to large distances (about 1000

fm), where the wave function is matched with its asymptotics. The method has been applied to the analysis of the three-body continuum structure of the two-neutron halo nuclei ^6He and ^{14}Be, diagonal and eigen phases of the three-body collision matrix have been calculated and a new $^{14}Be(2^+)$ resonance was predicted at E_x=3.4 MeV. Recent experimental studies with the data $E_x(exp)$ = 3.54(16) MeV have confirmed our prediction.

3) We have shown that for the reproduction of the experimental data on the delayed beta decay of the ^{6}He halo nucleus into the $\alpha+d$ continuum channel, it is necessary to use microscopically founded $\alpha-d$ potentials with a forbidden state in the S-wave, reproducing phase shifts and the ground state energy. In that case, the internal and halo components of the Gamow-Teller matrix elements almost completely cancel each other, and as a result, the transition probability is strongly reduced consistently with the experimental data. These results for the first time demonstrated the importance of the potential models with forbidden states, which have a microscopic background, in beta-decay processes.

4) The method of hyperspherical harmonics on a Lagrange mesh has been applied to the analysis of the magnetic M1-transition of the isobar-analog state $^6Li(0+)$ to the $^6Li(1+)$ ground state and to the $\alpha + d$ continuum channel in the three-body formalism. The theoretical estimation for the width of the transition to the ground state 7.49 eV is well consistent with the experimental data 8.19±0.19 eV. And the calculated magnetic moment of the ^6Li nucleus ($\mu = 0.86\mu_N$) reproduced the experimental data $0.82\mu_N$ fairly well. Theoretical estimations for the probabilities of the M1-transition per time and energy units of the isobar-analog state $^6Li(0+)$ to the $\alpha + d$ continuum have been obtained. The integral width of the transition 0.9 meV is well consistent with the previous simplified calculations. It was shown that the isobar-analog state $^6Li(0+)$ has a well developed halo structure, like the nucleus $^6He(0+)$.

5) The theoretical estimations for the transition probabilities per time and energy units of the beta-decay of the halo nucleus ^{11}Li to the two-body $^9Li + d$

continuum channel have been obtained, very consistent with new experimental data. In this case, a resonance in the S-wave of the $^9Li + d$ system at the energy position of about 0.7 MeV plays the main role, not depending on which potential model is used: with a repulsive core or with a forbidden state. In this case, the halo components strongly dominate over the internal components. For the integral probability of the process the theoretical estimation 7.3E-3 s^{-1} is within the error bar of the experimental data 8.8 $\pm$1.9 E-3 s^{-1} for the energy cut-off $E > 0.2$ MeV.

6) The branching ratio for the β delayed np emission by ^{11}Li, a very exotic decay process, unique among nuclei with known two-neutron separation energies, has been estimated in the frame of the cluster potential model. Reasonable estimates of the branching ratio and of the energy distribution of the decays are obtained with shifted three-body Coulomb functions. The obtained branching ratio is estimated between 0.8×10^{-10} and 2.2×10^{-10}, which is much smaller than for the hindered deuteron decay of ^{6}He, $(2.6 \pm 1.3) \times 10^{-6}$. The reason of this smallness is the small Q value of the process which leads to a limited phase space. The observation of this β delayed decay mode, as expected, requires a valuable experimental effort. The total transition probabilities are estimated to be of order 10^{-8} s^{-1}. These estimations show how rare the process is.

7) At the end, we have evaluated the beta decay probabilities per time and energy units of the one-neutron halo nuclei ^{11}Be, ^{19}C and ^{31}Ne to the two-body $core + p$ continuum channels in the cluster potential model. For the total transition probability of the ^{11}Be nucleus to the $^{10}Be + p$ continuum channel the estimation is 1.5E-9 s^{-1}, of the ^{19}C nucleus to the $^{18}C + p$ continuum it is 2.7 E-12 s^{-1}. The corresponding branching ratios are 3.0E-8 for the ^{11}Be and 1.8E-13 for the ^{19}C halo nuclei. The total transition probability of the ^{31}Ne nucleus to the $^{30}Ne + p$ continuum channel varies from 0 up to 1.E-6 s^{-1} due to uncertainty of the separation energy. For the separation energy between 0.25 and 0.35 MeV, the total decay probability is 3.3E-10 s^{-1}, which leads to a

branching ratio 1.6E-12.

The **main conclusion** of the dissertation is that the potential models developed in this work can not only describe adequately the existing experimental data in the field of low-energy nuclear physics, but also are able to predict new properties of light nuclei, if the parameters of the model are chosen from the condition to be consistent with the underlying microscopic features.

BIBLIOGRAPHY

[1] Day B.D. Three body correlations in nuclear matter // Physical Review - New York, 1981. - vol **C24**, N. 3. - pp. 1203-1271.

[2] Wiringa P.B., Smith R.A., Ainswoth T.L. Nucleon-nucleon potential with and without Delta(1232) degrees of freedom // Phys.Rev. - New York, 1984. - vol. **C29**, N. 4. - pp. 1207-1221.

[3] Machleidt R., Holinde, Elster Ch. The Bonn meson -exchange model for the nucleon-nucleon interaction // Phys. Rep.- Elsevier, Amsterdam, 1987. - vol. **149**, N. 1. - pp. 1-89.

[4] Epelbaum E., Nogga A., Glockle W., Kamada H., Meissner Ulf-G., Witala H. Three-nucleon forces from chiral effective field theory // Phys. Rev. - New York, 2002. - vol. **C 66**, N. 6. - 064001 (17 p.)

[5] Epelbaum E., Hammer H.-W., Meissner Ulf-G. Modern theory of nuclear forces // Rev. Mod. Phys. - New York, 2009. - vol.**81**, N. 4. - pp. 1773-1825.

[6] Nakamura K, et al. (Particle Data group). Review of Particle Physics // J. Phys. - London, 2010. - vol. **G37**, N. 7A. - 075021 (1422 p.)

[7] Klempt E., Richard J.M. Baryon spectroscopy // Rev. Mod. Phys. - New York, 2010. - vol.**82**, N.2. - pp. 1095-1153.

[8] Riska D.O., Brown G.E. Two-pion exchange interaction between constituent quarks // Nucl. Phys. - Elsevier, Amsterdam, 1999. - vol. **A653**, N. 3. - pp. 251-273.

[9] Holinde K. The nucleon-nucleon interaction // Nucl. Phys. - Elsevier, Amsterdam, 1992. - vol. **A543**, N. 1-2. - pp. 143-162.

[10] Proceedings of the International Workshop on Physics of Excited Nucleons (NSTAR 2013) Peniscola, Spain, 27-30 May 2013. - Int. J. Mod. Phys. CS. - Singapore, 2014. - vol. **26**.

[11] Anisovich A.V., Klempt ., Nikonov V.A., Sarantsev A.V., Thoma U. P -wave excited baryons from pion- and photo-induced hyperon production // European Physical Journal A. - Springer, Berlin, 2011. - vol. **47**, N. 2. - pp. 27-42.

[12] Tursunov E.M. Lower excitation spectrum of the nucleon and delta in a relativistic chiral quark model // J. Phys. G: Nucl. Part. Phys. - London, 2005. - vol. **31**, N. 7. - pp. 617-629.

[13] Tursunov E.M. Relativistic structure of one-meson and one-gluon exchange forces and the lower excitation spectrum of the Nucleon and the Delta // Journal of Physics G: Nuclear and Particle Phys.- London, 2009. - vol. **36**, N. 9. - 095006 (17 p.).

[14] Tursunov E.M. Convergence of the self-energy in a relativistic chiral quark model: excited Nucleon and Delta sector// J. Phys. G: Nucl.Part.Phys., - London, 2010 -vol. **37**, N. 10 - 105013 (8 p.).

[15] Tursunov, E. M. A periodic table for the excited N* and Δ* spectrum in a relativistic chiral quark model // arXiv:1103.3661, Los-Alamos, 2011. - 7 p.

[16] Tursunov, E. M., Krewald S. Spectrum of the excited N^* and Δ^* baryons in a relativistic chiral quark model // Phys. Rev. D - New York, 2014. - vol. **D90** - id. 074015 (16 p.)

[17] Tursunov, E. M., Krewald S. Spectrum of the excited N^* and Δ^* baryons in a relativistic chiral quark model. // Int. Jour. Mod. Phys. CS. - Singapore, 2014. -vol. **26** - 1460118 (5 p.).

[18] Oset E., Tegen R., Weise W. Nucleon charge form factors and chiral quark models // Nucl. Phys. - Elsevier, Amsterdam, 1984. - vol. **A426**, N. 3. - pp. 456-476.

[19] Gutsche Th. A Chiral Potential Model for the Light Quark Baryons: Ph.D. thesis. - Florida State Univ., USA, 1987. - 249 p.

[20] Gutsche Th., Robson D. Positive and convergent self-energy in a chiral potential model // Phys. Lett. - Elsevier, Amsterdam, 1989. - vol. **B229**, N. 4. - pp. 333-338.

[21] Fujiwara Y., Suzuki Y., Nakamoto C. Baryon-baryon interactions in the SU6 quark model and their applications to light nuclear systems // Prog. Part. Nucl. Phys. - Elsevier, Amsterdam, 2007. - vol. **58**, N. 2. - pp. 439-520.

[22] Tursunov E.M. Study of a three-body problem with the Moscow **NN** -potential: Ph.D thesis. - Tashkent, 1997. - 129 p.

[23] Kukulin V.I., Pomerantsev V.N., Faessler A., Buchmann A., Tursunov E.M. Moscow-type NN potentials and three-nucleon bound states // Phys.Rev. - New York, 1998. - vol. **C57**, N. 2. - pp. 535-554.

[24] Baye D. Supersymmetry between deep and shallow nucleus-nucleus potentials // Phys. Rev. Lett. - New York, 1987. - vol. **58**, N. 26. - pp. 2738-2741.

[25] Kukulin V.I., Obukhovsky I.T., Pomerantsev V.N., Faessler A. Two component dressed-bag model for NN interaction: deuteron structure and

phase shifts up to 1 GeV // Int. J. Mod. Phys. E. - Singapore, 2002. - vol. **11**, N. 1. - pp. 1-33.

[26] Neudatchin V.G., Kukulin V.I., Korotkikh V.L., Korennoy V. A microscopically substantiated local optical potential for $\alpha - \alpha$- scattering // Phys.Lett. - Elsevier, Amsterdam, 1971. - vol. **34B**, N. 7. - pp. 581-583.

[27] Buck B., Friedrich H., Wheatley C. Local potential models for the scattering of complex nuclei // Nucl.Phys. - Elsevier, Amsterdam, 1977. - vol. **A275**, N. 1. - pp. 246-268.

[28] Sofianos S. A., Adam R. M., Belyaev V. B. Alpha-cluster-model description of nuclei // Phys. Rev. - New York, 2011. - vol. **C84**, N. 6. - 064304 (6 p.).

[29] Filikhin I., Suslov V.M., Vlahovic B. 0+ states of the 12C nucleus: the Faddeev calculation in configuration space // J. of Phys.G:Nucl.Phys. - London, 2005. - vol. **31**, N. 11. - pp. 1207-1224.

[30] Yamada T., Schuck P. Single alpha-particle orbits and Bose-Einstein condensation in 12C // Euro.Phys.J. - Springer, Berlin, 2005. - vol. **A26**, N. 2. - pp.185-199

[31] Lashko Yu. A., Filippov G.F. The role of the Pauli principle in three-cluster systems composed of identical clusters // Nucl. Phys. - Elsevier, Amsterdam, 2009. - vol. **A826**, N. 1. - pp.24-48.

[32] Descouvemont P. Three-alpha continuum states. // J. of Phys.G:Nucl.Phys. - London, 2010. - vol. **37**, N. 6. - id. 064010 (16 p.)

[33] Descouvemont P. 12C spectroscopy above the 3-alpha threshold. // J. of Phys.:Conf. Ser. - London, 2011. - vol. **321**, N. 1. - id. 012013 (10 p.).

[34] Lazauskas R., Dufour M. Description of three-alpha bosonic states in the 12C nucleus with local and nonlocal potentials // Phys. Rev. - New York, 2011. - vol. **C84**, N.6. - id. 064318 (8 p.).

[35] Lu B.-N., Lähde T.A., Lee D, Meissner Ulf-G. Breaking and restoration of rotational symmetry on the lattice for bound state multiplets // Phys. Rev. - New York, 2014. - vol. **D90**, N. 2. - id. 034507 (10 p.).

[36] Hutzelmeyer H., Hackenbroich H.H. Carbon 12 as a nucleus of symmetry [444] // Z. Phys. - Springer, Vena, 1970. - vol. **232**, N. 4. - pp. 356-362.

[37] Smirnov Yu.F., Obukhovsky I.T., Tchuvil'sky Yu.M., Neudatchin V. G. The 12C nucleus as a 3 α system with forbidden states // Nucl.Phys. - Elsevier, Amsterdam, 1974. - vol. **A 235**, N. 2. - pp. 289-298.

[38] Horiuchi H. Many-Cluster Problem by the Orthogonality Condition Model –General Discussion and 12C Problem // Prog. Theor. Phys. - Tokyo, 1975. - vol. **53**, N. 2. - pp. 447-460.

[39] Toshaki-Suzuki A., Kamimura M., Ikeda K. Microscopic Study of the Interaction between Complex Nuclei // Prog. Theor. Phys.Suppl. - Tokyo, 1980. - vol. **68**. - pp. 359-385.

[40] Schmid E. W., Orlowski M. Approximative treatment of the Coulomb exchange interaction of clusters// Z.Phys. - Springer, Vienn, 1982.- vol. **A306**, N. 1. - pp. 51-55.

[41] Pichler R., Oberhummer H., Csoto A., Moszkowski S.A. Three-alpha structures in 12C // Nucl.Phys. - Elsevier, Amsterdam, 1997. - vol. **A618**, N. 1-2. -pp. 55-64.

[42] Ajzenberg-Selove F., Lauritsen T. Energy levels of light nuclei A = 5-10 // Nucl.Phys. - Elsevier, Amsterdam, 1988. - vol.**A490**, N. 1. - pp. 1-225.

[43] Ali S., Bodmer A.R. Phenomenological alpha-alpha potentials // Nucl.Phys. - Elsevier, Amsterdam, 1966. - vol. **A80**, N. 1. - pp. 99-112.

[44] Marsh S. The hyperspherical harmonics method applied to 12C // Nucl.Phys. - Elsevier, Amsterdam, 1982. - vol. **A389**, N. 1. - pp 45-55.

[45] Walliser H., Nakaichi-Maeda S. Pauli repulsion of α-particles and the 3α overbinding problem // Nucl.Phys. - Elsevier, Amsterdam, 1987. - vol. **A464**, N. 3. - pp. 366-380.

[46] Tursunov E.M. Variational calculations of the ^{12}C nucleus structure in a 3α model using a deep potential with forbidden states // J. Phys.G: Nucl.Part.Phys - London, 2001. - vol. **27**, N. 7. - pp. 1381-1389.

[47] Tursunov, E.M., Baye D., Descouvemont P. Comparative variational studies of 0+ states in three-alpha models// Nuclear Physics. - Elsevier, Amsterdam, 2003. - vol. **A723**, N. 3-4. - pp. 365-374.

[48] Fujiwara Y., Suzuki Y., Kohno M. Case of almost redundant components in three-alpha Faddeev equations // Phys. Rev. - New York, 2007. - vol. **C69**, N.3. - id. 037002 (4 p.).

[49] Fujiwara Y., Miyagawa K., Kohno M., Suzuki Y., Baye D., Sparenberg J.-M. Faddeev calculation of three-alpha and $\alpha\alpha\Lambda$ systems using resonating-group method kernels // Phys. Rev. - New York, 2004. - vol. **C70**, N.2. - id. 024002 (18 p.).

[50] Theeten M., Baye D., Descouvemont P. Comparison of local, semi-microscopic, and microscopic three-cluster models // Phys. Rev. - New York, 2006. - vol. **C74**, N.4. - 044304 (14 p.).

[51] Theeten M., Matsumura H., Orabi M., Baye D., Descouvemont P., Fujiwara Y., Suzuki Y. Three-body model of light nuclei with microscopic

nonlocal interactions // Phys. Rev. - New York, 2007. - vol. **C76**, N.5. - id. 054003 (11 p.).

[52] Pf*ü*tzner M., Karny M, Grigorenko L.V., Riisager K. Radioactive decays at limits of nuclear stability // Rev. Mod. Phys. - New York, 2012. - vol. **84**, N. 2. - pp. 567-619.

[53] Grieser M., Litvinov Yu.A., Raabe R. et al. Storage ring at HIE-ISOLDE. Technical design report // Euro.Phys.J. Special Topics - Springer, Berlin, 2012. - vol. **207**. - pp.1-117

[54] Tanihata I., Savajols H., Kanungo R. Recent experimental progress in nuclear halo structure studies // Prog. Part. Nucl. Phys. - Elsevier, Amsterdam, 2013. - vol. **68**, N.1. - pp.215-313.

[55] Borge, M. J. G. Beta-delayed particle emission // Physica Scripta - IoP Publishing, London, 2013. - Vol. **152**, N.1 - id. 014013 (17 p.).

[56] Borge M.J.G., Fraile L.M., Fynbo H.O.U., Jonson B., Kirsebom O.S., Nilsson T., Nyman G., Possnert G., Riisager K., Tengblad O. Rare β-p decays in light nuclei // J. of Phys.G:Nucl.Phys. - London, 2013. - Vol. **40**, N. 3. - id. 035109 (10 p).

[57] Tanihata I., Hamagaki H., Hashimoto O., Shida Y., Yoshikawa N., Sugimoto K., Yamakawa O., Kobayashi T., Takahashi N. Measurements of Interaction Cross Sections and Nuclear Radii in the Light p -Shell Region // Phys. Rev. Lett. - New York, 1985. - vol. **55**, N. 24. - pp. 2676-2679.

[58] Hansen P.G., Jonson B. The Neutron Halo of Extremely Neutron-Rich Nuclei // Europhys. Lett. - London, 1987. - vol. **4**, N. 4. - pp. 409-413.

[59] Tanihata I. Neutron halo nuclei // J. Phys. G - London, 1996. - vol. **22**, N. 2. - pp. 157-198.

[60] Zhukov M.V., Fedorov D.F., Danilin B.V., Vaagen J.S., Bang J.M. A simplified three-body model for 11Li and associated 9Li and neutron momentum distributions // Nucl. Phys. - Elsevier, Amsterdam, 1991. - vol. **A529**, N. 1. - pp. 53-67.

[61] Timofeyuk N. K., Blokhintsev L. D., Tostevin J. A. Pre-asymptotic behavior of single-particle overlap integrals of non-Borromean two-neutron halos // Phys. Rev. - New York, 2003. - vol. **C68**, N. 2. - 021601 (5 p.).

[62] Jonson B. Light dripline nuclei // Phys. Rep. - Elsevier, Amsterdam, 2004. - vol. **389**, N. 1. - pp. 1-59.

[63] Zhukov M.V., Danilin B.V., Fedorov D.V., Bang J.M., Thompson I.J., Vaagen J.S. Bound state properties of Borromean halo nuclei: 6He and 11Li // Phys. Rep. - Elsevier, Amsterdam, 1993. - vol. **231**, N. 4. - pp. 51-199.

[64] Alt E. O., Blokhintsev L. D., Mukhamedzhanov A. M., Sattarov A. I. Deuteron elastic scattering and stripping processes off C12 as a three-body problem // Phys Rev - New York, 2007. - vol. **C75**, N. 5. - 054003 (11 p.)

[65] Morse P.M., Feshbach H. Methods in Theoretical Physics. - McGraw-Hill, New York, 1953 - vol. 2. - 997 p.

[66] Lin C.D. Hyperspherical coordinate approach to atomic and other Coulombic three-body systems // Phys. Rep. - Elsevier, Amsterdam, 1995. - vol. **257**, N. 1. - pp. 1-83.

[67] Descouvemont P., Daniel C., Baye D. Three-body systems with Lagrange-mesh techniques in hyperspherical coordinates // Phys. Rev. - New York, 2003. - vol. **C67**, N. 4. - 044309 (14 p.).

[68] Aumann T., Aleksandrov D., Axelsson L., et al. (collaboration). Continuum excitations in 6He // Phys. Rev. - New York, 1999. - vol. **C59**, N. 3. - pp. 1252-1262.

[69] Lazauskas R., Carbonell J. Ab-Initio Calculations of Four-Nucleon Elastic Scattering // Few-Body-Systems. - Springer, Berlin, 2004. - vol. **34**, N. 2. - pp. 105-111.

[70] Kukulin V. I., Rubtsova O.A. Elastic scattering on a nucleus and the breakup of the composite projectile via wave-packet continuum discretization // Phys. Rev. - New York, 2007. - vol. **C76**, N. 4. - 047601 (4 p.).

[71] Belyaev V. B., Levin S. B., Yakovlev S. L. Three charged particles in the continuum: astrophysical examples // J. Phys. B: Atomic, Molecular, and Optical Physics. - London,2004. - vol. **37**, N. 6. - pp. 1369-1380.

[72] Ershov S.N., Danilin B.V., Vaagen J.S. Continuum spectroscopy of Borromean two-neutron halo nuclei // Phys. Rev. - New York, 2006. - vol. **C74**, N. 1. - 014603 (10 p.).

[73] Vaagen J. S., Danilin B. V., Ershov S. N. Continuum Spectroscopy of Halo Nuclei // Int. J. Mod. Phys., Singapore, 2007. - vol. **E16**, N. 4. - pp. 1033-1045.

[74] Mukhamedzhanov A. M., Lieber M. Asymptotic wave function for three charged particles in the continuum // Phys. Rev. - New York, 1996. - vol. **A54**, N. 4. - pp. 3078-3085.

[75] Alt E.O., Irgaziev B.F., Mukhamedzhanov A.M. Three-body Coulomb interaction effects in the final state of the 208Pb(8B,7Bep)208Pb Coulomb breakup reaction // Phys. Rev. - New York, 2005. - vol. **C71**, N. 2. - 024605 (15 p.).

[76] Matsumoto T., Hiyama E., Ogata K., Iseri Y., Kamimura M., Chiba S., Yahiro M. Continuum-discretized coupled-channels method for four-body nuclear breakup in 6He + 12C scattering // Phys. Rev. - New York, 2004. - vol. **C70**, N.6. - id. 061601 (5 p.)

[77] [5] C. Beck, N. Keeley, A. Diaz-Torres. Coupled-channel effects in elastic scattering and near-barrier fusion induced by weakly bound nuclei and exotic halo nuclei // Phys. Rev. - New York, 2007. - vol. **C75**, N.5. - id. 054605 (11 p.)

[78] Rubtsova O.A., Kukulin V.I., Moro A.M. Continuum discretization methods in a composite particle scattering off a nucleus: Benchmark calculations // Phys. Rev. - New York, 2008. - vol. **C78**, N.3. - id. 034603 (9 p.)

[79] Rodriguez-Gallardo M., Arias J.M., Gomez-Camacho J., Johnson R.C., Moro A.M., Thompson I.J., Tostevin J.A. Four-body continuum-discretized coupled-channels calculations using a transformed harmonic oscillator basis // Phys. Rev. - New York, 2008. - vol. **C77**, N.6. - id. 064609 (9 p.)

[80] Moro A.M., Arias J.M., Gomez-Camacho J., Perez-Bernal F. Analytical transformed harmonic oscillator basis for continuum discretized coupled channels calculations // Phys. Rev. - New York, 2009. - vol. **C80**, N.5. - id. 054605 (10 p.)

[81] Egami T., Matsumoto T., Ogata K.,Yahiro M. Description of Four-Body Breakup Reaction with the Method of Continuum-Discretized Coupled-Channels // Prog. Theor. Phys. - Tokio, 2009. - vol. **121**, N.4. - pp. 789-807

[82] Druet T., Baye D., Descouvemont P., Sparenberg J.-M. CDCC calcula-

tions with the Lagrange-mesh technique // Nucl. Phys. - Elsevier, Amsterdam, 2010. - vol. **A845**, N. 1. - pp.88-105.

[83] Khaldi K., Elster Ch., Glöckle W. The n+n+alpha system in a continuum Faddeev formulation // Phys. Rev. - New York, 2010. - vol. **C82**, N.5. - id. 054002 (14 p.)

[84] Romero-Redondo C., Quaglioni S., Navrrtil P., Hupin G. He4+n +n continuum within an ab initio framework // Phys. Rev. Lett. - New York, 2014. - vol. **113**, N.3. - id. 032503 (5 p.)

[85] Carbonell J., Deltuva A., Fonseca A.C., Lazauskas R. Bound state techniques to solve the multiparticle scattering problem // Prog. Part. Nucl. Phys. - Elsevier, Amsterdam, 2014. - vol. **74**, N. 1. - pp. 55-80.

[86] Ho Y.K. The method of complex coordinate rotation and its applications to atomic collision processes // Phys. Rep. - Elsevier, Amsterdam, 1983. - vol **99**, N. 1. - pp. 1-68.

[87] Kukulin V.I., Krasnopol'sky V.M. Description of few-body systems via analytical continuation in coupling constant // J. Phys. A - London, 1977. - vol. **10**, N. 2. - pp. L33-L37.

[88] Lane A.M., Thomas R.G. R-Matrix Theory of Nuclear Reactions // Rev. Mod. Phys. - New York, 1958. - vol. **30**, N. 2. - pp. 257-353.

[89] Thompson I.J., Danilin B.V., Efros V.D., Vaagen J.S., Bang J.M., Zhukov M.V. Pauli blocking in three-body models of halo nuclei // Phys. Rev. - New York, 2000. - vol. **C61**, N. 2. - 024318 (11 p.).

[90] Burke V.M., Noble C.J. Farm - A flexible asymptotic R-matrix package // Comput. Phys. Commun. - Elsevier, Amsterdam, 1995. - vol. **85**, N. 3. - pp. 471-500.

[91] Descouvemont P., Tursunov E.M., Baye D. Three body continuum states on a Lagrange mesh // Nucl.Phys. - Elsevier, Amsterdam, 2006. - vol. **A765**, N. 3-4, pp. 370-389

[92] Riisager K., Borge M.J.G., Gabelmann H., et al. (collaboration). First observation of beta-delayed deuteron emission. // Phys. Lett. - Elsevier, Amsterdam, 1990. - vol. **B235**, N. 1-2. - pp. 30-34.

[93] Borge M. J. G., Johannsen L., Jonson B., et al. (collaboration). Study of charged particles emitted in the beta-decay of 6,8He // Nucl. Phys. - Elsevier, Amsterdam, 1993. - vol. **A560**, N. 2. - pp. 664-676.

[94] Anthony D., Buchmann L., Bergbusch P., et al. (collaboration). Beta-delayed deuteron emission from 6He // Phys. Rev. - New York, 2002. - vol. **C65**, N. 3. - 034310 (7 p).

[95] Raabe R., B*ü*scher J., Ponsaers J. et al. Measurement of the branching ratio of the He6 beta-decay channel into the alpha+d continuum // Phys. Rev. - New York, 2009. - vol. **C80**, N.5. - id. 054307 (6 p.)

[96] Mukha I., Borge M.J.G., Guillemaud-Mueller D., et al. (ISOLDE collaboration). Observation of the 11Li(beta d) decay // Phys. Lett. - Elsevier, Amsterdam, 1996. - vol. **B367**, N. 1-4. - pp. 65-69.

[97] Borge M.J.G., Grigorenko L., Guillemaud-Mueller D., et al. (ISOLDE collaboration). Probing the 11Li halo structure through beta-decay into the 11Be*(18 MeV) state // Nucl. Phys. - Elsevier, Amsterdam, 1997. - vol. **A613**, N. 3. - pp. 199-208.

[98] Raabe R., Andreyev A., Borge M.J.G., et al. (collaboration). Beta - Delayed Deuteron Emission from Li11 : Decay of the Halo // Phys. Rev. Lett. - New York, 2008. - vol. **101**, N. 21. - 212501 (4 p).

[99] Descouvemont P., Leclercq-Willain C. Beta-delayed deuteron emission of 6He in a potential model // J. Phys. G: Nucl. Part. Phys. - London, 1992. - vol. **18**, N. 5. - pp. L99-L104.

[100] Zhukov M.V., Danilin B.V., Grigorenko L.V., Shulgina N.B. He6 beta-decay to the alpha+d channel in a three-body model // Phys. Rev. - New York, 1993. - vol. **C47**, N. 6. - pp. 2937-2940.

[101] Baye D., Suzuki Y., Descouvemont P. Evidence for Halo in Quenching of 6He beta-decay into alpha and Deuteron // Prog. Theor. Phys. - Tokyo, 1994. - vol. **91**, N. 2. - pp. 271-286.

[102] Varga K., Suzuki Y., Ohbayashi Y. Microscopic multicluster description of the neutron-rich helium isotopes // Phys. Rev. - New York, 1994. - vol. **C50**, N. 1. - pp. 189-195.

[103] Barker F.C. Deuteron emission following 6He beta-decay // Phys. Lett. - Elsevier, Amsterdam, 1994. - vol. **B322**, N. 1-2. - pp. 17-21.

[104] Csótó A., Baye D. Microscopic description of the beta-delayed deuteron emission from He6 // Phys. Rev. - New York, 1994. - vol. **C49**, N. 2. - pp. 818-823.

[105] Tursunov E.M., Baye, D., Descouvemont P. Analysis of the He-6 beta-decay into the α+d continuum within a three-body model // Phys. Rev. - New York, 2006. - vol. **C73**, N.1. - 014303 (9 p.); vol. **C74**, N. 6. - 069904(E).

[106] Tursunov E.M., Baye D., Descouvemont P. Electromagnetic and weak processes with light halo nuclei// Uzbek. Phys. Journal - Tashkent, 2010.- vol. **12**, N. 4-6. - pp. 280-289.

[107] Csótó A., Langanke K. Parity-violating beta-decay of the 3.56 MeV (J^{π},T)

= (0^+,1) state of 6Li // Nucl. Phys. - Elsevier, Amsterdam, 1996. - vol. **A601**, N. 2. - pp. 131-140.

[108] Grigorenko L.V., Shulgina N.B. Parity-violating $^6Li(0+1) \Rightarrow \alpha + d$ decay and 6Li(0+1) $\Rightarrow \alpha + d + \gamma$ M1-transition // Phys. Atom. Nucl. - Moscow, 1998. - vol. **61**, N. 9. - pp. 1472-1478.

[109] Suzuki Y., Yabana K. Isobaric analogue halo states // Phys. Lett. - Elsevier, Amsterdam, 1991. - vol. **B272**, N. 3-4. - pp. 173-177.

[110] Tursunov E.M., Descouvemont P., Baye D. Gamma-delayed deuteron emission of the 6Li(0+) state // Nucl.Phys. - Elsevier, Amsterdam, 2007. - vol. **A793**, N. 1. - pp. 52-66.

[111] Audi G., Wapstra A.H., Thibault C. The Ame2003 atomic mass evaluation: (II). Tables, graphs and references // Nucl. Phys. - Elsevier, Amsterdam, 2003. - vol. **A729**, N. 1. - pp. 337-676.

[112] Bachelet C., Audi G., Gaulard C., Guénaut G., Herfurth F., Lunney D., Saint Simon M. de, Thibault C. and the ISOLDE collaboration. Mass measurement of short-lived halo nuclides // Eur. Phys. J. - Springer, Berlin, 2005. - vol. **A25**, N. 1, Suppl. 1. - pp. 31-32.

[113] Bachelet C., Audi G., Gaulard C., Guenaut C., Herfurth, F., Lunney D., de Saint Simon M., Thibault, C. New Binding Energy for the Two-Neutron Halo of Li11 // Phys. Rev. Lett. - New York, 2008. - vol. **100**, N.18. - id. 182501 (4 p.)

[114] Gaulard C., Bachelet C., Audi G., et al. (collaboration). Mass measurements of the exotic nuclides 11Li and 11,12Be performed with the Mistral spectrometer // Nucl. Phys. - Elsevier, Amsterdam, 2009. - vol. **A826**, N. 1-2. - pp. 1-23.

[115] Kelley J. H., Kwan E., Purcell J. E., Sheu C.G., Weller H. R. Energy levels of light nuclei A=11 // Nucl. Phys. - Elsevier, Amsterdam, 2012. - vol. **A880**, N. 2. - pp.88-195.

[116] Marqués F.M., Labiche M., Orr N.A., et al. (collaboration). Three-body correlations in Borromean halo nuclei // Phys. Rev. - New York, 2001. - vol. **C64**, N. 6. - 061301 (5 p.).

[117] D. Baye. Lagrange-mesh calculations of halo nuclei // Nucl. Phys. - Elsevier, Amsterdam, 1997. - vol. **A627**, N. 2. - pp. 305-323.

[118] Thompson I.J., Zhukov M.V. Effects of ^{10}Li virtual states on the structure of ^{11}Li // Phys. Rev. - New York, 1994. - vol. **C49**, N. 4. - pp. 1904-1907.

[119] Borge M.J.G., Fynbo H., Guillemaud-Mueller D., et al. (ISOLDE collaboration). Elucidating halo structure by beta decay: beta gamma from the 11Li decay // Phys. Rev. - New York, 1997. -vol. **C55**, N. 1. - pp. R8-R11.

[120] Langevin M., Detraz C., Epherre M., et al. (ISOLDE collaboration). Observation of beta-delayed triton emission // Phys. Lett. - Elsevier, Amsterdam, 1984. - vol. **B146**, N. 3-4. - pp. 176-178.

[121] Ohbayasi Y., Suzuki Y. An exploratory study of 11Li beta-decay into 9Li and a deuteron. Phys. Lett. - Elsevier, Amsterdam, 1995. - vol. **B346**, N. 3-4. - pp. 223-226.

[122] Zhukov M.V., Danilin B.V., Grigorenko L.V., Vaagen J.S. Beta-decay of Li 11 to the deuteron channel and halo analog states in Be11 // Phys. Rev. - New York, 1995. - vol. **C52**, N. 5. - pp. 2461-2467.

[123] Baye D., Tursunov E.M., Descouvemont P. Beta-decay of 11Li into 9Li and a deuteron within a three-body model // Phys. Rev. - New York, 2006. - vol. **C74**, N. 6. - 064302 (7 p.).

[124] Tursunov E.M., Baye D., Descouvemont P. Theoretical study of the 11Li beta-decay into the deuteron channel in a cluster model // Int. J. Mod. Phys.E. - Singapore, 2011. - vol. **20**, N. 4 - pp. 803-806.

[125] Baye D., Descouvemont P., Tursunov E.M. Unique decay process: beta -delayed emission of a proton and a neutron by the 11Li halo nucleus // Phys. Rev.C -New York, 2010 - vol. **82**, N.5 - 054318 (6 p.).

[126] Baye D., Tursunov E.M. Beta-delayed emission of a proton by a one-neutron halo nucleus // Phys. Lett. B - Amsterdam, 2011.- vol. **696**, N. 5 - pp. 464-467.

[127] Tursunov E M. Variational calculations of 12C structure with the Buck and Ali-Bodmer alpha - alpha potentials // Europen Conf. on Advances in Nucl. Phys. and Related Areas. Thessaloniki, Greece 8-12 July 1997: Abstracts. - Thessaloniki, 1997. - p. 194

[128] E.M. Tursunov E.M. On the convergence of the many-body Pauli projector // arXiv:1002.0455. - Los Alamos, 2010. - 3 p.

[129] Voronchev V.T., Krasnopolsky V.M., Kukulin V.I. A variational study of the ground and excited states of light nuclei in a three-body model on the complete basis. I. General formalism // J. of Phys.G:Nucl.Phys. - London, 1982. - vol. **8**, N. 5. - pp. 649-666.

[130] Tursunov E.M., Razikov Kh.D., Kukulin V.I., Voronchev V.T., Pomerantsev V.N. High accuracy variational method for few-body calculations: Application to a 3N system // Physics of Atomic Nuclei. - Moscow, 1994. - vol. **57**, N. 12. - pp. 2075-2088.

[131] Kukulin V.I., Pomerantsev V.N., Tursunov E.M. New class of nonlocal models for describing interactions of composite particles and testing of

these models in the three-body problem // Physics of Atomic Nuclei. - Moscow, 1996. - vol. **59**, N. 5. - pp. 757-765.

[132] Varga K., Suzuki Y. Precise solution of few-body problems with the stochastic variational method on a correlated Gaussian basis // Phys.Rev. - New York, 1995. - vol. **C52**, N. 6. - pp. 2885-2905.

[133] Kameyama H., Kamimura M., Fukushima Y. Coupled-rearrangement-channel Gaussian-basis variational method for trinucleon bound states // Phys.Rev. - New York, 1989. - vol. **C40**, N. 2. - pp. 974-987.

[134] Baye D., Kruglanski M., Vincke M. Lagrange-mesh calculation of a three-body model for 6He // Nucl.Phys. - Elsevier, Amsterdam, 1994. - vol. **A573**, N. 3. - pp. 431-447.

[135] Kukulin V.I., Pomerantsev V.N. The orthogonal projection method in scattering theory // Ann.Phys. - Elsevier, Elsevier, Amsterdam, 1978. - vol. **111**, N. 2. - pp. 330-363.

[136] Matsumura H., Orabi M., Suzuki Y., Fujiwara Y. Removal of forbidden states in three-α-system // Nucl.Phys. - Elsevier, Amsterdam, 2006. - vol. **A776**, N. 1-2. - pp. 1-16.

[137] Suzuki Y., Matsumura H., Orabi M., Fujiwara Y., Descouvemont P., Theeten M., Baye D. Local versus nonlocal $\alpha - \alpha$ interactions in a 3α description of ^{12}C // Phys. Lett. - Elsevier, Amsterdam, 2008. - vol. **B659**, N. 1-2. - pp. 160-164.

[138] Baye D., Hesse M., Sparenberg J.-M., Vincke M. Analysis of the R-matrix method on Lagrange meshes // J. Phys. B - London, 1998. - vol. **31**, N. 15. - pp. 3439-3454.

[139] Hesse M., Sparenberg J.-M., Van Raemdonck F., Baye D. Coupled-

channel R-matrix method on a Lagrange mesh // Nucl. Phys. - Elsevier, Amsterdam, 1998. - vol. **A640**, N. 1. - pp. 37-51.

[140] Baye D., Hesse M., Vincke M. The unexplained accuracy of the Lagrange-mesh method // Phys. Rev. - New York, 2002. - vol. **E 65**, N. 2. - 026701 (8 p.).

[141] Raynal J., Revai J. Transformation coefficients in the hyperspherical approach to the three-body problem // Nuovo Cimento A, Series 10 - Springer, Berlin, 1970. - vol. **68**, N. 4. - pp. 612-622.

[142] Vasilevsky V., Nesterov A.V., Arickx F., Broeckhove J. Algebraic model for scattering in three-s-cluster systems. I. Theoretical background // Phys. Rev. - New York, 2001. - vol. **C63**, N. 3. - 034606 (16 p.).

[143] Vasilevsky V., Nesterov A.V., Arickx F., Broeckhove J. Algebraic model for scattering in three-s -cluster systems. II. Resonances in the three-cluster continuum of 6He and 6Be // Phys. Rev. - New York, 2001. - vol. **C63**, N. 3. - 034607 (7 p.).

[144] Abramowitz M, Stegun I.A. Handbook of Mathematical Functions. - Dover Publication, New York, 1999. - 1046 p.

[145] Kanada H., Kaneko T., Nagata S., Nomoto M. Microscopic Study of Nucleon-4He Scattering and Effective Nuclear Potentials // Prog. Theor. Phys. - Tokyo, 1979. - vol. **61**, N. 5. - pp. 1327-1341.

[146] Thompson I.J., Barnett A.R. Coulomb and Bessel Functions of Complex Arguments and Order // J. Comput. Phys. - Elsevier, Amsterdam, 1986. - vol. **64**, N. 2. - pp. 490-509.

[147] J. Raynal. Computing as a Language of Physics // Lectures Presented at an International Seminar Course at Trieste from 2 to 20 Aug. 1971.- IAEA, Vienna, 1972. - pp. 281-302.

[148] Gailitis M. New forms of asymptotic expansions for wavefunctions of charged-particle scattering // J. Phys. - London, 1976. - vol. **B9**, N. 5. - pp. 843-854.

[149] Baye D., Descouvemont P. Electromagnetic transitions and radiative capture in the generator-coordinate method // Nucl. Phys. - Elsevier, Amsterdam, 1983. - vol. **A407**, N. 1-2. - pp. 77-97.

[150] Descouvemont P., Vincke M. Iterative method for resonance properties in the R-matrix theory // Phys. Rev. - New York, 1990. - vol. **A42**, N. 7. - pp. 3835-3843.

[151] Hesse M., Roland J., Baye D. Solving the resonating-group equation on a Lagrange mesh // Nucl. Phys. - Elsevier, Amsterdam, 2002. - vol. **A709**, N. 1-4. - pp. 184-200.

[152] Thompson D.R., LeMere M., Tang Y.C. Systematic investigation of scattering problems with the resonating-group method // Nucl. Phys. - Elsevier, Amsterdam, 1977. - vol. **A286**, N. 1. - pp. 53-66.

[153] Tilley D.R., Cheves C.M., Godwin J.L., et al. (collaboration). Energy levels of light nuclei A=5, 6, 7 // Nucl. Phys. - Elsevier, Amsterdam, 2002. - vol. **A708**, N. 1-2. - pp. 3-161.

[154] Danilin B.V., Thompson I.J., Vaagen J.S., Zhukov M.V. Three-body continuum structure and response functions of halo nuclei (I): 6He // Nucl. Phys. - Elsevier, Amsterdam, 1998. - vol. **A632**, N. 3. - pp. 383-416.

[155] Danilin B.V., Rogde T., Vaagen J.S., Thompson I.J., Zhukov M.V. Three-body continuum spatial correlations in Borromean halo nuclei // Phys. Rev. - New York, 2004. - vol. **C69**, N. 2. - 024609 (10 p.).

[156] Adahchour A., Baye D., Descouvemont P. 14Be in a Lagrange-mesh cal-

culation // Phys. Lett. - Elsevier, Amsterdam, 1995. - vol. **B356**, N. 4. - pp. 445-449.

[157] Thompson I.J., Zhukov M.V. Structure and reactions of the Be 12, 14 nuclei // Phys. Rev. - New York, 1996. - vol. **C53**, N. 2. - pp. 708-714.

[158] Tarutina T., Thompson I.J., Tostevin J.A. Study of 14Be with core excitation // Nucl. Phys. - Elsevier, Amsterdam, 2004. - vol. **A733**, N. 1-2. - pp. 53-66.

[159] Descouvemont P. Halo structure of Be 14 in a microscopic Be 12 +n+n cluster model // Phys. Rev. - New York, 1995. - vol. **C52**, N. 2. - pp. 704-710.

[160] Thoennessen M., Yokoyama S., Hansen P.G. First evidence for low lying s-wave strength in 13Be // Phys. Rev. - New York, 2001. - vol. **C63**, N. 1. - 014308(3 p.).

[161] Audi G., Wapstra A.H. The 1993 atomic mass evaluation: (I) Atomic mass table // Nucl. Phys. - Elsevier, Amsterdam, 1993. - vol. **A565**, N. 1. - pp. 1-65.

[162] Tanihata I., Kobayashi T., Yamakawa O., et al. (collaboration). Measurement of interaction cross sections using isotope beams of Be and B and isospin dependence of the nuclear radii // Phys. Lett. - Elsevier, Amsterdam, 1988. - vol. **B206**, N. 4. - pp. 592-596.

[163] Aksyutina Yu., Aumann T., Boretzky K., et al. (collaboration). Study of the ^{14}Be Continuum: Identification and Structure of its Second 2^+ State // Phys. Rev. Lett. - New York, 2013. - vol. 111, N. 24. - 242501 (5 p.).

[164] Feshbach H. A unified theory of nuclear reactions // Ann. Phys. - Elsevier, Amsterdam, 1962. - vol. **19**, N. 2.- pp. 287-313.

[165] Fynbo H. O. U., Diget C. A., Bergmann, U. C., et al. (collaboration). Revised rates for the stellar triple-alpha process from measurement of 12C nuclear resonances // Nature. - London, 2005. - vol. **433**, N. 7022. - pp. 136-139.

[166] Baye D., Heenen P.H. Generalised meshes for quantum mechanical problems // J. Phys. A - London, 1986. - vol. **19**, N. 11. - pp. 2041-2059.

[167] Dubovichenko S.B., Dzhazairov-Kakhramanov A.V. Calculation of Coulomb form factors of lithium nuclei in a cluster model based on potentials with forbidden states // Phys. Atom. Nucl. - Moscow, 1994. - vol. **57**, N. 5. - pp. 733-740.

[168] Voronchev V.T., Kukulin V.I., Pomerantsev V.N., Ryzhikh G.G. Three-Body Calculations of A = 9 Nuclei with Supersymmetric alpha-alpha Potentials // Few-Body Syst. - Springer, Berlin, 1995. - vol. **18**, N. 2-4. - pp. 191-202.

[169] Baye D., Descouvemont P. Microscopic theory of beta-decay towards unbound states // Nucl. Phys. - Elsevier, Amsterdam, 1988. - vol. **A481**, N. 3. - pp. 445-457.

[170] Wilkinson D.H. Analysis of neutron beta-decay // Nucl. Phys. - Elsevier, Amsterdam, 1982. - vol. **A377**, N. 2-3. - pp. 474-504.

[171] Dubbers D., Mampe W., Dohner J. Determination of the weak-coupling constants from free-neutron decay experiments // Europhys. Lett. - London, 1990. - vol. **11**, N. 3. - pp. 195-200.

[172] Grüebler W, Schmelzbach P.A., König V., Risler R., Boerma D. Phase-shift analysis of d-alpha elastic scattering between 3 and 17 MeV // Nucl. Phys. - Elsevier, Amsterdam, 1975. - vol. **A242**, N. 2. - pp. 265-284.

[173] Jenny B., Grüebler W., König V., Schmelzbach P.A., Schweizer C. Phase-shift analysis of d-alpha elastic scattering between 3 and 43 MeV // Nucl. Phys. - Elsevier, Amsterdam, 1983. - vol. **A397**, N. 1. - pp. 61-101.

[174] Merkur'ev S.P. Coordinate asymptotic behavior of three-particle wave functions. // Theoretical and Mathematical Physics. - Springer, Berlin, 1971. - vol. **8**, N. 2. - pp. 798-809.

[175] Puchalski M., Moro A.M., Pachucki K. Isotope Shift of the 3S1/22-2S1/22 Transition in Lithium and the Nuclear Polarizability // Phys. Rev. Lett. - New York, 2006. - vol. **97**, N. 13. - 133001 (4 p.)

[176] Arai K., Suzuki Y., Varga K. Neutron-proton halo structure of the 3.563-MeV 0+ state in ^{6}Li // Phys. Rev. - New York, 1995. - vol. **C51**, N. 5. - pp. 2488-2493.

[177] Kukulin V.I., Pomerantsev V.N., Razikov Kh.D., Voronchev V.T., Ryzhikh G.G. Detailed study of the cluster structure of light nuclei in a three-body model (IV). Large space calculation for A = 6 nuclei with realistic nuclear forces // Nucl. Phys. - Elsevier, Amsterdam, 1995. - vol. **A586**, N. 1. - pp. 151-189.

[178] Jeppesen H.B., Ames F., Van den Bergh P., et al. (ISOLDE collaboration, REX-ISOLDE collaboration). Low energy reactions with radioactive ions at REX-ISOLDE-the 9Li + 2H case // Nucl. Phys. - Elsevier, Amsterdam, 2005. - vol. **A748**, N. 3-4. - pp. 374-392.

[179] Baye D., Capel P., Descouvemont P., Suzuki Y. Four-body calculation of He-6 breakup with the Coulomb-corrected eikonal method // Phys. Rev. - New York, 2009. - vol. **79**, N. 2. - 024607 (16 p.)

[180] Madurga M., Borge M.J.G., Alcorta M., et al. (ISOLDE collaboration).

Kinematic identification of the beta t branch in the decay of 11Li // Eur. Phys. J. - Springer, Berlin, 2009. - vol. **A42**, N. 3. - pp. 415-419.

[181] Baye D., Brainis E. Zero-energy determination of the astrophysical S factor and effective-range expansions // Phys. Rev. - New York, 2000. - vol. **C61**, N. 2. - 025801 (10 p.).

[182] Ringle R., Brodeur M., Brunner T., et al. (collaboration). High-precision Penning trap mass measurements of 9,10Be and the one-neutron halo nuclide 11Be // Phys. Lett. - Elsevier, Amsterdam, 2009. - vol. **B675**, N. 2. - pp. 170-174.

[183] Audi G., Bersillon O., Blachot J., Wapstra A.H. The Nubase evaluation of nuclear and decay properties // Nucl. Phys. - Elsevier, Amsterdam, 2003. - vol. **A729**, N. 1. - pp. 3-128.

[184] Capel P., Goldstein G., Baye D. Time-dependent analysis of the breakup of Be 11 on C 12 at 67MeV/nucleon // Phys. Rev. - New York, 2004. - vol. **C70**, N.6. - 064605 (9 p.).

[185] Riisager K., Forstner O., Borge M.J.G. et al. (ISOLDE collaboration). Be11(β-p), a quasi-free neutron decay? // Phys. Lett. - Elsevier, Amsterdam, 2014. - vol. **B732**, N.3. - pp.305-308.

[186] Riisager K. Beta-decay to continuum states: the case of 11Be // In. "INPC 2013 - International Nuclear Physics Conference, Firenze, Italy", Edited by S. Lunardi et al. - EPJ Web of Conferences, 2014 - Vol. 66. - id.02090 (4 p.)

[187] Sohler D., Stanoiu M., Dombrádi Z., et al. (collaboration). In-beam gamma-ray spectroscopy of the neutron-rich nitrogen isotopes $^{19-22}$N // Phys. Rev. - New York, 2008. - vol **C77**, N. 4. - 044303 (8 p.).

[188] Nakamura T., Kobayashi N., Kondo Y., et al. (collaboration). Halo Structure of the Island of Inversion Nucleus ^{31}Ne // Phys. Rev. Lett. - New York, 2009. - vol. **103**, N. 26. - 262501 (4 p.).

[189] Horiuchi W., Suzuki Y., Capel P., Baye D. Probing the weakly-bound neutron orbit of Ne 31 with total reaction and one-neutron removal cross sections // Phys. Rev. - New York, 2010. - vol. **C81**, N. 2. - 024606 (11 p.).

[190] Hamamoto I. Interpretation of Coulomb breakup of Ne 31 in terms of deformation // Phys. Rev. - New York, 2010. - vol. **C81**, N. 2. - 021304 (4 p.).

[191] Rodberg L.S., Thaler R.M. Introduction to the quantum theory of scattering. - Academic Press, New York, 1967. - 298 p.

[192] Rose H.J., Brink D.M. Angular Distributions of Gamma Rays in Terms of Phase-Defined Reduced Matrix Elements // Rev. Mod. Phys. - New York, 1967. - vol. **39**, N. 2. - pp. 306-347.

[193] Baye D., Descouvemont P. Microscopic description of nucleus-nucleus bremsstrahlung // Nucl. Phys. - Elsevier, Amsterdam, 1985. - vol. **A443**, N. 2. - pp. 302-320.

APPENDIX

1. Gamma-delayed transition probabilities to continuum states

Let us assume a bound initial state at energy E_i with spin and parity J_i, π_i of a nucleus at rest, decaying to a final unbound state at relative energy E, and with spin and parity J_f, π_f. In the final state, both nuclei are characterized by spins I_1 and I_2, and by internal wave functions ϕ^{I_1} and ϕ^{I_2}. According to Ref. [191], the transition probability per time unit is given by

$$dW_\gamma = \frac{2\pi}{\hbar}\frac{|T_{fi}|^2}{(2\pi\hbar)^6} d\boldsymbol{p}\, d\boldsymbol{P}\, d\boldsymbol{p_\gamma}\, \delta(\boldsymbol{P}+\boldsymbol{p_\gamma})\delta(E+E_\gamma-E_i), \qquad \text{(A.1.1)}$$

where we neglect recoil effects. In (A.1.1), $(\boldsymbol{p}, \boldsymbol{P}, \boldsymbol{p_\gamma})$ are the relative, total, and photon momenta. The transition matrix element T_{fi} is obtained from

$$|T_{fi}|^2 = \frac{1}{2J_i+1}\frac{2\pi\hbar c}{k_\gamma}\sum_{\nu_1,\nu_2,M_i,q} |\langle \Psi_f^{\nu_1\nu_2(-)}(\boldsymbol{p})|H_\gamma^q|\Psi^{J_iM_i\pi_i}\rangle|^2, \qquad \text{(A.1.2)}$$

where k_γ is the photon wave number,

(ν_1, ν_2) are the spin orientations in the exit channel,

H_γ^q is the electromagnetic-emission hamiltonian with polarization q. The final state is described by an ingoing wave $\Psi_f^{\nu_1\nu_2(-)}$ with relative momentum $\boldsymbol{p} = (p, \Omega_p)$, related to the corresponding outgoing wave $\Psi_f^{\nu_1\nu_2(+)}$ by

$$\Psi_f^{\nu_1\nu_2(-)}(\boldsymbol{p}) = (-1)^{I_1+I_2-\nu_1-\nu_2} K \Psi_f^{-\nu_1-\nu_2(+)}(-\boldsymbol{p}), \tag{A.1.3}$$

where K is the time-reversal operator. The outgoing wave function is written in a partial wave expansion as

$$\Psi_f^{\nu_1\nu_2(+)}(\boldsymbol{p}) = \sum_{JM\pi\ell I\nu} \langle I_1 I_2 \nu_1 \nu_2 | I\nu \rangle \langle \ell I m \nu | JM \rangle \Psi_{\ell I}^{JM\pi}(E) \mathcal{D}_{0m}^{\ell *}(\Omega_p), \tag{A.1.4}$$

where $\mathcal{D}_{0m}^{\ell}(\Omega_p)$ are Wigner functions. When the relative coordinate $\boldsymbol{r}$ is large, the asymptotic behaviour of the partial wave is given by

$$\begin{aligned} \Psi_{\ell I}^{JM\pi}(E) \longrightarrow \; & \tfrac{[\pi(2\ell+1)]^{1/2}}{kr} i^{\ell+1} \exp(i\sigma_\ell) \left(I_\ell(kr) - U^{J\pi} O_\ell(kr) \right) \\ & \times \left[[\phi^{I_1} \otimes \phi^{I_2}]^I \otimes Y_\ell(\Omega_r) \right]^{JM}, \end{aligned} \tag{A.1.5}$$

where σ_ℓ are the Coulomb phase shifts,

I_ℓ and O_ℓ are the ingoing and outgoing Coulomb functions, respectively. Here and in the following, we assume a single-channel problem or, in other words, that the dimension of the collision matrix $\boldsymbol{U}$ is unity.

After integration over $\boldsymbol{P}$ and p_γ, Eq. (A.1.1) is transformed as

$$dW_\gamma = \frac{k_\gamma^2}{(2\pi\hbar)^5 c} |T_{fi}|^2 \, d\boldsymbol{p} \, d\Omega_\gamma. \tag{A.1.6}$$

First, we expand H_γ^q in electric ($\sigma = E$) and magnetic ($\sigma = M$) multipoles [192]. Then we integrate over the orientations Ω_p and Ω_γ. We have

$$\int |T_{fi}|^2 d\Omega_p d\Omega_\gamma \;=\; \frac{32\pi^2}{2J_i+1} \sum_{\sigma\lambda J_f \pi_f} \frac{|\alpha_\lambda^\sigma|^2}{2\lambda+1}$$

$$\times \frac{2J_f+1}{2\ell_f+1} |\langle \Psi^{J_f\pi_f}_{\ell_f I_f}(E)||\mathcal{M}^\sigma_\lambda||\Psi^{J_i\pi_i}\rangle|^2, \qquad \text{(A.1.7)}$$

where $\mathcal{M}^\sigma_\lambda$ are the multipole operators of order λ (coefficients α^σ_λ are given, for instance, in Ref. [192]). Let use define

$$\Gamma_\gamma(E) = \sum_{\sigma\lambda J_f\pi_f} \frac{8\pi k_\gamma^{2\lambda+1}}{\lambda(2\lambda+1)!!^2} \frac{2J_f+1}{2J_i+1} |\langle \Psi^{J_f\pi_f}_{\ell_f I_f}(E)||\mathcal{M}^\sigma_\lambda||\Psi^{J_i\pi_i}\rangle|^2. \quad \text{(A.1.8)}$$

Using (A.1.7) in (A.1.6) gives

$$\frac{dW_\gamma}{dE} = \frac{\mu k}{2\pi^2\hbar^3} \frac{\Gamma_\gamma(E)}{2\ell_f+1}, \qquad \text{(A.1.9)}$$

where μ is the reduced mass. An interesting case concerns transitions to a narrow resonance with energy E_R and particle width Γ. In such a case, the scattering wave function can be approximated as [193]

$$\Psi^{J_f\pi_f}_{I_f\ell_f}(E) \approx \frac{1}{k} \frac{[\pi\hbar v(2\ell_f+1)\Gamma]^{1/2}}{E_R - E - i\Gamma/2} \Psi^{J_f\pi_f}_{BSA}, \qquad \text{(A.1.10)}$$

where $\Psi^{J_f\pi_f}_{BSA}$ is the bound-state approximation of the wave function, and v the relative velocity. Using this approximation in (A.1.9) and integrating over E gives

$$W_\gamma = \Gamma^{BSA}_\gamma/\hbar, \qquad \text{(A.1.11)}$$

where Γ^{BSA}_γ is the γ width in the bound-state approximation. This result corresponds to the usual definition of the transition probability between two bound states.

2. Matrix elements of the M1 transition operator in hyperspherical coordinates

Let us write the three-body wave function (4.8) as

$$\Psi^{JM\pi}_{^6\mathrm{Li}}(\rho,\Omega_5) = \rho^{-5/2}\sum_{\gamma K}\chi^{J\pi}_{\gamma K}(\rho)\mathcal{Y}^{JM}_{\gamma K}(\Omega_5) = \sum_{\gamma K}\Psi^{JM\pi}_{\gamma K}(\rho,\Omega_5), \tag{A.2.1}$$

where index γ stands for $(\ell_x\ell_y LS)$.

A reduced matrix element of ℓ_x is obtained from

$$\begin{aligned}\langle\Psi^{J\pi}_{\gamma K}||\ell_x||\Psi^{J'\pi'}_{\gamma' K'}\rangle &= \delta_{\ell_x\ell'_x}\delta_{\ell_y\ell'_y}\delta_{SS'}\delta_{KK'}[\ell_x(\ell_x+1)]^{1/2}\hat{\ell}_x\hat{L}\hat{L}'\hat{J}'(-)^{\ell_x+\ell_y+S+L+L'+J'}\\ &\times\left\{\begin{array}{ccc} L & \ell_x & \ell_y\\ l_x & L' & 1\end{array}\right\}\left\{\begin{array}{ccc} L & J & S\\ J' & L' & 1\end{array}\right\}I_\rho,\end{aligned} \tag{A.2.2}$$

where we use the notation $\hat{\ell}=\sqrt{2\ell+1}$, and where the integral I_ρ is defined as

$$I_\rho = \int\chi^{J\pi}_{\gamma K}(\rho)\chi^{J'\pi'}_{\gamma' K'}(\rho)d\rho. \tag{A.2.3}$$

Matrix elements of ℓ_y are obtained by swapping ℓ_x and ℓ_y. For the crossed term in (5.12), the calculation is more tedious. We have

$$\begin{aligned}\langle\Psi^{J\pi}_{\gamma K}||\boldsymbol{x}\times\boldsymbol{p_y}+\boldsymbol{y}\times\boldsymbol{p_x}||\Psi^{J'\pi'}_{\gamma' K'}\rangle &= \delta_{SS'}(-)^{L+S+J'+\ell_x+\ell_y}\sqrt{6}\hat{\ell}_x\hat{\ell}_y\hat{\ell}'_x\hat{\ell}'_y\hat{L}\hat{L}'\hat{J}'I_\rho I_\alpha\\ \times\left(\begin{array}{ccc}\ell'_x & 1 & \ell_x\\ 0 & 0 & 0\end{array}\right)&\left(\begin{array}{ccc}\ell'_y & 1 & \ell_y\\ 0 & 0 & 0\end{array}\right)\left\{\begin{array}{ccc} L & J & S\\ J' & L' & 1\end{array}\right\}\left\{\begin{array}{ccc}\ell_x & \ell_y & L\\ \ell'_x & \ell'_y & L'\\ 1 & 1 & 1\end{array}\right\},\end{aligned} \tag{A.2.4}$$

where the angular integral reads

$$I_\alpha = \int_0^{\pi/2}d\alpha\cos^2\alpha\sin^2\alpha\phi^{\ell_x\ell_y}_K(\alpha)\left(\frac{d}{d\alpha}+\frac{\Delta l_y}{\tan\alpha}-\frac{\Delta l_x}{\cot\alpha}\right)\phi^{\ell'_x\ell'_y}_{K'}(\alpha). \tag{A.2.5}$$

In this expression, $\Delta\ell = 1 + [\ell'(\ell'+1) - \ell(\ell+1)]/2$. Integration over α is performed numerically. For the hyperradius ρ, the use of Lagrange functions makes the integral very simple.

For the spin part of the M1 operator, we have

$$\begin{aligned}\langle \Psi^{J\pi}_{\gamma K} || \boldsymbol{s}_1 || \Psi^{J'\pi'}_{\gamma' K'} \rangle &= \delta_{\ell_x \ell'_x} \delta_{\ell_y \ell'_y} \delta_{LL'} \delta_{KK'} \hat{s}_1 \hat{S} \hat{S}' \hat{J}' [s_1(s_1+1)]^{1/2} (-)^{s_1+s_2+L-J} \\ &\times \left\{ \begin{array}{ccc} J & S & L \\ S' & J' & 1 \end{array} \right\} \left\{ \begin{array}{ccc} S & s_1 & s_2 \\ s_1 & S' & 1 \end{array} \right\} I_\rho, \end{aligned} \tag{A.2.6}$$

where we have assumed that the core spin is zero ($s_3 = 0$).

For transitions to the continuum, the previous formula can still be applied, but the final-state wave functions are now defined by Eq. (5.4). It is clear that with the restriction to the S-wave final state, the orbital components $\ell_{x,\mu}$ and $\ell_{y,\mu}$ do not contribute to the M1 transition. The matrix element of the crossed term is performed over the Jacobi coordinates. Using the S-wave character of the scattering state, we have

$$\begin{aligned}\langle \Psi^{0^+}_{^6\mathrm{Li}} || \boldsymbol{x} \times \boldsymbol{p_y} + \boldsymbol{y} \times \boldsymbol{p_x} || \Psi^{1^+}_{\alpha d} \rangle &= \sqrt{2\mu_{pn}\mu_{\alpha d}/9} \sum_K \int dx dy \phi^{11}_K(\alpha) \chi^{0^+}_{1111K}(\rho) \\ &\times xy\rho^{-5/2} \left(x\frac{\partial}{\partial y} - y\frac{\partial}{\partial x} \right) u_d(x/\sqrt{\mu_{pn}}) u_E(y/\sqrt{\mu_{\alpha d}}), \end{aligned} \tag{A.2.7}$$

where ρ and α are given in Eq. (5.2). The spin contribution is obtained with the same technique, with the help of Eq. (A.2.6). Note that the bra and ket have been swapped with respect to Eq. (5.10). The ordering is simply restored with a factor $-1/\sqrt{3}$.